The Rac1 homolog CED-10 plays key roles in cytoskeletal regulation during asymmetric divisions in the early *Caenorhabditis elegans* embryo

By

HELEN LAMB

DISSERTATION

Submitted in partial satisfaction of the requirements for the degree of

DOCTOR OF PHILOSOPHY

in

Biochemistry, Molecular, Cellular, & Developmental Biology

in the

OFFICE OF GRADUATE STUDIES

of the

UNIVERSITY OF CALIFORNIA

DAVIS

Approved:

_____

Lesilee Rose, Chair

_____

Bruce Draper

_____

Daniel Starr

Committee in Charge

2022

Table of Contents

Acknowledgements

I am grateful to many people for their support in this undertaking – it would have been impossible to complete my doctoral degree without the support of my community. First and foremost is my doctoral advisor, Lesilee S. Rose, for welcoming me into her lab and for her patient encouragement and generous mentorship throughout my years as her student. From conception of the research projects to final proofreading of this dissertation, Dr. Rose's constant support has been fundamental to my success. Thanks also to my dissertation committee members Bruce W. Draper and Dan A. Starr, who provided valuable guidance and advice in formal and informal settings. Special thanks to Jon Sack, my academic advisor, and Enoch Baldwin, master advisor for the graduate group, for compassionate and honest advice. Thanks to Kyoko Okada for scientific, professional, and personal mentorship.

Thanks to the Biochemistry, Molecular, Cellular, and Developmental Biology Graduate Group at UC Davis – faculty, staff, and students – for providing a collegial, supportive environment in which to study and for fostering a deep appreciation for the interdisciplinary nature of modern biology. Thanks to my qualifying exam committee, Dan A. Starr, Bruce W. Draper, Kassandra Ori-McKenney, Priya Shah, and Geoffrey Attardo, for helping me start my research with a solid foundation. Thanks to Francis J. McNally for honest advice and insightful scientific feedback at many lab meetings. Thanks to Sara K. Olson at Pomona College for fostering my interest in scientific research and serving as a role model. Thanks to Hsin-Yi "Henry" Ho for training and guidance early in my time at UC Davis and for encouraging me to continue my doctoral studies. Thanks to the Molecular & Cellular Biology T32 Training program, especially James Trimmer, Frederic Chedin, and Gayathri Gomes, for valuable scientific and professional training as well as exposure to a breadth of scientific topics,

techniques, and philosophical approaches. Thanks to Bruce Hammock for a memorable and extremely valuable conversation over lunch.

Thanks to Brigette Monroy, Kari Price, Deena Leerberg, Malgorzata Liro, and Dean Natwick for their kind and generous mentorship early in my studies. I am deeply grateful to several peers, in particular Sara Konopelski-Snavely, Cindy Khuu, Mikaela Louie, Megan Liou, Sydney Wyatt, Jennifer Baily, Laurel Koch, and Ayswarya Jay: as the saying goes, “sorrow shared is halved; joy shared is doubled.” Special and heartfelt thanks are due to my parents, Lowell D. and Victoria R. Lamb, for encouraging me to pursue a doctoral degree, cheering me on at every stage, and listening to many iterations of arcane scientific lectures; and to my brother, John R. Lamb, for inspiring me to be a better scientist and person.

Abstract

In multicellular organisms, asymmetric cell division generates cell type diversity during both development and tissue homeostasis. For successful asymmetric division to proceed, a cellular axis of polarity, or asymmetry, must be established via any of several molecular mechanisms. This step is followed by two sequential processes requiring precise coordination of the various components of the cytoskeleton. First, the mitotic spindle must be positioned in alignment with the axis of polarity; second, cytokinesis must occur at the right position and time, as instructed by the spindle, to segregate chromosomes and bisect the axis of polarity. In this dissertation I present my contributions to two research projects related to cytoskeletal regulation during asymmetric cell division.

Chapter I reviews the state of the field prior to my studies and introduces the two research projects in context. Chapter II is a manuscript in revision for *Journal of Cell Science* that relates our findings from the first project, which aimed to understand the role of the DEPDC1 homolog LET-99 during cytokinesis. LET-99 was previously characterized as a negative regulator of the dynein-containing force generating complex during spindle positioning, but had also been shown to play a separable role in cytokinesis. With others, I demonstrated that during the first mitotic division LET-99 and the Rac1 homolog CED-10 have antagonistic roles in regulating the balance of branched vs linear actin during cytokinesis to achieve robust and timely furrowing. These roles appear to be global rather than spatially restricted to the contractile ring. However, the findings suggest that CED-10 does not interact with LET-99 to promote spindle positioning in the first mitotic division, further confirming that LET-99's role as a regulator of the actomyosin cytoskeleton and cytokinesis is separable from its role in spindle positioning.

Chapter III is a manuscript in preparation that documents our investigations into the role of CED-10 in spindle orientation of the asymmetrically dividing EMS cell. Two signaling pathways that regulate this spindle orientation were previously identified: a Wnt/Frizzled pathway and a MES-1/SRC-1 pathway. I determined that CED-10 works upstream or at the level of SRC-1 in the MES-1/SRC-1 signaling pathway and furthermore that CED-10 contributes to cortical localization of the same dynein-containing force generating complex involved in spindle positioning at the one-cell stage. I also found that CED-10's molecular function in this context may be to promote branched actin formation at the EMS/P2 contact, but this evidence is partially contradicted by our findings that loss of the branched-actin regulator GEX-3 does not enhance the rate of EMS spindle rotation defects in Wnt/MOM-2-depleted embryos. An additional curious finding is that CED-10 has a previously unreported role in P1 spindle rotation, as do the branched actin nucleator Arp2/ARX-2 (Arp2) and the Frizzled ortholog MOM-5.

Although this research was performed using nematodes as a model organism, the results have broad implications for all animals because most of the molecular components involved are evolutionarily conserved. By understanding in detail the mechanisms of different types of asymmetric divisions, we can understand both normal development and diseases such as cancer, which involves the dysregulation of asymmetric division.

Chapter I

Introduction: Cytoskeletal regulation during asymmetric cell division

During the embryonic development of multicellular organisms, cells must proliferate, take on distinct identities, and move into the correct positions to form an individual. All three of these major cellular behaviors require a precisely regulated and dynamically tuned cytoskeleton. The focus of this dissertation is asymmetric cell division, which occurs in all multicellular organisms and is necessary for cell fate diversification during both embryonic development and adult tissue homeostasis (Gillies and Cabernard 2011, Inaba and Yamashita 2012, Venkei and Yamashita 2018). In many asymmetric divisions, establishment of a polarity or asymmetry axis is followed by orientation of the mitotic spindle in alignment with that axis. This spindle orientation defines a division plane that, in coordination with the actin cytoskeleton, bisects the axis of asymmetry and creates daughter cells with different fates (D'avino, Glover et al. 2005, Morin and Bellaiche 2011, McNally 2013, Pillitteri, Guo et al. 2016). The work presented here aims to add to the current understanding of molecular mechanisms underlying asymmetric cell division using the early *Caenorhabditis elegans* embryo as a model system.

Asymmetric cell division in metazoans relies on conserved molecular mechanisms

Multiple possible sources exist for the cue that instructs spindle orientation. The cue can be mechanical in nature, as in the case of tension forces present in the enveloping cell layer of the zebrafish gastrula (Campinho, Behrndt et al. 2013), or signal-based, as in the case of *Drosophila* sensory organ precursor cells polarized by planar cell polarity (PCP) signaling (Segalen, Johnston et al. 2010). Furthermore, it can originate outside the cell, as in the case of vertebrate neuroepithelia responding to semaphorin signaling (Arbeille, Reynaud et al. 2015), or within the cell, as in the case of *C. elegans* germline progenitors polarized by asymmetric

localization of partitioning-defective (PAR) proteins (Cheng, Kirby et al. 1995). In most types of asymmetric division studied to date, the axis of asymmetry is determined by a combination of partially redundant cues, some more essential than others (Tsou, Ku et al. 2003, di Pietro, Echard et al. 2016).

One mechanism that is central to many types of metazoan asymmetric divisions is the establishment of molecular asymmetry at the cortex by PAR proteins. These highly conserved yet versatile proteins form a regulatory network, driven by mutual stabilization or destabilization, resulting in their localization to restricted cortical "domains" (Lang and Munro 2017). The most conserved PAR proteins are the small GTPase Cdc42, the scaffold PAR-3/Bazooka, the adaptor PAR-6, and the kinases PAR-1 and aPKC (PKC-3 in worms) (Gillies and Cabernard 2011, Lang and Munro 2017). Together, Cdc42, PAR-3, PAR-6, and aPKC have been termed the anterior or apical PARs (aPARs) because they colocalize at the apical domains of *Drosophila* epithelial cells and the anterior domain of the *C. elegans* zygote; in many systems, including the *C. elegans* zygote, aPAR localization is restricted by posterior PARs (pPARs) such as PAR-1 (Rose and Gonczy 2014, di Pietro, Echard et al. 2016, Lang and Munro 2017).

In many animal cell divisions requiring an oriented spindle, the forces necessary to move the spindle are produced by the asymmetric localization of a conserved cortical force-generating complex. This complex, which can be regulated by the PAR proteins described above and/or by other types of cues, retains the motor dynein and its partner dynactin at the cortex, converting its minus-end directed "walking" into pulling forces that move the microtubules. Linking dynein and dynactin to the cortex are the adaptor proteins GPR-1/2 (LGN/Pins) and LIN-5 (NuMA/Mud) and a cortical anchor such as the heterotrimeric G protein subunit $G\alpha_i$ (Morin and Bellaiche 2011, McNally 2013, di Pietro, Echard et al. 2016). Alternative anchors such as the

PDZ domain-containing DLG-1 (Discs Large) or the actin-binding scaffold AFD-1 (Afadin/Canoe), can also work with LIN-5 to keep dynein at the cortex, but these alternative anchors can also interact with other motors like myosin in a dynein-independent mechanism (di Pietro, Echard et al. 2016).

Mechanisms of asymmetric cell divisions in the early *C. elegans* embryo

The early *Caenorhabditis elegans* embryo serves as an excellent model for studying the molecular mechanisms of asymmetric division: it follows an invariant division pattern that includes multiple asymmetric divisions. Furthermore, the nematode genome contains homologs for many highly conserved molecular components for asymmetry establishment, spindle orientation, and fate specification, allowing researchers to gain insights into the fundamental principles of asymmetric cell division. The research reported here focuses on the first through third rounds of mitotic division, each of which includes at least one asymmetric division (Rose and Gonczy 2014). The first mitotic division is asymmetric: in response to fertilization, the zygote (or P0 cell) establishes opposing aPAR and pPAR domains that define anterior and posterior embryonic poles (Fig. 1A). Following pronuclear meeting, the newly formed mitotic spindle rotates to align with the anterior/posterior axis and thus division creates an anterior cell, AB, and a posterior cell, P1 (Fig. 1A, 1C). In the second round of mitosis, the AB daughter divides symmetrically to give rise to ABa and ABp at the anterior and dorsal aspects of the embryo, respectively; the P1 cell divides asymmetrically to give rise to the EMS and P2 cells at the ventral and posterior aspects of the embryo, respectively (Rose and Gonczy 2014). While the ABa and ABp blastomeres divide symmetrically again, both EMS and P2 divide asymmetrically (Fig. 1C).

The asymmetric divisions of the germline "P" lineage blastomeres (i.e., P0, P1, and P2) are instructed by PAR polarity. In these cells, a PAR and pPAR domains form, and at least in the one-cell, these PAR proteins antagonize one another's cortical localization to form mutually exclusive "anterior" and "posterior" domains (Rose and Gonczy 2014) (Fig. 1B). In response to the formation of the PAR domains, a cytoplasmic gradient of cell fate determinants forms, also along the axis of PAR asymmetry (Rose and Gonczy 2014). Studies in the one-cell embryo have shown that the force-generating complex described previously localizes asymmetrically on the cortex and exerts microtubule pulling forces that orient and position the spindle along the axis of PAR asymmetry (Srinivasan, Fisk et al. 2003, Park and Rose 2008, Rose and Gonczy 2014, di Pietro, Echard et al. 2016). The resulting mitotic division gives rise to daughters that have inherited different quantities of PARs and cytoplasmic fate determinants and therefore proceed to adopt different fates.

In contrast, the division axis of EMS is not aligned with PAR polarity, which at this stage becomes "inner-outer" rather than "anterior-posterior" (Fig. 1A). Instead, the EMS mitotic spindle rotates into an orientation perpendicular to the PAR polarity axis and parallel with the anterior-posterior axis of the embryo. Following EMS cytokinesis, the anterior daughter MS becomes a mesoderm progenitor, while E, closer to P2, becomes an endoderm progenitor (Rocheleau, Downs et al. 1997, Thorpe, Schlesinger et al. 1997, Bei, Hogan et al. 2002, Walston, Tuskey et al. 2004) (Fig. 1C). The induction of endoderm fate in requires that the E blastomere be born in the correct position to contact P2; therefore, proper orientation of the EMS division is essential to produce endoderm from only one daughter and mesoderm from the other. EMS spindle rotation is instructed by two redundant signals from the neighboring cell P2: a well-described Wnt/β-catenin pathway and a poorly understood MES-1/SRC-1 kinase signaling

pathway. Both pathways also work to induce endoderm fate specification in the E blastomere (Bei, Hogan et al. 2002) (Fig. 1D).

Two partially redundant signaling pathways instruct EMS spindle orientation and endoderm fate

In the Wnt pathway, the Wnt ligand MOM-2 is secreted by the P2 blastomere. Binding to the Frizzled receptor (MOM-5) on the EMS surface activates the effector protein Disheveled (DSH-2) and results in removal of the divergent β-catenin WRM-1 from the cortex (Schlesinger, Shelton et al. 1999, Walston, Tuskey et al. 2004, Kim, Ishidate et al. 2013). Because *wrm-1(RNAi)* suppresses the EMS spindle orientation defect of embryos lacking both Wnt/Frizzled and MES-1/SRC-1 pathway components, the removal of WRM-1 is thought to "un-mask" a cortical cue for spindle positioning (Kim, Ishidate et al. 2013). In the MES-1/SRC-1 pathway, the receptor tyrosine kinase-like membrane protein MES-1 activates the proto-oncogene kinase SRC-1, which signals to unknown downstream effectors (Berkowitz and Strome 2000, Bei, Hogan et al. 2002). MES-1 localizes exclusively to the EMS/P2 contact, while an antibody that stains SRC-1-dependent tyrosine phosphorylation is present on all cell-cell contacts but enriched at the EMS/P2 contact (Bei, Hogan et al. 2002). These localization patterns hint at a mechanism for EMS spindle positioning that relies on spatially restricted pathway components.

In response to these signaling pathways, the mitotic spindle orients to the anterior-posterior axis, which requires a rotation of the spindle from its initial left-right orientation (Fig. 1A). Loss of the dynein heavy chain (DHC-1), dynactin (DNC-1), or LIN-5 results in strong spindle orientation defects, suggesting these proteins act in both pathways (Zhang, Skop et al. 2007, Liro and Rose 2016). However, it is not clear whether the same heterotrimeric Gα proteins that anchor the force-generating complex in P0 have any role in this division, raising the possibility that other anchors could recruit LIN-5 to the EMS/P2 contact (Liro and Rose 2016).

At the eight-cell stage, Wnt/Frizzled and MES-1/SRC-1 signaling work together to induce endoderm fate in the E blastomere. They apparently converge on regulation of β-catenin localization: WRM-1 (and possibly HMP-2) moves to the nucleus and drives endoderm fate specification through nuclear export of the LEF-1/TCF-7 ortholog POP-1 (Lin, Thompson et al. 1995, Rocheleau, Downs et al. 1997, Thorpe, Schlesinger et al. 1997, Bei, Hogan et al. 2002, Sugioka, Mizumoto et al. 2011).

The MES-1/SRC-1 signaling pathway, in addition to its importance in EMS spindle positioning and endoderm fate specification, is required for P2 asymmetric division (Berkowitz and Strome 2000, Bei, Hogan et al. 2002). At birth, P2 inherits the posterior PARs uniformly around the cortex. During the cell cycle, new PAR domains form, but in a different orientation from the previous P lineage divisions: "anterior" PARs such as PAR-3 localize to the anterior-dorsal aspect of the cell, while "posterior" PARs including PAR-2 occupy the posterior-ventral aspect including the EMS/P2 cell contact (Kemphues and Strome 1997, Arata, Lee et al. 2010, Rose and Gonczy 2014) (Fig. 1A). The spindle then forms on the axis of PAR polarity. This reorientation of the axis of PAR polarity requires MES-1/SRC-1 signaling (Arata, Lee et al. 2010).

Despite major progress in uncovering the mechanisms of this type of asymmetric division in the early *C. elegans* embryo, several questions regarding the details of MES-1/SRC-1 signaling remain. First, the mechanism for spatial restriction of MES-1 and active SRC-1 has not been elucidated. The identity of the relevant SRC-1 phosphorylation target(s) is unknown, and it is also unclear whether the same target(s) are involved in EMS spindle positioning and P2 PAR domain reorientation or spindle positioning. Additionally, the cortical anchor(s) for the force-generating complex has yet to be identified.

Recent advances in understanding EMS asymmetric division

Double mutant analysis has been the standard mechanism for assigning genes to the EMS asymmetric division pathways. For example, the MES-1/SRC-1 and Wnt pathways were identified as separate, redundant pathways because *mes-1* and *src-1* mutants had the same low frequency of spindle rotation defects as *mes-1;src-1* double mutants, but when either was combined with mutation of a Wnt pathway component, the rate of spindle rotation failure increased to ~95% (Bei, Hogan et al. 2002). Using similar analyses, our lab has identified three new EMS spindle positioning components: in the Wnt pathway, the kinase PAR-1; and in the MES-1/SRC-1 pathway, the PAR-1-like kinase PIG-1 and the G-protein regulator LET-99 (Liro and Rose 2016, Liro, Morton et al. 2018). All three genes also contribute to the first asymmetric division of the P0 cell.

In P0, PAR-1 acts redundantly with PAR-2 to inhibit aPARs from localizing to the posterior cortex. PIG-1 was identified as a kinase whose function is also partially redundant with both PAR-1 and PAR-2 in maintaining the posterior PAR domain (Kemphues, Priess et al. 1988, Morton, Hoose et al. 2012). Both the posterior and anterior PARs negatively regulate the cortical localization of LET-99, restricting it to a posterior-lateral band. LET-99, a negative regulator of force-generating complex localization, then mediates the spatial restriction of the dynein-containing complex responsible for microtubule pulling forces (Rose and Kemphues 1998, Krueger, Wu et al. 2010) (Fig. 1B). While LET-99 forms a similar band in P1 and P2 and is thought to perform the same function, in EMS it localizes to all cell-cell contacts at first but is removed from the EMS/P2 contact over the course of the cell cycle (Tsou, Hayashi et al. 2003). Furthermore, loss of LET-99 suppresses the EMS rotation defects of *mes-1, src-1*, and *pig-1* mutants (Liro, Morton et al. 2018). These observations were interpreted to mean that LET-99 is a

negative regulator of MES-1/SRC-1 dependent EMS spindle orientation; thus its removal from the P2/EMS contact permits signaling to proceed in a mechanism similar to the Wnt-instructed removal of β-catenin from the cortex, by unmasking a cortical cue for rotation (Liro and Rose 2016). Given this evidence and our understanding of each protein's function in the first asymmetric division, we have previously proposed a model in which PIG-1 inhibits LET-99 in response to MES-1/SRC-1 signaling. However, as mentioned previously, it is not clear if $G\alpha_i$ is the anchor for the force generating complex in this context, leaving open the possibility that LET-99 could be regulating other factors instead of or in addition to its known targets.

CED-10 (Rac1) is a key cytoskeletal regulator in development

The work presented here identifies CED-10 as another molecular component of the MES-1/SRC-1 pathway. CED-10 is an ortholog of the small GTPase Rac1, which is conserved to varying degrees throughout eukaryotes and acts as a "molecular switch" in various cellular signaling pathways (Boreaux, Vignal et al. 2007, Hall 2012). As a member of the Rho GTPase family, Rac1 is primarily involved in cytoskeletal regulation across diverse developmental contexts including gastrulation; neuronal growth, synaptogenesis, and maturation; hematopoiesis; and immune cell chemotaxis (Bustelo, Sazeau et al. 2007, Hall 2012, Duquette and Lamache-Vane 2014, Nguyen, Kholodenko et al. 2018). Rac1 is thought to facilitate these diverse processes by partnering with different combinations of regulators and effectors. In humans, over 80 guanine exchange factors (GEFs), nearly 70 GTPase activating factors (GAPs), and at least 3 GTP-disassociation inhibitors (GDIs) have been identified as Rac1 regulators. Various kinases such as p21-activated kinases (PAKs), members of the NADPH oxidase complex, and scaffolding proteins including Wiskott-Aldrich family (Wasf) proteins are just a handful of the many known effectors (Bustelo, Sazeau et al. 2007, Hall 2012). Given Rac1's

pleiotropic roles in cellular behaviors, especially in cell shape and migration, it is unsurprising that dysregulation or constitutive activation of Rac1 is also associated with poor prognosis in cancer, making it an important potential therapeutic target (Bailly, Beignet et al. 2022).

CED-10 has known branched-actin-dependent roles in the *C. elegans* embryo that provide clues to its possible function in the EMS division. CED-10 participates in the branched-actin-dependent processes of cell corpse engulfment (where it is a downstream effector of Src signaling) and gonad distal tip migration in concert with CED-5/DOCK180 and CED-2/CrkII (Lundquist 2006). It is also required for branched-actin-mediated cell movements during ventral enclosure of the epidermis and axonal pathfinding (Lundquist 2006). Notably, in the *C. elegans* intestine, the branched actin regulators Arp-2/3 and WAVE/SCAR (both of which are regulated in early morphogenesis by CED-10) have been shown to be required for apical accumulation of the force generating component DLG-1/Discs Large (Patel, Bernadskaya et al. 2008, Bernadskaya, Patel et al. 2011).

A previous study using a maternal-effect lethal, putative null allele of CED-10, *ced-10(t1875)*, found that in the eight-cell embryo, CED-10 is part of a Wnt pathway for spindle orientation of the ABar blastomere. The same study reported that *ced-10* mutant embryos exhibited abnormal EMS spindle positioning in the four-cell embryo (Cabello, Neukomm et al. 2010). However, this phenotype was not analyzed in detail, nor was the relationship between CED-10 and the known signaling pathways promoting EMS spindle positioning. A prior graduate student in the Rose lab, Małgorzata Liro, performed a preliminary genetic analysis that confirmed a role for CED-10 in EMS spindle positioning (Liro 2017).

In my dissertation research, I set out to define the genetic and molecular role(s) CED-10 plays in the asymmetric division of EMS. Another question that the present work aims to address

is how the initial MES-1/SRC-1 signal results in regulation of the dynein-containing force generating complex. I also contributed to analysis of the role of CED-10 and branched actin in cytokinesis and their interactions with LET-99. The results inform our understanding of both systems and highlight the importance of coordination between the microtubule cytoskeleton and the actomyosin cytoskeleton during asymmetric divisions.

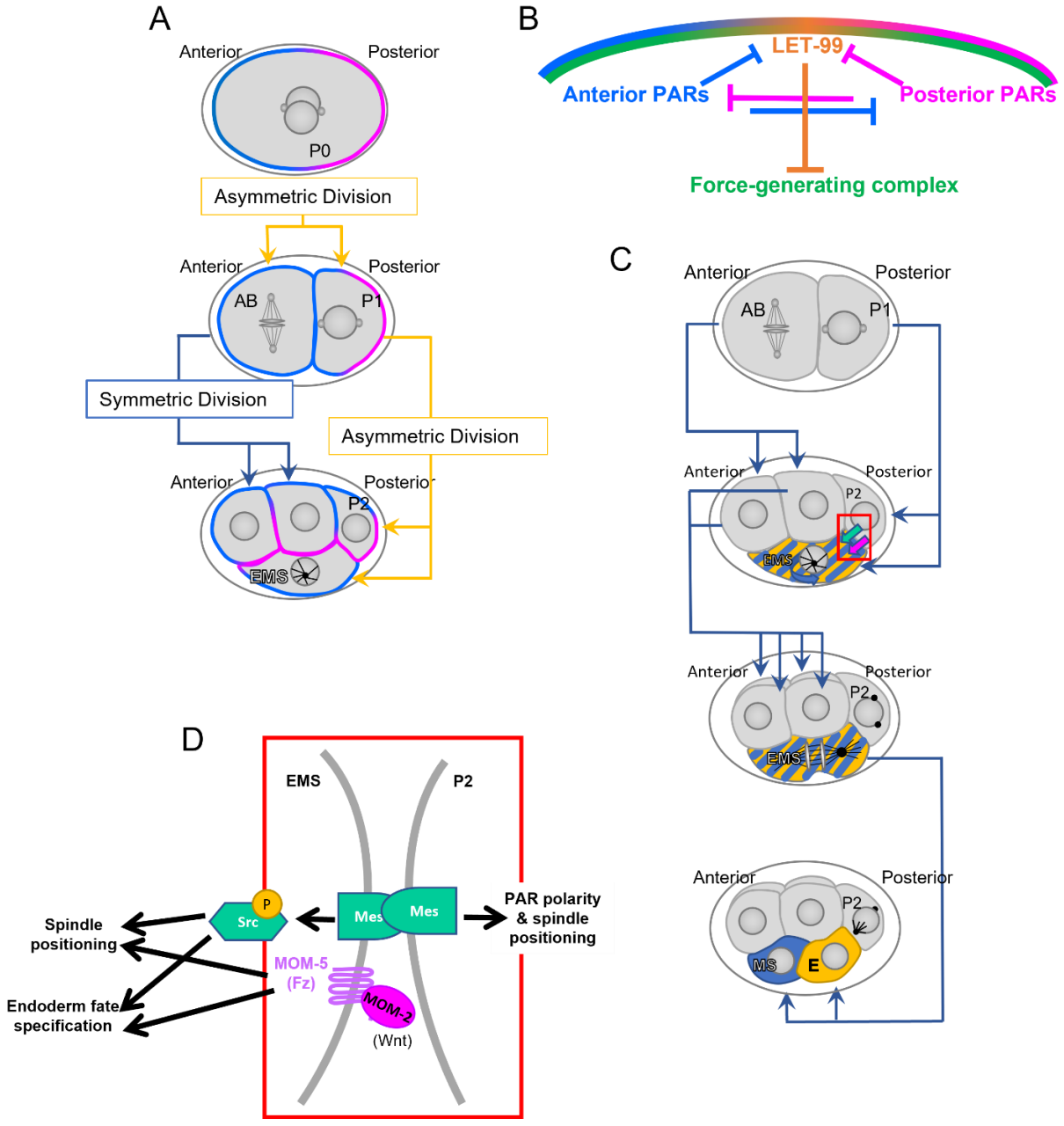

Figure 1. Asymmetric divisions of the early *C. elegans* embryo.
(A) Diagram illustrating the progression from two cells to four cells in the early *C. elegans* embryo, with an emphasis on the cortical localization of the PAR polarity proteins and the asymmetric divisions of the P lineage. Blue represents anterior PARs and pink represents posterior PARs. In all figures throughout this paper, the anterior of the embryo is presented at the left and the posterior at the right; ventral, defined by the position of the EMS cell, is on the bottom.
(B) Diagram illustrating the network of regulatory interactions among anterior PARs (blue), posterior PARs (pink), the DEPDC1 protein LET-99 (orange), and the dynein-containing force generating complex (green) at the cell cortex in the zygote, P0.
(C) Diagram illustrating the progression from two cells to seven cells in the early *C. elegans* embryo, with an emphasis on the signal-instructed mitotic spindle positioning of the EMS cell, a daughter of P1 and sister of P2. Blue represents mesoderm fate and gold represents endoderm fate. The red rectangle indicates the EMS/P2 contact, which is illustrated in more detail in (D).
(D) Diagram illustrating key features of the two signaling pathways at the EMS/P2 cell-cell contact instructing EMS asymmetric division. EMS is represented on the left, P2 on the right.

References

Arata, Y., Lee, J.-Y., Goldstein, B., & Sawa, H. (2010). Extracellular control of PAR protein localization during asymmetric cell division in the C. elegans embryo. *Development*(137), 3337-3345.

Arbeille, E., Reynaud, F., Sanyas, I., Bozon, M., Kindbeiter, K., Causeret, F., . . . Castellani, V. (2015). Cerebrospinal fluid-derived Semaphorin3B orients neuroepithelial cell divisions in the apicobasal axis. *Nature Communications, 6*, 6366. doi:https://doi.org/10.1038/ncomms7366

Bailly, C., Beignet, J., Loirand, G., & Sazeau, V. (2022). Rac1 as a therapeutic anticancer target: Promises and limitations. *Biochemical Pharmachology, 203*. doi:10.1016/j.bcp.2022.115180

Bei, Y., Hogan, J., Berkowitz, L. A., Soto, M., Rocheleau, C. E., Pang, K. M., . . . Mello, C. C. (2002). SRC-1 and Wnt signaling act together to specify endoderm and to control cleavage orientation in early C. elegans embryos. *Developmental Cell*, 113-125.

Berkowitz, L. A., & Strome, S. (2000). MES-1, a protein required for unequal divisions of the germline in early C. elegans embryos, resembles receptor tyrosine kinases and is localized to the boundary between the germline and gut cells. *Development, 127*, 4419-4431.

Bernadskaya, Y. Y., Patel, F. B., Hsu, H.-T., & Soto, S. C. (2011). Arp2/3 promotes junction formation and maintenance in the Caenorhabditis elegans intestine by regulating membrane association of apical proteins. *Molecular Biology of the Cell*, 2886-2899.

Boreaux, A., Vignal, E., Faure, S., & Fort, P. (2007). Evolution of the Rho Family of Ras-like GTPases in Eukaryotes. *Molecular Biology and Evolution, 24*(1), 203-216. doi:10.1093/molbev/msl145

Bustelo, X. R., Sazeau, V., & Berenjeno, I. M. (2007). GTP-binding proteins of the Rho/Rac family: regulation, effectors and functions in vivo. *BioEssays, 29*(4), 356-370. doi:10.1002/bies.2055

Cabello, J., Neukomm, L. J., Gunesdogan, U., Burkart, K., Charette, S. J., Lochnit, G., . . . Schnabel, R. (2010). The Wnt pathway controls cell death engulfment, spindle orientation, and migration through CED-10/Rac. *PLOS Biology*, e1000297.

Campinho, P., Behrndt, M., Ranft, J., Risler, T., Minc, N., & Heisenberg, C.-P. (2013). Tension-oriented cell divisions limit anisotropic tissue tension in epithelial spreading during zebrafish epiboly. *Nature Cell Biology, 15*(12), 1405-1414. doi:10.1038/ncb20869

Cheng, N. N., Kirby, C. M., & Kemphues, K. J. (1995). Control of cleavage spindle orientation in Caenorhabditis elegans: the role of the genes par-2 and par-3. *Genetics, 139*(2), 549-559. doi:https://doi.org/10.1093/genetics/139.2.549

D'avino, P. P., Glover, D., & Glover, D. M. (2005). Cleavage furrow formation and ingression during animal cytokinesis: a microtubule legacy. *Journal of Cell Science*, 1549-1558.

di Pietro, F., Echard, A., & Morin, X. (2016). Regulation of mitotic spindle orientation: an integrated view. *EMBO reports*, 1106-1130.

Duquette, P. M., & Lamache-Vane, N. (2014). Rho GTPases in embryonic development. *Small GTPases, 5*(2), 1-9. doi:10.4161/sgtp29716

Gillies, T. E., & Cabernard, C. (2011). Cell Division Orientation in Animals. *Current Biology, 21*, R599-R609. doi:10.1016/j.cub.2011.06.055

Hall, A. (2012). Rho family GTPases. *Biochemical Society Transactions, 40*(6), 1378-1383. doi:10.1042/BST20120103

Inaba, M., & Yamashita, Y. M. (2012). Asymmetric Stem Cell Division: Precision for Robustness. *Cell Stem Cell*(11), 461-469.

Kemphues, K. J., Priess, J. R., Morton, D. G., & Cheng, N. S. (1988). Identification of genes required for cytoplasmic localization in early C. elegans embryos. *Cell, 52*, 311-320.

Kim, S., Ishidate, T., Sharma, R., Soto, M. C., Conte, D., Mello, C. C., & Shirayama, M. (2013). Wnt and CDK-1 regulate cortical release of WRM-1/beta-catenin to control cell division orientation in early Caenorhabditis elegans embryos. *PNAS*, E918-E927.

Krueger, L. E., Wu, J. C., Tsou, M. F., & Rose, L. S. (2010). LET-99 inhibits lateral posterior pulling forces during asymmetric spindle elongation in C. elegans embryos. *Journal of Cell Biology, 189*, 481-495.

Lang, C. F., & Munro, E. (2017). The PAR proteins: from molecular circuits to dynamic self-stabilizing cell polarity. *Development, 144*, 3405-3416. doi:10.1242/dev.139063

Lin, R., Thompson, S., & Priess, J. R. (1995). pop-1 encodes an HMG box protein required for the specification of a mesoderm precursor in early C. elegans embryos. *Cell, 83*, 599-609.

Liro, M. J. (2017). *Spindle positioning and endoderm specification in response to Wnt and Src polarity cues during asymmetric division in C. elegans.* Ph.D., University of California, Davis.

Liro, M. J., & Rose, L. S. (2016). Mitotic spindle positioning in the EMS cell of C. elegans requires LET-99 and LIN-5/NuMA. *Genetics*, 1177-1189.

Liro, M. J., Morton, D., & Rose, L. S. (2018). The kinases PIG-1 and PAR-1 act in redundant pathways to regulate asymmetric division in the EMS blastomere of C. elegans. *Developmental Biology*, 9-19.

Lundquist, E. A., Reddien, P. W., Hartwieg, E., Horvitz, H., & Bargmann, C. I. (2001). Three C. elegans Rac proteins and several alternative Rac regulators control axon guidance, cell migration and apoptotic cell phagocytosis. *Development, 128*, 4475-4488.

McNally, F. J. (2013). Mechanisms of spindle positioning. *Journal of Cell Biology*, 131-140.

Morin, X., & Bellaiche, Y. (2011). Mitotic spindle orientation in asymmetric and symmetric cell divisions during animal development. *Developmental Cell*, 102-119.

Morton, D. G., Hoose, W. A., & Kemphues, K. J. (2012). A genome-wide RNAi screen for enhancers of par mutants reveals new contributors to early embryonic polarity in Caenorhabditis elegans. *Genetics, 192*, 929-942.

Nguyen, L. K., Kholodenko, B. N., & von Kriegsheim, A. (2018). Rac1 and RhoA: Networks, loops and bistability. *Small GTPases, 9*(4), 316-321. doi:10.1080/21541248.2018.1224399

Park, D. H., & Rose, L. S. (2008). Dynamic localization of LIN-5 and GPR-1/2 to cortical force generation domains during spindle positioning. *Developmental Biology*, 42-52.

Patel, F. B., Bernadskaya, Y. Y., Chen, E., Jobanputra, A., Pooladi, Z., Freeman, K. L., . . . Soto, M. C. (2008). The WAVE/SCAR complex promotes polarized cell movements and actin enrichment in epithelia during C. elegans embryogensis. *Developmental Biology, 324*, 297-309.

Pillitteri, L. J., Guo, X., & Dong, J. (2016). Asymmetric cell division in plants: mechanisms of symmetry breaking and cell fate determination. *Cell & Molecular Life Sciences, 73*(22), 4213-4229. doi:10/1007/s00018-016-2290-2

Price, K. L., H. Lamb, J. V. Alvarado and L. S. Rose (2022). "The DEPDC1 protein LET-99 is required for cortical stability and antagonizes branched actin formation to promote robust cytokinesis." *bioRxiv*.

Rocheleau, C. E., Downs, W. D., Lin, R., Wittmann, C., Bei, Y., Cha, Y. H., . . . Mello, C. C. (1997). Wnt signaling and an APC-related gene specify endoderm in early C. elegans embryos. *Cell*(90), 707-716.

Rose, L. S., & Gonczy, P. (2014). Polarity establishment, asymmetric division and segregation of fate determinants in early C. elegans embryos. *WormBook: The Online Review of C. Elegans Biology*.

Rose, L. S., & Kemphues, K. (1998). The let-99 gene is required for proper spindle orientation during cleavage of the C. elegans embryo. *Development, 125*, 1337-1346.

Schlesinger, A., Shelton, C. A., Maloof, J. N., Meneghini, M., & Bowerman, B. (1999). Wnt pathway components orient a mitotic spindle in the early Caenorhabditis elegans embryo without requiring gene transcription in the responding cell. *Genes & Development, 13*, 2028-2038.

Segalen, M., Johnston, C. A., Martin, C. A., Dumortier, J. G., Prehoda, K. E., David, N. B., . . . Bellaiche, Y. (2010). The Fz-Dsh planar cell polarity pathway induces oriented cell division via Mud/NuMA in Drosophila and zebrafish. *Developmental Cell, 19*(5), 740-752. doi:10.1016/j.devcel.2010.10.004

Srinivasan, D. G., Fisk, R. M., Xu, H., & van den Heuvel, S. (2003). A complex of LIN-5 and GPR proteins regulates G protein signaling and spindle function in C. elegans. *Genes & Development*, 1225-1239.

Sugioka, K., Mizumoto, K., & Sawa, H. (2011). Wnt regulates spindle asymmetry to generate asymmetric nuclear B-catenin in C. elegans. *Cell, 146*(6), 942-954. doi:https://doi.org/10.1016/j.cell.2011.07.043

Thorpe, C. J., Schlesinger, A., Carter, J. C., & Bowerman, B. (1997). Wnt signaling polarizes an early C. elegans blastomere to distinguish endoderm from mesoderm. *Cell*(90), 695-705.

Tsou, M.-F. B., Hayashi, A., & Rose, L. S. (2003). LET-99 opposes G-alpha/GPR signaling to generate asymmetry for spindle positioning in response to PAR and MES-1/SRC-1 signaling. *Development*, 5717-5730.

Tsou, M.-F. B., Ku, W., Hayashi, A., & Rose, L. S. (2003). PAR-dependent and geometry-dependent mechanisms of spindle positioning. *Journal of Cell Biology, 160*(6), 845-855. doi:10.1083/jcb.200209079

Tsou, M.-F. B., A. Hayashi, L. R. DeBella, G. McGrath and L. S. Rose (2002). "LET-99 determines spindle position and is asymmetrically enriched in response to PAR polarity cues in C. elegans embryos." *Development* 129(19): 4469-4481.

Venkei, Z. G., & Yamashita, Y. M. (2018). Emerging mechanisms of asymmetric stem cell division. *Journal of Cell Biology*, 3785-3795.

Walston, T., Tuskey, C., Edgar, L., Hawkins, N., Ellis, G., Bowerman, B., . . . Hardin, J. (2004). Multiple Wnt signaling pathways converge to orient the mitotic spindle in early C. elegans embryos. *Developmental Cell*, 831-841.

Zhang, H., Skop, A. R., & White, J. G. (2007). Src and Wnt signaling regulate dynactin accumulation to the P2-EMS cell border in C. elegans embryos. *Journal of Cell Science*, 155-161.

Chapter II

The DEPDC1 protein LET-99 is required for cortical stability and antagonizes branched actin formation to promote robust cytokinesis

This chapter has been submitted for publication in the Journal of Cell Science.

Kari L. Price*, Helen Lamb*, Jocelyn V. Alvarado, and Lesilee S. Rose
Department of Molecular and Cellular Biology, University of California, Davis

*co-first authors

Contributions: I co-first authored this publication with Dr. Price. I analyzed spindle positioning (centration and angle at NEB, elongation and position at anaphase) for Figures 4 and 6. I carried out statistical analyses and generated all figures. Dr. Price initiated the project and carried out the majority of the experiments with the aid of Ms. Alvarado and Dr. Rose. I co-wrote the manuscript with Dr. Price and Dr. Rose. In addition, I performed an experiment to measure the accumulation of mKate::myosin in the furrow and analyzed the resulting images; I also analyzed cortical GFP::utrophin foci in *ced-10* and *ced-10;let-99* mutants. Although these data are not included in the current manuscript, they will likely be used to address reviewers' comments.

Abstract

During cytokinesis, signals from the central spindle stimulate the accumulation of active RhoA-GTPase and thus contractile ring components at the equator, while the astral microtubules inhibit such components at the polar cortex. The DEPDC1 family protein LET-99 is required for furrow ingression in the absence of the central spindle signal, and for timely onset of furrowing even in the presence of the central spindle signal. Here we show that LET-99 works downstream or independently of RhoA-GTP and antagonizes branched F-actin and the Rac protein CED-10 to promote furrow initiation. This interaction with CED-10 is separable from LET-99's function in spindle positioning. We also characterize a new role for LET-99 in regulating cortical stability, where LET-99 acts in parallel with the actomyosin scaffolding protein anillin, but LET-99 does not antagonize CED-10 in this case. We propose that LET-99 acts in a pathway that inhibits the Rac CED-10 to promote the proper balance of branched versus linear F-actin for cytokinesis, and that LET-99 also regulates another factor that contributes to cortical stability.

Introduction

During cell division, after segregation of the duplicated chromosomes by the mitotic spindle, the mother cell is physically separated into daughter cells by the process of cytokinesis. In animal cells, cytokinesis is achieved via an actomyosin ring that pulls the cell membrane into a progressively constricting furrow. Proper timing and spatial positioning of the furrow are essential for the fidelity of chromosome segregation and the accurate partitioning of cytoplasmic components into the daughter cells (reviewed in (Green, Paluch et al. 2012, Glotzer 2017, Pollard and O'Shaughnessy 2019, Verma, Mogilner et al. 2019).

The actomyosin contractile ring assembles in an equatorial band at the cortex in response to the localized recruitment and activation of the GTPase RhoA. When RhoA is activated by binding GTP (RhoA-GTP) it directly activates the diaphanous family of formins that promote the formation of linear actin filaments (linear F-actin). RhoA-GTP also activates Rho Kinase, which stimulates nonmuscle myosin II motor activity. In the contractile ring, myosin helps align bundles of linear F-actin, and the complex of contractile myosin and actin provides the driving force for constriction (Green, Paluch et al. 2012, Chircop 2014, Glotzer 2017, Pollard and O'Shaughnessy 2019, Verma, Mogilner et al. 2019).

The localization of RhoA-GTP and its effectors to the cell equator occurs in response to signals from the anaphase mitotic spindle. The overlapping, non-kinetochore-based microtubules of the central spindle recruit the centralspindlin complex, a heterotetramer of the kinesin protein MKLP1 and the Rac GTPase MgcRacGAP. The centralspindlin complex then promotes the accumulation of RhoA-GTP. In contrast, the long, centrosomal-emanating astral microtubules that touch the polar cortex inhibit the localization of RhoA-GTP from the poles (Werner, Munro et al. 2007, Werner and Glotzer 2008, von Dassow 2009, Lewellyn, Dumont et al. 2010, Green, Paluch et al. 2012, Glotzer 2017, Mangal, Sacher et al. 2018, Pollard and O'Shaughnessy 2019, Verma, Mogilner et al. 2019).

In several systems, the additive effects of the astral and central spindle microtubules in stimulating cytokinesis can be observed at the level of the timing of cytokinesis or the extent of furrow ingression (Werner, Munro et al. 2007, von Dassow 2009, Lewellyn, Dumont et al. 2010, Green, Paluch et al. 2012, Glotzer 2017, Mangal, Sacher et al. 2018, Pollard and O'Shaughnessy 2019, Verma, Mogilner et al. 2019). For example, *C. elegans* embryos with changes in the proximity of the astral microtubules to the cortex exhibit delays in the timing of furrow initiation

but cytokinesis completes. In embryos or cells missing a central spindle or depleted of the centralspindlin protein MKLP1, substantial ingression occurs but cytokinesis ultimately fails. Simultaneous perturbation of both centralspindlin activity and the astral signal results in a dramatic reduction or complete loss of furrow formation and ingression (Dechant and Glotzer 2003, Bringmann and Hyman 2005, Werner, Munro et al. 2007, Piekny and Glotzer 2008, Werner and Glotzer 2008, Lewellyn, Dumont et al. 2010, Tse, Piekny et al. 2011, Zanin, Desai et al. 2013, Mangal, Sacher et al. 2018). Further, in *C. elegans* one-cell embryos, laser ablation of the spindle results in spatially separated astral versus central spindle induced furrows (Bringmann and Hyman 2005) and mutants with a small misplaced spindle exhibit a centralspindlin-dependent furrow adjacent to the spindle, and an astral-mediated furrow away from the asters that does not require centralspindlin activity (Werner, Munro et al. 2007).

The depletion of several proteins significantly reduces furrowing only in conjunction with loss of centralspindlin components. Anillin (ANI-1 in *C. elegans*) is a scaffolding protein that binds myosin, actin, RhoA-GTP and other components, and is required for proper myosin organization during cytokinesis. Anillin binds active RhoA and is a downstream effector. Nonetheless, in some systems including *C. elegans*, the defects in cytokinesis observed upon loss of anillin are much more severe when the cell is dependent on astral inhibition to induce furrowing (Maddox, Habermann et al. 2005, Piekny and Glotzer 2008, Werner and Glotzer 2008, Tse, Piekny et al. 2011, van Oostende Triplet, Jaramillo Garcia et al. 2014). This could reflect a greater need for anillin in large cells where the central spindle is far from cortex and/or a greater need for anillin when flow of actomyosin and RhoA-GTP away from the poles concentrates contractile ring components at the equator in response to astral inhibition (Werner and Glotzer 2008, von Dassow 2009, Reymann, Staniscia et al. 2016). On the other hand, the *C. elegans*

protein NOP-1 activates RhoA, primarily as part of the aster-directed furrowing pathway, in parallel to centralspindlin (ZEN-4/CYK-4 in *C. elegans*) activation of RhoA at the equator. While *nop-1* mutants exhibit normal cytokinesis, *zen-4; nop-1* double mutant embryos do not exhibit any furrow ingression (Tse, Werner et al. 2012, Price and Rose 2017).

Several regulators of spindle positioning during the first asymmetric division also enhance the furrow ingression defects of embryos without a central spindle or of *zen-4* mutants (Bringmann, Cowan et al. 2007, Verbrugghe and White 2007). Some of these regulators appear to affect actomyosin organization and furrowing indirectly, due to reduced spindle elongation or failure to displace the spindle posteriorly (Werner, Munro et al. 2007, Price and Rose 2017). However, the role of the LET-99 protein in cytokinesis is genetically separable from its role in asymmetric division. For example, the PAR polarity proteins restrict the localization of LET-99 to a lateral posterior band in asymmetrically dividing cells (Tsou, Hayashi et al. 2002, Wu and Rose 2007). However, the localization of LET-99 to the prospective cleavage furrow is determined by the spindle and occurs in both asymmetrically and symmetrically dividing cells, and loss of LET-99 enhances the furrow ingression defects of *zen-4* mutants in both types of cells as well (Bringmann, Cowan et al. 2007, Price and Rose 2017). Changes in the dynamics of cortical myosin have been reported for *let-99* mutants, and *let-99; zen-4* double mutants exhibit greatly reduced myosin accumulation at the furrow. In contrast, loss of *let-99* does not enhance the cytokinesis phenotype of *nop-1* mutants (Bringmann, Cowan et al. 2007, Goulding, Canman et al. 2007, Werner, Munro et al. 2007, Price and Rose 2017). However, it is not known if LET-99 affects furrowing by acting upstream of RhoA activation like NOP-1, if LET-99 functions with downstream RhoA-GTP effectors, or if rather LET-99 influences the actomyosin cytoskeleton via a separate pathway. Interestingly, the DEPDC1A and DEPDC1B family of

proteins to which LET-99 is most related have a region with homology to Rho-GTPase activating proteins, and DEPDC1B has been shown to physically and genetically interact with Rac (Sendoel, Maida et al. 2014, Yang, Liu et al. 2014, Wu, Zhu et al. 2015). These findings raise the possibility that LET-99 could genetically interact with Rac or other small G proteins during cytokinesis in *C. elegans*.

The small GTPases Cdc42 and Rac promote the formation of branched F-actin networks via the Arp2/3 nucleating complex. While depletion of Cdc42 and Rac typically do not cause failure of cytokinesis, studies in *C. elegans* and other systems has revealed that a proper balance of branched versus linear F-actin is critical for proper timing and mechanics of membrane ingression (Severson, Baillie et al. 2002, Canman, Lewellyn et al. 2008, Bastos, Penate et al. 2012, Loria, Longhini et al. 2012, Chircop 2014, Zhuravlev, Hirsch et al. 2017, Chan, Silva et al. 2019, Pal, Ellis et al. 2020). In *C. elegans*, the Rac CED-10 negatively regulates cytokinetic furrowing: Hypomorphic mutations in *ced-10* can rescue the furrowing ingression defects of centralspindlin mutants. Similar results have been observed for depletion of Arp2 (ARX-2). Recent studies also found that strong depletion of ARX-2 affects timely furrow initiation and ingression rate; this effect can be rescued by partial depletion of the formin CYK-1, which promotes linear F-actin (Canman, Lewellyn et al. 2008, Loria, Longhini et al. 2012, Zhuravlev, Hirsch et al. 2017, Chan, Silva et al. 2019, Pal, Ellis et al. 2020). The regulation of levels of branched versus linear F-actin are also critical for normal cell shape during cytokinesis and cell migration in many cell types, and ARX-2 and CED-10 have been implicated in regulating cortical stability in the early *C. elegans* embryo (Severson, Baillie et al. 2002, Bustelo, Sauzeau et al. 2007, Roh-Johnson and Goldstein 2009, Loria, Longhini et al. 2012, Chircop 2014) .

In this study, we further investigate LET-99's role in regulating the actomyosin cytoskeleton. Our results indicate that LET-99 does not act upstream of activation of RhoA to promote cytokinetic furrowing, which together with prior work indicates that LET-99 is not specific to the astral inhibition pathway for cytokinesis. Rather, we show that LET-99 promotes timely furrow formation in a mechanism that acts antagonistically to branched F-actin and the Rac CED-10. Further, we characterize a new role for LET-99 in promoting cortical stability. The cortical stability and cytokinesis defects of *let-99* embryos are enhanced by simultaneous loss of anillin. Surprisingly the cortical stability defects of *let-99* mutants are also enhanced, rather than suppressed by loss of CED-10. These results indicate that LET-99 is not in a simple linear pathway where it inhibits CED-10 to regulate both cytokinesis and cortical stability. From these and other data, we propose that LET-99 regulates the actomyosin cytoskeleton globally via two mechanisms: LET-99 inhibits branched F-actin formation and also influences other actomyosin regulators.

Results

LET-99 antagonizes branched F-actin filament formation to promote timely cytokinesis onset

The loss of LET-99 function enhances the cytokinetic furrow ingression defects of mutants missing the spindle midzone or the ZEN-4 component of the centralspindlin complex. In addition, embryos from *let-99* single mutant mothers (hereafter referred to as *let-99* embryos or mutants) were reported to have a delay in the onset of cytokinesis, even though cytokinesis completed (Bringmann, Cowan et al. 2007, Price and Rose 2017). We first confirmed that depletion of LET-99 by RNA interference (RNAi) results in a cytokinesis delay, so that this background could be used in further analyses of contractile ring components. The time from

nuclear envelope breakdown (NEB) to furrowing onset (FO, defined by the first indentation of the membrane) was measured from DIC movies (Fig.2A, A'). We found that *let-99(RNAi)* embryos exhibited a delay in cytokinesis that was similar to that produced by the *let-99(dd17)* null mutant. Because loss of LET-99 also affects spindle positioning and elongation, which can indirectly affect furrowing, embryos with spindles misoriented at late anaphase were excluded from this and all subsequent analyses of furrowing kinetics (see Methods).

To determine if LET-99 acts upstream of recruitment of activated RhoA, we examined embryos expressing GFP::AHPH, which contains the C-term half of anillin including its RhoA-GTP binding and plekstrin homology domains; this transgene has been validated as a sensor for active RhoA (Tse, Werner et al. 2012). Images were taken from a cortical view during the first cell division and enrichment in the contractile ring region was quantified (Fig. 2B, B'). No difference in the average fluorescence intensity between controls and *let-99(RNAi)* embryos was observed. The overall appearance of anillin labeled by GFP::ANI-1 (Tse, Piekny et al. 2011), and the levels in the contractile ring were also comparable in control and *let-99(RNAi)* embryos (Fig. 2B, B'). These results suggest that LET-99 is not required for activation of RhoA and recruitment of anillin to the contractile ring.

RhoA-GTP promotes the accumulation of myosin and linear F-actin at the furrow. We previously reported lower levels of myosin at the furrow in single *let-99* mutants (Price and Rose 2017). To examine F-actin localization during cytokinesis, we examined embryos expressing the GFP::Utrophin actin binding probe (GFP-Utr contains the calponin homology domain of Drosophila utrophin, which binds act (Tse, Werner et al. 2012). Total levels of F-actin at the furrow as assayed by GFP-Utr intensity were similar between control and *let-99(RNAi)* embryos (Fig. 1B, B'). However, we observed a qualitative increase in the number of small cortical foci

of GFP:: Utr in *let-99* embryos. Cortical actin foci are indicative of branched actin filaments, because they are abolished by loss of ARX-2. In contrast depletion of CYK-1 lowers the levels of linear F-actin, making it easier to visualize the ARX-2 dependent foci (Xiong, Mohler et al. 2011, Shivas and Skop 2012, Chan, Silva et al. 2019). Thus to more easily visualize foci and quantify the effect of loss of LET-99 on branched F-actin, we depleted CYK-1 by RNAi in the GFP:: Utr-CH background, with or without *let-99(dd17*) and counted the number of foci. Both *cyk-1(RNAi)* and *cyk-1(RNAi); let-99(dd17)* embryos showed reduced levels of total GFP-Utr at the furrow compared to controls, as expected for knockdown of CYK-1 (Fig. 2C, C'). However, compared to *cyk-1(RNAi)* embryos, *cyk-1(RNAi); let-99(dd17)* embryos exhibited an increase in the number of GFP:: Utr-CH foci at the cleavage furrow as well as across the entire embryo cortex (Fig. 2D, E). These results indicate that there are increased levels of branched F-actin in *let-99* mutants.

The proper balance of Arp-2/3 dependent branched F-actin versus formin dependent linear F-actin is necessary for proper actomyosin organization during contractile ring assembly and thus for proper timing of furrowing onset, as indicated by the first shallow deformation of the membrane (Chan, Silva et al. 2019). We therefore tested whether reducing branched F-actin filaments, via RNAi of ARX-2, could rescue the furrowing delay of *let-99(dd17)* mutant embryos. The time to furrowing onset in *arx-2(RNAi)* embryos was similar to controls, consistent with prior results for partial depletion of ARX-2 (Chan, Silva et al. 2019). However, *arx-2(RNAi); let-99(dd17)* embryos exhibited a time to furrowing onset that was reduced compared to *let-99(dd17)* embryos (Fig. 2F). These results are consistent with a role for *let-99* in antagonizing branched F-actin filament formation during cytokinesis.

LET-99 and CED-10/Rac have opposing roles during cytokinetic furrowing

In *C. elegans* embryos as in many systems, branched F-actin is promoted by both Rac and Cdc42 (CED-10 and CDC-42 in *C. elegans*)(Bustelo, Sauzeau et al. 2007, Chircop 2014). While neither *cdc-42* nor *ced-10* mutant embryos have overt cytokinesis phenotypes, several studies have shown that CED-10 antagonizes aspects of cytokinesis. For example, partial loss of function mutations in *ced-10* increases the extent of furrow ingression in embryos lacking centralspindlin function, as also seen for depletion of Arp2/3 (Jantsch-Plunger, Gönczy et al. 2000, Canman, Lewellyn et al. 2008, Loria, Longhini et al. 2012, Zhuravlev, Hirsch et al. 2017). The latter result is opposite to the effect of *let-99* mutations on furrow ingression in *centralspindlin* mutants (Price and Rose 2017). We therefore tested whether loss of CED-10 function could rescue the delay in onset of furrowing exhibited by *let-99(RNAi)* embryos, using a maternal effect lethal allele that is a predicted null, *ced-10(t1875)* (Kinchen, Cabello et al. 2005). In embryos from *ced-10(t1875)* mothers (hereafter referred to as *ced-10* embryos or mutants), there were no overt cytokinesis defects and the time from NEB to furrowing onset was comparable to controls (Fig. 2G), as reported previously for hypomorphic alleles or depletion of maternal CED-10 by RNAi. The mean time to furrowing onset in *let-99(RNAi) ced-10(t1875)* embryos was reduced compared to *let-99(RNAi)* embryos and was not significantly different than wild-type controls (Fig. 2G). Thus, similar to depletion of ARX-2, the loss of CED-10 restored furrow timing in *let-99(RNAi)* embryos.

Having established an antagonistic role between CED-10 and LET-99 for furrowing onset, we examined other aspects of cytokinesis. A balance of branched vs linear F-actin is also required for the timely transition from furrowing onset to the formation of a double-membraned furrow canal, also known as back-to-back membrane configuration, and for the rate of furrow

ingression (Chan, Silva et al. 2019). To measure these aspects more accurately we utilized strains expressing endogenously tagged non-muscle myosin, NMY-2::mKate2, imaged in cross-section (Rehain-Bell, Love et al. 2017)(Fig. 3A, see Methods). The time from NEB to furrowing onset in NMY-2::mKate2 control embryos was similar to that of wild-type embryos, and *let-99(dd17)* embryos showed a delay in furrowing onset, indicating that this background did not alter the cytokinesis phenotypes being scored (Fig. 3B). We found that in addition, *let-99(dd17)* embryos exhibited a longer time for the transition to back-to-back membrane formation compared to controls (Fig. 3C). The rate of furrow ingression in *let-99(dd17)* embryos was not statistically different from controls (Fig. 3D), consistent with a previous analysis of constriction of the entire furrow from an end on view (Bringmann, Cowan et al. 2007). *ced-10(t1875)* embryos did not show any significant differences from controls in any of these measurements. In the *ced-10(t1875) let-99(dd17)* double mutant embryos, the time to furrowing onset was comparable to controls, and the time for back-to-back membrane formation was also significantly reduced in *ced-10(t1875) let-99(dd17)* double mutants compared to *let-99(dd17)* embryos (Fig. 3B, C). Together these data confirm that loss of CED-10 rescues the *let-99* mutant furrowing onset delay, and also reveal an antagonistic role between CED-10 and LET-99 in the transition from furrowing onset to back-to-back membrane formation.

Loss of LET-99 also enhances the furrow ingression defects of centralspindlin deficient embryos in the AB cell; unlike the one-cell, the AB cell divides symmetrically and *let-99* mutants do not have defects in spindle elongation in this cell that could also impact cytokinesis (Price and Rose 2017). We therefore examined furrow formation in the AB cell using the NMY-2::mKate background (Fig. 3A,E). The time from NEB to back-to-back membrane formation in the AB cell was slower in *let-99(dd17)* embryos compared to controls. In *ced-10(t1875) let-*

99(dd17) double mutants, this timing was restored to control levels. These results confirm the antagonist relationship between LET-99 and CED-10 in cytokinetic furrowing and demonstrate that it is not specific to asymmetrically dividing cells.

CED-10 does not affect spindle positioning in the one-cell embryo

Prior work showed that *let-99*'s enhancement of the cytokinesis defects of centralspindlin mutants did not correlate with defects in spindle position or elongation (Bringmann, Cowan et al. 2007, Price and Rose 2017). Interestingly however, CED-10 is required for spindle orientation in certain cells of the eight-cell embryo and later in the vulval lineage (Kishore and Sundaram 2002, Cabello, Neukomm et al. 2010). These observations raised the possibility that *let-99* and *ced-10* interact during spindle positioning. We therefore characterized spindle positioning in *ced-10(t1875)* and *ced-10(t1875) let-99(RNAi)* one-cell embryos in comparison to wildtype and *let-99(RNAi*) embryos.

In wild-type one-cell embryos, the male and female pronuclei meet in the posterior and then the nuclear-centrosome complex moves to the center of the embryo (centration); the complex also rotates so that the centrosomes are aligned on the polarized AP axis prior to NEB in most embryos (Figure 4A-D, Movie 1). The spindle is displaced posteriorly during metaphase and anaphase resulting in an unequal cleavage where the anterior AB cell is larger than the posterior P1 cell (Fig. 4A,B,E and Fig. 5A)(reviewed in (Rose and Gonczy 2014)). In *let-99(RNAi)* or mutant embryos, there is a failure of centration, and variable rotation prior to NEB, which is accompanied by rocking of the nuclear centrosome complex. Nonetheless, the spindle aligns along the AP axis in most embryos prior to anaphase. Spindle elongation and displacement are both reduced but the overall spindle position is posterior and cleavage is

unequal, because of the earlier centration defect (Fig. 4A-F, Movie 2, Fig. 5A) (Rose and Kemphues 1998, Tsou, Hayashi et al. 2002, Krueger, Wu et al. 2010).

In *ced-10(t1875)* embryos, the nuclear-centrosome complex centered and the spindle oriented onto the anterior-posterior axis before NEB, as observed in controls. The spindle then displaced back towards the posterior so that the one-cell divided unequally (Fig. 4A-E, Movie 3, Fig. 5A). In addition, spindle elongation was comparable to controls. (Fig. 4F). The *ced-10(t1875) let-99(RNAi)* double mutant embryos exhibited nuclear centrosome rocking and defects in centration and nuclear rotation that were indistinguishable from those of *let-99(RNAi)* embryos (Fig. 4A-D, Movie 4). The position of the posterior spindle pole was abnormal, and spindle length was reduced in the double mutant embryos, again comparable to *let-99(RNAi)* embryos (Fig. 4E, F). Thus, the loss of CED-10 does not suppress the spindle positioning or spindle elongation defects of *let-99* mutants. Overall, these results show that first, CED-10 has no apparent role in spindle positioning during the first division, and second, that the genetic interaction between *let-99* and *ced-10* mutations is specific to cytokinesis.

LET-99 affects cortical stability

Although the normal timing of furrowing was restored in the *ced-10(t1875) let-99(RNAi)* embryos, many double mutants exhibited an ectopic furrow resulting in a wedge-like structure between the AB and P1 cells (Fig. 5A). Similar ectopic furrow structures were previously reported in *let-99* single mutants at the end of cytokinesis and were correlated with disorganization of the contractile ring as viewed end-on (Bringmann, Cowan et al. 2007), but their genesis was not determined. We therefore examined the formation of these furrows in more detail. In *let-99(RNAi)* embryos, a single cytokinetic furrow formed and ingressed, similar to controls. However, 4/10 *let-99(RNAi)* embryos exhibited a protrusion of the AB cell membrane

that extended toward the P1 cell and shifted the cell-cell contact region. We refer to this deformation as a half-wedge, because in all four of these embryos a second furrow emerged within the protrusion to produce the wedge structure (Fig. 5A, Movie 2). Although some protrusions in *let-99(RNAi)* embryos started during cytokinesis, the progression to the wedge occurred well after cytokinesis completion; the protrusions and extra furrows were also dynamic and resolved before the AB cell entered mitosis (Fig 5A, Movie 2). These observations indicate that *let-99* embryos do not initiate ectopic cytokinesis furrows at the start of cytokinesis, but rather suggest that *let-99* embryos have altered cortical activity of the AB cell.

Wild-type embryos have higher levels of cortical myosin at the anterior during cytokinesis of the one-cell and in the AB cell, and the AB cell cortex/membrane undulates during and after cytokinesis (Munro, Nance et al. 2004, Werner, Munro et al. 2007, Fujita and Onami 2012, Loria, Longhini et al. 2012, Ozugergin, Mastronardi et al. 2022). Undulations of the AB cortex in control embryos occurred both in the polar regions and near the furrow, most lasting only 10-20 sec in one location (Movie 1). All *let-99(RNAi)* exhibited these typical rapid undulations of the AB cortex, but the furrow protrusions that developed into wedge structures lasted much longer, for more than 100 sec; two of the *let-99(RNAi)* embryos exhibited an additional protrusion of 40 sec or more (Fig. 5C). Thus, to compare the protrusive activity in single and double mutants, we quantified the number of "persistent" protrusions that lasted at least 40 sec in each embryo. Persistent protrusions near the furrow were also observed during or after cytokinesis in 4/10 *ced-10(t1875)* embryos, but these were of shorter duration than *let-99* protrusions, and in only one case did a wedge form (Fig. 5A-C). In general, there were more undulations of the entire AB cell membrane in *ced-10* embryos compared to controls (Fig. 5A, Movie 3), consistent with prior observations of the anterior membrane during cytokinesis (Loria,

Longhini et al. 2012). Although the number of protrusions per embryo was similar in all mutant backgrounds, a higher proportion of *ced-10(t1875) let-99(RNAi)* double mutant embryos (9/10) exhibited persistent protrusions compared to either single mutant (Fig. 5B). In the subset of double mutant embryos which could be followed until late prophase of the AB cell, 4/5 embryos exhibited protrusions that progressed into wedges, and then ectopic furrows resolved (Fig. 4A, Movie 4). Some furrow protrusions in these embryos lasted longer compared to *let-99(RNAi)* embryos, but the overall mean persistence time was only significantly different from *ced-10* embryos (Fig. 5C). Similar results were observed in the NMY-2 background, where 92% of *ced-10(t1875) let-99(dd17)* (n= 12) exhibited a persistent wedge or half-wedge protrusion, compared to 41% of *let-99(dd17)* embryos (n = 17). Thus, this protrusion phenotype of *let-99* is enhanced rather than suppressed by simultaneous loss of *ced-10* and the data suggest that LET-99 regulates cortical stability.

We also observed a distinct type of cortical instability in *ced-10(t1875)* embryos, consisting of multiple very small bleb like structures (Movie 3). These structures were most apparent later in the two-cell stage compared to during cytokinesis, and could also be observed in the one-cell embryo at the end of the pseudocleavage stage through NEB. These small protrusions are similar to structures observed in *arx-2(RNAi)* embryos, which have been shown to be true blebs, that is, breaks in the cortical cytoskeleton through which membrane protrudes (Severson, Baillie et al. 2002, Roh-Johnson and Goldstein 2009). These small blebs were observed in *let-99(dd17) ced-10(t1875)* embryos as well. Together with the enhancement of the furrow protrusion phenotype, these results indicate that LET-99 and CED-10 are not in a simple linear pathway whereby LET-99 inhibits CED-10 to regulate both cytokinesis and cortical stability.

let-99; ani-1 double mutant embryos exhibit enhanced cortical instability

We previously showed *let-99(dd17);ani-1(RNAi);zen-4(RNAi)* embryos exhibit an even greater reduction in the extent of furrow ingression compared to *let-99(dd17);zen-4(RNAi)* or *ani-1(RNAi);zen-4(RNAi)* embryos, suggesting that LET-99 and ANI-1 act in parallel to promote cytokinetic furrowing (Price and Rose 2017). We therefore tested whether loss of ANI-1 enhances the *let-99(dd17)* mutant phenotype even in the presence of ZEN-4, by examining the time to furrowing onset from DIC time-lapse movies. On average, *ani-1(RNAi)* embryos exhibited a normal time to furrowing onset. The *let-99(dd17);ani-1(RNAi)* embryos showed a delay which was significantly longer than in *let-99(dd17)* single mutants (Fig. 6A, F). However, *let-99(dd17); ani-1(RNAi)* embryos showed similar spindle positioning defects as the *let-99(dd17)* single mutants, and spindle elongation was not more defective in the double mutants (Fig. 6B-E). These results show that LET-99 and ANI-1 act in parallel to promote timely furrowing onset, independently of effects on spindle elongation or position.

The loss of anillin has been reported to result in protrusions at the furrow in HeLa cells and cortical deformations have been observed in *C. elegans* one-cell embryos depleted of ANI-1 in combination with other cytokinesis regulators (Pacquelet, Uhart et al. 2015, Price and Rose 2017). We observed many protrusions near the furrow after cytokinesis in *ani-1(RNAi)* embryos and in *let-99(dd17);ani-1(RNAi)* embryos. In addition, we observed deformations of the cortex at anterior or posterior pole of the embryo during anaphase. We refer to these deformations as polar extrusions as they appear distinct from both furrow protrusions and the normal undulations of the AB membrane. A small number of *let-99(dd17)* single mutant embryos exhibited polar extrusions at the anterior (2/8, Fig. 6F, G; Movie 5; 0/10 *let-99(RNAi)* embryos exhibited extrusions). Several *ani-1(RNAi)* embryos (4/11) exhibited extrusions, all at the posterior pole

(Fig. 6F,G; Movie 6). The majority of *let-99(dd17); ani-1(RNAi)* double mutant embryos had polar extrusions and these could be at the anterior or pole posterior pole or both (11/12 embryos; Fig. 6F, G; Movie 7). Strikingly, some extrusions in both the *ani-1(RNAi)* and *ani-1(RNAi); let-99(dd17)* embryos "traveled", resolving at a distance from the site of initiation (Fig. 6F and Movie 7). Although the mean persistence time of the protrusions in the double mutant was not longer, the total number of extrusions per embryo was higher compared to the single mutants (Fig. 6G, H). Thus, simultaneous loss of LET-99 and ANI-1 results in enhanced instability of the cortex. Together with the analysis of *ced-10 let-99* double mutant embryos, these results identify a new role for LET-99 in regulating cortical stability. These data also provide evidence that LET-99 regulates the cortical cytoskeleton throughout the embryo, not just at the cytokinetic furrow.

Discussion

The LET-99 protein was first identified as a regulator of spindle positioning during asymmetric division in *C. elegans*. Subsequent work revealed a redundant role for LET-99 in cytokinesis of both asymmetrically and symmetrically dividing cells. Although LET-99 accumulates asymmetrically at the cortex in response to polarity cues early in the cell cycle, the spindle promotes an equatorial enrichment of LET-99 at anaphase, independent of polarity (Rose and Kemphues 1998, Tsou, Hayashi et al. 2002, Bringmann, Cowan et al. 2007, Price and Rose 2017). These and other data pointed to a role for LET-99 in regulating the actomyosin cytoskeleton during furrowing in a pathway separable from its role in spindle position. In this report, we further define the action of LET-99 during cytokinesis and identify a novel role for LET-99 in overall cortical stability.

Although *let-99* single mutants complete cytokinesis, they exhibit delays in furrowing onset, and here we identified a delay in the transition to the fully formed cleavage furrow. The

loss of LET-99 also enhances the furrow ingression defects of embryos missing the central spindle or mutant for *zen-4*. In contrast, loss of LET-99 does not enhance the phenotype of *nop-1* mutants, and loss of LET-99 affects furrow ingression of the astral-mediated furrow in experiments where the astral and central spindle signals are spatially separated (Bringmann, Cowan et al. 2007, Werner, Munro et al. 2007, Price and Rose 2017). These genetic results initially placed LET-99 in the pathway for responding to astral inhibition signals. However, our recent work showed that the enrichment of LET-99 at the equator in anaphase can respond to signals from either the astral microtubules or the central spindle (Price and Rose 2017). In the current study, we found that loss of LET-99 does not affect the contractile ring accumulation of a biosensor for active RhoA or full-length Anillin. These data together argue against models in which LET-99 is a specific component of the astral pathway that acts with NOP-1 to promote RhoA activation. Rather, LET-99 acts downstream from RhoA-GTP or in a separate pathway, and the genetic interactions reflect a greater need for LET-99 function when the actomyosin cytoskeleton is responding to astral signals, similar to the case for anillin. The effects of loss of anillin on myosin organization are distinct from those seen in LET-99 mutants (Adams, Tavares et al. 1998, Bringmann, Cowan et al. 2007, Werner, Munro et al. 2007, Tse, Piekny et al. 2011, Price and Rose 2017) and here we showed that *let-99; ani-1* double mutant embryos have enhanced defects in both cytokinesis and cortical stability. Thus, LET-99 and anillin regulate the actomyosin cytoskeleton through different mechanisms.

Our observations of increased branched F-actin foci in *let-99* embryos coupled with the rescue of *let-99's* cytokinesis delays by reduction of Arp2 or the Rac CED-10 suggest that LET-99 has an antagonistic role to the formation of branched F-actin. The increased branched F-actin in the forming furrow of *let-99* mutant embryos may interfere directly with the alignment of

linear F-actin and myosin in the contractile furrow (Canman, Lewellyn et al. 2008, Zhuravlev, Hirsch et al. 2017, Descovich, Cortes et al. 2018). LET-99 accumulates to highest levels at the equator. However, there are lower levels of LET-99 throughout the entire cortex (Tsou, Hayashi et al. 2002, Price and Rose 2017), and the changes to actin foci observed were present throughout the cortex. Thus, the excess branched F-actin present in *let-99* mutants could also delay furrowing by increasing overall cortical stiffness outside the furrow or changing the dynamics of actomyosin globally (Taneja, Bersi et al. 2020). In either case, loss of Arp2 or the Rac CED-10 in a *let-99* mutant would reduce branched F-actin, allowing for furrow formation with normal timing.

LET-99 could antagonize the formation of branched F-actin to promote furrowing through a number of different molecular mechanisms. There is cross-talk between Rho and Rac pathways in many processes, and the levels of Arp-dependent branched F-actin vs formin-dependent linear F-actin must be regulated precisely for proper cytokinesis. In several systems, depletion of Arp2/3 components or the small GTPase Rac increases the extent of furrow ingression in mutants with reduced RhoA-GTP activity caused by loss of centralspindlin. Similarly, although depletion of Arp2 doesn't cause cytokinesis failure, it changes the timing of furrowing onset, back-to-back membrane formation, and furrow ingression. These effects can be ameliorated by simultaneous reduction of formin. Likewise defects caused by partial depletion of formin can be rescued by reduction of Arp2 (Canman, Lewellyn et al. 2008, Bastos, Penate et al. 2012, Loria, Longhini et al. 2012, Chircop 2014, Lawson and Burridge 2014, Glotzer 2017, Zhuravlev, Hirsch et al. 2017, Chan, Silva et al. 2019, Pollard and O'Shaughnessy 2019, Pal, Ellis et al. 2020). A number of mechanisms, which are not mutually exclusive, have been implicated in this balancing act between branched and linear F-actin during cytokinesis in *C.*

elegans. These include opposite effects of Rho and Rac on cortical rigidity, direct inhibition of Rac at the furrow by the centralsplindlin component MgcRacGAP (CYK-4), and global inhibition of the formin CYK-1 by Arp2/3 (Loria, Longhini et al. 2012, Zhuravlev, Hirsch et al. 2017, Chan, Silva et al. 2019). LET-99 could be a new player in one of these pathways.

A mechanism in which LET-99 binds to Rac to directly inhibit its function is appealing because LET-99 is a member of the DEPDC1A and B family of proteins (Sendoel, Maida et al. 2014). This protein family contains an N-terminal DEP domain and a region with homology to Rho-GAP proteins near the C-terminus. Although the Rho-GAP motif is missing the catalytic residue for GAP activity in all family members, the domain could potentially bind small G proteins. Several studies have shown a genetic interaction between DEPDC1B and Rac or RhoA; one report showed that DEPDC1B binds Rac in vitro, and overexpression of DEPDC1B inhibited Rac activity and F-actin polymerization in Hela cells (Marchesi, Montani et al. 2014, Su, Liang et al. 2014, Yang, Liu et al. 2014, Wu, Zhu et al. 2015). We have been unable to detect a consistent interaction between LET-99 and CED-10/Rac in vitro using recombinant proteins (unpublished results). This could reflect an in vivo requirement for other proteins to facilitate a LET-99 - Rac interaction. Alternatively, LET-99 could act indirectly via one of the pathways outlined above. Indeed, any model for LET-99 regulation of the actomyosin cytoskeleton must also take into account the observation that while loss of CED-10 suppressed the cytokinetic furrowing of *let-99* embryos, the double mutant embryos had enhanced cortical protrusive activity. Thus, we propose that LET-99 ultimately affects at least one other actomyosin cytoskeletal regulator or component in addition to branched F-actin. Precedence for this idea comes from known cross talk pathways for Rho and Rac. For example, Rho-kinase promotes

myosin contractility but also activates negative regulators of Rac (Chircop 2014, Lawson and Burridge 2014).

LET-99 has been well-characterized as a key intermediate that acts downstream of PAR polarity cues to regulate spindle positioning in asymmetrically dividing cells. In that pathway, LET-99 acts to promote asymmetric pulling forces on the spindle, by inhibiting cortical localization of the Gα-dependent complex that recruits dynein (Park and Rose 2008, Rose and Gonczy 2014). Although the position of the astral microtubules is critical for myosin organization and flow in the astral mediated pathway for furrowing, prior work showed that LET-99's requirement in furrowing does not correlate with spindle positioning or elongation defects (Bringmann, Cowan et al. 2007, Price and Rose 2017). Our current findings provide further evidence that LET-99 influences the actomyosin cytoskeleton in a mechanism independent of that used for spindle positioning. In particular, although CED-10 plays a role in spindle positioning in other cells (Kishore and Sundaram 2002, Cabello, Neukomm et al. 2010), we found no role for CED-10 in the first division, and the *ced-10* null mutation neither enhanced or suppressed the spindle positioning defects of *let-99* mutant embryos. Similarly, the genetic enhancement between loss of LET-99 and ANI-1 is specific for cytokinesis and cortical instability. Thus, LET-99 appears to be a multifunctional protein that can act with either heterotrimeric or small G proteins in distinct mechanisms. Elucidating the molecular details of LET-99's interactions will lead to a better understanding of the regulation of spindle positioning and the actomyosin cytoskeleton and should also give insight into the DEPDC1 family of proteins.

Materials and Methods

C. elegans strains

C. elegans strains were maintained on MYOB plates with *E. coli* OP50 as a food source (Brenner, 1974; Church et al., 1995). The following strains were used in this study.

Strain #	*Genotype*
N2	*Wild type, Bristol strain*
AZ244	*unc-119(ed3) III; ruls57[pie-1::GFP::b-tubulin + unc-119(+)] V?*
GE4047	*ced-10(t1875)/ nTI[qIs50(pha::GFP) let- ?]*
FM126	*ltIs37[pie-1p::mCherry::his-58 + unc-119(+)] him-8(e1489) IV; ruls57[pie-1::GFP::b-tubulin + unc-119(+)] V?*
LP229	*nmy-2(cp52[nmy-2::mKate2 + LoxP unc-119(+) LoxP]) I; unc-119(ed3) III*
MG542	*ltIs28 [pASM14; pie-1::GFP-TEV-STag::ani-1; unc-119 (+)]; ltIs37[pie-1p::mCherry::his-58; unc-119 (+)].*
MG589	*mgSi3[gfp::utrophin + Cbr-unc-119(+)]II; unc-119(ed3)III*
MG617	*mgSi5[gfp::ani-1(ahph) + Cbr-unc-119(+)].*
RL175	*unc-22(e66) let-99(dd17) / nT1[unc-? (n754d) let-?].*
RL231	*unc-22(e66) let-99(dd17) / nT1[qIs51(pha::GFP) let-?] IV*
RL356	*ced-10(t1875) dpy-20(e1282) unc-22(e66) let-99(dd17) / nT1 [qIs51(pha::GFP)] V*
RL263	*ced-10(t1875)/nT1; qIs50[pha::GFP]; (ruIs57 [GFP::tubulin; unc-119(+)]*
RL359	*ced-10(t1875) dpy-20(e1282) /nT1 [qIs51(pha::GFP)]*
RL361	*mgSi3[cb-unc-119(+) GFP::Utrophin] II; ltIs37[pie-1p::mCherry::his-58 + unc-119(+)] him-8(e1489) IV*
RL369	*nmy-2(cp52[nmy-2::mkate2 + LoxP unc-119(+) LoxP]) I; unc-119(ed3) III; ced-10(t1875) dpy-20(e1282) IV /nT1 [qIs51(pha::GFP)] V*
RL408	*nmy-2(cp52[nmy-2::mKate2]) I; let-99(dd17) unc-22(e66)/ nT1 [qIs51(pha::GFP)] IV*
RL409	*nmy-2(cp52[nmy-2::mKate2]) I; let-99(dd17) unc-22(e66) ced-10(t1875) dpy-20/ nT1 [qIs51(pha::GFP)] V*

RNAi

RNAi was performed by feeding (Timmons, Court et al. 2001). Constructs used to induce RNAi were obtained from the Ahringer RNAi library (Kamath, Fraser et al. 2003)and include *ani-1 (III-6E18), let-99 (IV-6P07), cyk-1(III-8B02), arx-2(V-7M13).* The extent of RNAi penetrance was determined from examining embryos for published strong loss of function phenotypes as follows: 1) *ani-1:* lack of pseudocleavage (Maddox, Habermann et al. 2005), 2) *let-99:* severe nuclear-centrosome rocking, failure of centration in the one-cell, and failure of P1 nuclear rotation (Tsou, Hayashi et al. 2002), 3) *cyk-1:* weak pseudocleavage and reduced F-actin in the cleavage furrow (Swan, Severson et al. 1998, Ding, Ong et al. 2017) and 4) *arx-2:* increased number of anterior, cortical blebs (Severson, Baillie et al. 2002). In cases where a double mutant background might suppress one mutant phenotype, the RNAi strength was also assessed by examining control embryos treated in parallel.

Microscopy

Worms were dissected in egg buffer (25 mM HEPES, pH 7.4, 120 mM NaCl, 48 mM KCl, 2 mM $CaCl_2$, $MgCl_2$) and embryos were mounted on 2% agarose pads in the same buffer and imaged. For the analyses of furrowing onset, spindle positioning, cortical stability in Figures 1 and 3-5, embryos were examined in differential interference contrast (DIC) using an Olympus BX60 compound microscope, using a PlanApo N 60x, 1.42 numerical aperture oil-immersion objective. Single plane time-lapse images were acquired every 5 or 10 seconds using a Hamamatsu Orca 12-bit digital camera and Micromanager software (Edelstein, Amodaj et al. 2001). For analysis of cytokinesis in embryos expressing NMY-2::mKate-2 in Figure 2, embryos were mounted as above and imaged with the same system; images were taken every 5

sec in bright field through NEB, then in widefield fluorescence from metaphase through cytokinesis completion. Room temperature during imaging was 23-25°C.

To image GFP::AHPH, GFP::ANI-1 and GFP::Utr from a cortical view, embryos were mounted as above and imaged using the spinning disk module of a Marianas SDC Real-Time 3D Confocal-TIRF microscope (Intelligent Imaging Innovations, 3i) fit with a Yokogawa spinning disk head, a 63x 1.3 numerical aperture oil-immersion objective, and EMCCD camera. Acquisition was controlled by Slidebook 6 software (3i Incorporated). Single focal planes images were acquired first in midfocal plan to score NEB and anaphase onset timing; the focal plane was then moved to a cortical view during anaphase, and images were obtained every 3 sec at 100ms exposure. Room temperature during imaging was 24-25°C. Raw images were exposed and scaled with the same parameters for each experiment, and all images were processed using Fiji software (Schindelin, Arganda-Carreras et al. 2012).

Analysis of cytokinetic furrowing

Cytokinetic furrowing rate measurements for both the P_0 cell and the AB cell were taken relative to nuclear envelope breakdown (NEB). For all analyses, NEB was scored under DIC or brightfield conditions, NEB was scored as the first frame in which the pronuclei or nucleus began to shrink in size. The time of furrowing onset was scored as the frame in which the first cortical indentation (aka shallow deformation) that proceeded to furrow formation was observated. Membrane ingression in the one-cell C. *elegans* embryos is asymmetric: although furrowing onset occurs fairly uniformly around the circumference, one furrow (the leading furrow) transitions to the back-to-back membrane (BB) configuration faster and ingresses farther; the other furrow forms with more variable timing (Maddox, Lewellyn et al. 2007). Thus measurements of back-to-back membrane and furrow ingression are only reported for the leading

furrow and could only be scored accurately in fluorescence in the NMY-2::mKate2 background. BB formation was scored as the first frame where the membranes changed from a "V" configuration to back-to-back membranes where a furrow tip was visible. To measure ingression rate, the Manual Tracking plugin in Fiji software (Schindelin, Arganda-Carreras et al. 2012) was used to track the movement of the furrow tip until cytokinesis completion. The tracked distance during the first 50 seconds after BB was divided by time to give an average velocity. For this and all analyses, a sample of at least n = 10 embryos was obtained for each genotype. However, in some cases embryos were excluded so the final n for each genotype varies. In particular, because misoriented spindles at late anaphase could affect signaling from the spindle to the cortex and impact cytokinesis separately from LET-99's function in furrowing, only embryos in which the spindle was aligned on the anterior-posterior axis by mid-anaphase were quantified for cytokinesis assays. In addition, we observed that a small number of *let-99(dd17)* embryos appeared to have a much slower cell cycle overall, where the time for all stages was approximately 1.5x that of other *let-99* embryos and controls, and the spindle at NEB plus 160s was clearly still in metaphase instead of anaphase. We thus used failure to progress into anaphase in a timely fashion as a criterion to exclude such embryos from all single and double mutant analyses using *let-99(dd17).* This slow phenotype was not observed after RNAi of *let-99*. Furrowing measurements were assembled in excel and then imported into Prism for statistical analysis and graphing.

Analysis of cortical contractile ring components

To measure enrichment of contractile ring components for Fig.1B, B', mean pixel intensity values corresponding to a 20 pixel x 60 pixel region of interest placed over the forming furrow were obtained and normalized to the signal on the posterior side of the contractile ring.

For measurements of GFP::ANI-1, measurements were made at ~90 sec after anaphase onset, as determined by monitoring mCherry: H2B labeling of the DNA in cross section. The GFP::AHPH and GFP::Utrophin strains did not have a DNA marker; for these, measurements were made within 20-50 sec after furrowing onset, which is similar in timing to 90 sec after anaphase onset. To determine the number of GFP::Utrophin foci at the cortex in *cyk-1* backgrounds (Fig.1 C, C'), images were first thresholded in ImageJ using the Shanbhag image thresholding plugin with a minimum value of two pixels required to define a focus. Foci were then counted using the Particle Analysis tool in Fiji (Schindelin et al., 2012) either over the entire cortex or in a 20 x 60 pixel ROI over the furrow region. Data were compiled in Microsoft Excel and then exported into Prism for statistical analysis.

Analysis of spindle positioning and elongation

Parameters of nuclear and spindle positioning were measured in Image J (https://imagej.nih.gov/ij/) using the line and angle tools, as shown in Fig. 3 and the corresponding text. Centration and rotation were measured at NEB. The position of the posterior spindle pole and spindle length were measured at NEB plus 160 sec, when anaphase spindles have elongated in controls embryos, but furrowing has not initiated. Measurements were compiled in Microsoft Excel and then exported into Prism for statistical analysis.

Analysis of cortical stability

Protrusions were measured manually by scoring the first frame where a deformation of the cortex was observed (start) and the first frame where the protrusion had completely disappeared (resolution). The total time was calculated as (resolution frame – start frame) x frame rate. In controls, undulations of the entire cortex and protrusions near the furrow typically lasted only 10 or 20 sec, but an occasional deformation lasted 30 sec. Therefore, only protrusions

lasting 40 sec or longer were scored as persistent. In all *let-99* embryos that were imaged through the second division, furrow protrusions began during one-cell cytokinesis or within 90 sec of furrowing completion, and all protrusions resolved before the AB cell underwent NEB. For scoring other genotypes, movies that lasted at least 400sec after NEB were used to score the the number of protrusions that initiated. For quantifying mean persistence time, only protrusions that resolved before the movie ended were used. The persistence of polar extrusions were measured in a similar manner. Data were assembled in excel and then imported into Prism for statistical analysis and graphing.

Acknowledgements

We thank members of the Rose and McNally labs for helpful discussions. We are grateful to Michael Glotzer, Bob Goldstein, Amy Maddox and Frank McNally for provided strains. We also thank the *Caenorhabditis* Genetics Center, which is funded by the National Institutes of Health Office of Research Infrastructure Programs (P40 OD010440) for strains. The 3i Marianas spinning disk confocal used in this study was purchased using a National Institutes of Health Shared Instrumentation Grant [1S10RR024543-01]. We thank the MCB Light Microscopy Imaging Facility, which is a UC-Davis Campus Core Research Facility, for the use of this microscope. We are grateful to Kathie Urrutia-Paniagua for media preparation. This work was funded by the National Institutes of Health Grant [R01GM68744] and the National Institute of Food and Agriculture [CA-D*-MCB-6239-H]. Student support was also provided by the Floyd and Mary Schwall Dissertation Year Fellowship [KLP], the UC Davis BMCDB Graduate Group [KLP, HL] and a National Institutes of Health training grant [T32 GM 007377].

References

Adams, R.R., Tavares, A.A.M., Salzberg, A., Bellen, H.J., Glover, D.M., 1998. pavarotti encodes a kinesin-like protein required to organize the central spindle and contractile ring for cytokinesis. Genes & Development 12, 1483-1494.

Bastos, R.N., Penate, X., Bates, M., Hammond, D., Barr, F.A., 2012. CYK4 inhibits Rac1-dependent PAK1 and ARHGEF7 effector pathways during cytokinesis. The Journal of Cell Biology 198, 865.

Bringmann, H., Cowan, C.R., Kong, J., Hyman, A.A., 2007. LET-99, GOA-1/GPA-16, and GPR-1/2 Are Required for Aster-Positioned Cytokinesis. Current Biology 17, 185-191.

Bringmann, H., Hyman, A.A., 2005. A cytokinesis furrow is positioned by two consecutive signals. Nature 436, 731-734.

Bustelo, X.R., Sauzeau, V., Berenjeno, I.M., 2007. GTP-binding proteins of the Rho/Rac family: regulation, effectors and functions in vivo. Bioessays 29, 356-370.

Cabello, J., Neukomm, L.J., Gunesdogan, U., Burkart, K., Charette, S.J., Lochnit, G., Hengartner, M.O., Schnabel, R., 2010. The Wnt pathway controls cell death engulfment, spindle orientation, and migration through CED-10/Rac. PLoS Biol 8, e1000297.

Canman, J.C., Lewellyn, L., Laband, K., Smerdon, S.J., Desai, A., Bowerman, B., Oegema, K., 2008. Inhibition of Rac by the GAP Activity of Centralspindlin Is Essential for Cytokinesis. Science 322, 1543-1546.

Chan, F.Y., Silva, A.M., Saramago, J., Pereira-Sousa, J., Brighton, H.E., Pereira, M., Oegema, K., Gassmann, R., Carvalho, A.X., 2019. The ARP2/3 complex prevents excessive formin activity during cytokinesis. Mol Biol Cell 30, 96-107.

Chircop, M., 2014. Rho GTPases as regulators of mitosis and cytokinesis in mammalian cells. Small GTPases 5.

Dechant, R., Glotzer, M., 2003. Centrosome Separation and Central Spindle Assembly Act in Redundant Pathways that Regulate Microtubule Density and Trigger Cleavage Furrow Formation. Developmental Cell 4, 333-344.

Descovich, C.P., Cortes, D.B., Ryan, S., Nash, J., Zhang, L., Maddox, P.S., Nedelec, F., Maddox, A.S., 2018. Cross-linkers both drive and brake cytoskeletal remodeling and furrowing in cytokinesis. Mol Biol Cell 29, 622-631.

Ding, W.Y., Ong, H.T., Hara, Y., Wongsantichon, J., Toyama, Y., Robinson, R.C., Nédélec, F., Zaidel-Bar, R., 2017. Plastin increases cortical connectivity to facilitate robust polarization and timely cytokinesis. The Journal of Cell Biology 216, 1371.

Edelstein, A., Amodaj, N., Hoover, K., Vale, R., Stuurman, N., 2001. Computer Control of Microscopes Using μManager, Current Protocols in Molecular Biology. John Wiley & Sons, Inc.

Fujita, M., Onami, S., 2012. Cell-to-cell heterogeneity in cortical tension specifies curvature of contact surfaces in Caenorhabditis elegans embryos. PLoS One 7, e30224.

Glotzer, M., 2017. Cytokinesis in Metazoa and Fungi. Cold Spring Harb Perspect Biol 9.

Goulding, M.B., Canman, J.C., Senning, E.N., Marcus, A.H., Bowerman, B., 2007. Control of nuclear centration in the C. elegans zygote by receptor-independent Gα signaling and myosin II. The Journal of Cell Biology 178, 1177-1191.

Green, R.A., Paluch, E., Oegema, K., 2012. Cytokinesis in Animal Cells. Annual Review of Cell and Developmental Biology 28, 29-58.

Jantsch-Plunger, V., Gönczy, P., Romano, A., Schnabel, H., Hamill, D., Schnabel, R., Hyman, A.A., Glotzer, M., 2000. Cyk-4: A Rho Family Gtpase Activating Protein (Gap) Required for Central Spindle Formation and Cytokinesis. The Journal of Cell Biology 149, 1391-1404.
Kamath, R.S., Fraser, A.G., Dong, Y., Poulin, G., Durbin, R., Gotta, M., Kanapin, A., Le Bot, N., Moreno, S., Sohrmann, M., Welchman, D.P., Zipperlen, P., Ahringer, J., 2003. Systematic functional analysis of the Caenorhabditis elegans genome using RNAi. Nature 421, 231-237.
Kinchen, J.M., Cabello, J., Klingele, D., Wong, K., Feichtinger, R., Schnabel, H., Schnabel, R., Hengartner, M.O., 2005. Two pathways converge at CED-10 to mediate actin rearrangement and corpse removal in C. elegans. Nature 434, 93-99.
Kishore, R.S., Sundaram, M.V., 2002. ced-10 Rac and mig-2 function redundantly and act with unc-73 trio to control the orientation of vulval cell divisions and migrations in Caenorhabditis elegans. Dev Biol 241, 339-348.
Krueger, L.E., Wu, J.-C., Tsou, M.-F.B., Rose, L.S., 2010. LET-99 inhibits lateral posterior pulling forces during asymmetric spindle elongation in C. elegans embryos. The Journal of Cell Biology 189, 481-495.
Lawson, C.D., Burridge, K., 2014. The on-off relationship of Rho and Rac during integrin-mediated adhesion and cell migration. Small GTPases 5, e27958.
Lewellyn, L., Dumont, J., Desai, A., Oegema, K., 2010. Analyzing the Effects of Delaying Aster Separation on Furrow Formation during Cytokinesis in the Caenorhabditis elegans Embryo. Molecular Biology of the Cell 21, 50-62.
Loria, A., Longhini, Katrina M., Glotzer, M., 2012. The RhoGAP Domain of CYK-4 Has an Essential Role in RhoA Activation. Current Biology 22, 213-219.
Maddox, A.S., Habermann, B., Desai, A., Oegema, K., 2005. Distinct roles for two C. elegans anillins in the gonad and early embryo. Development 132, 2837-2848.
Maddox, A.S., Lewellyn, L., Desai, A., Oegema, K., 2007. Anillin and the septins promote asymmetric ingression of the cytokinetic furrow. Dev Cell 12, 827-835.
Mangal, S., Sacher, J., Kim, T., Osório, D.S., Motegi, F., Carvalho, A.X., Oegema, K., Zanin, E., 2018. TPXL-1 activates Aurora A to clear contractile ring components from the polar cortex during cytokinesis. The Journal of Cell Biology 217, 837-848.
Marchesi, S., Montani, F., Deflorian, G., D'Antuono, R., Cuomo, A., Bologna, S., Mazzoccoli, C., Bonaldi, T., Di Fiore, P.P., Nicassio, F., 2014. DEPDC1B coordinates de-adhesion events and cell-cycle progression at mitosis. Dev Cell 31, 420-433.
Munro, E., Nance, J., Priess, J.R., 2004. Cortical Flows Powered by Asymmetrical Contraction Transport PAR Proteins to Establish and Maintain Anterior-Posterior Polarity in the Early C. elegans Embryo. Developmental Cell 7, 413-424.
Ozugergin, I., Mastronardi, K., Law, C., Piekny, A., 2022. Diverse mechanisms regulate contractile ring assembly for cytokinesis in the two-cell Caenorhabditis elegans embryo. J Cell Sci 135.
Pacquelet, A., Uhart, P., Tassan, J.-P., Michaux, G., 2015. PAR-4 and anillin regulate myosin to coordinate spindle and furrow position during asymmetric division. The Journal of Cell Biology 210, 1085-1099.
Pal, D., Ellis, A., Sepulveda-Ramirez, S.P., Salgado, T., Terrazas, I., Reyes, G., De La Rosa, R., Henson, J.H., Shuster, C.B., 2020. Rac and Arp2/3-Nucleated Actin Networks Antagonize Rho During Mitotic and Meiotic Cleavages. Front Cell Dev Biol 8, 591141.
Park, D.H., Rose, L.S., 2008. Dynamic localization of LIN-5 and GPR-1/2 to cortical force generation domains during spindle positioning. Developmental Biology 315, 42-54.

Piekny, A.J., Glotzer, M., 2008. Anillin Is a Scaffold Protein That Links RhoA, Actin, and Myosin during Cytokinesis. Current Biology 18, 30-36.
Pollard, T.D., O'Shaughnessy, B., 2019. Molecular Mechanism of Cytokinesis. Annu Rev Biochem 88, 661-689.
Price, K.L., Rose, L.S., 2017. LET-99 functions in the astral furrowing pathway, where it is required for myosin enrichment in the contractile ring. Mol Biol Cell 28, 2360-2373.
Rehain-Bell, K., Love, A., Werner, M.E., MacLeod, I., Yates, J.R., 3rd, Maddox, A.S., 2017. A Sterile 20 Family Kinase and Its Co-factor CCM-3 Regulate Contractile Ring Proteins on Germline Intercellular Bridges. Curr Biol 27, 860-867.
Reymann, A.-C., Staniscia, F., Erzberger, A., Salbreux, G., Grill, S.W., 2016. Cortical flow aligns actin filaments to form a furrow. eLife 5, e17807.
Roh-Johnson, M., Goldstein, B., 2009. In vivo roles for Arp2/3 in cortical actin organization during C. elegans gastrulation. J Cell Sci 122, 3983-3993.
Rose, L., Gonczy, P., 2014. Polarity establishment, asymmetric division and segregation of fate determinants in early C. elegans embryos. WormBook, 1-43.
Rose, L.S., Kemphues, K., 1998. The let-99 gene is required for proper spindle orientation during cleavage of the C. elegans embryo. Development 125, 1337-1346.
Schindelin, J., Arganda-Carreras, I., Frise, E., Kaynig, V., Longair, M., Pietzsch, T., Preibisch, S., Rueden, C., Saalfeld, S., Schmid, B., Tinevez, J.-Y., White, D.J., Hartenstein, V., Eliceiri, K., Tomancak, P., Cardona, A., 2012. Fiji - an Open Source platform for biological image analysis. Nature methods 9, 10.1038/nmeth.2019.
Sendoel, A., Maida, S., Zheng, X., Teo, Y., Stergiou, L., Rossi, C.A., Subasic, D., Pinto, S.M., Kinchen, J.M., Shi, M., Boettcher, S., Meyer, J.N., Manz, M.G., Bano, D., Hengartner, M.O., 2014. DEPDC1/LET-99 participates in an evolutionarily conserved pathway for anti-tubulin drug-induced apoptosis. Nat Cell Biol 16, 812-820.
Severson, A.F., Baillie, D.L., Bowerman, B., 2002. A Formin Homology protein and a profilin are required for cytokinesis and Arp2/3-independent assembly of cortical microfilaments in C. elegans. Curr Biol 12, 2066-2075.
Shivas, J.M., Skop, A.R., 2012. Arp2/3 mediates early endosome dynamics necessary for the maintenance of PAR asymmetry in Caenorhabditis elegans. Molecular Biology of the Cell 23, 1917-1927.
Su, Y.F., Liang, C.Y., Huang, C.Y., Peng, C.Y., Chen, C.C., Lin, M.C., Lin, R.K., Lin, W.W., Chou, M.Y., Liao, P.H., Yang, J.J., 2014. A putative novel protein, DEPDC1B, is overexpressed in oral cancer patients, and enhanced anchorage-independent growth in oral cancer cells that is mediated by Rac1 and ERK. J Biomed Sci 21, 67.
Swan, K.A., Severson, A.F., Carter, J.C., Martin, P.R., Schnabel, H., Schnabel, R., Bowerman, B., 1998. cyk-1: a C. elegans FH gene required for a late step in embryonic cytokinesis. J Cell Sci 111 (Pt 14), 2017-2027.
Taneja, N., Bersi, M.R., Baillargeon, S.M., Fenix, A.M., Cooper, J.A., Ohi, R., Gama, V., Merryman, W.D., Burnette, D.T., 2020. Precise Tuning of Cortical Contractility Regulates Cell Shape during Cytokinesis. Cell Rep 31, 107477.
Timmons, L., Court, D.L., Fire, A., 2001. Ingestion of bacterially expressed dsRNAs can produce specific and potent genetic interference in Caenorhabditis elegans. Gene 263, 103-112.
Tse, Y.C., Piekny, A., Glotzer, M., 2011. Anillin promotes astral microtubule-directed cortical myosin polarization. Molecular Biology of the Cell 22, 3165-3175.

Tse, Y.C., Werner, M., Longhini, K.M., Labbe, J.-C., Goldstein, B., Glotzer, M., 2012. RhoA activation during polarization and cytokinesis of the early Caenorhabditis elegans embryo is differentially dependent on NOP-1 and CYK-4. Molecular Biology of the Cell 23, 4020-4031.
Tsou, M.-F.B., Hayashi, A., DeBella, L.R., McGrath, G., Rose, L.S., 2002. LET-99 determines spindle position and is asymmetrically enriched in response to PAR polarity cues in C. elegans embryos. Development 129, 4469-4481.
van Oostende Triplet, C., Jaramillo Garcia, M., Haji Bik, H., Beaudet, D., Piekny, A., 2014. Anillin interacts with microtubules and is part of the astral pathway that defines cortical domains. Journal of Cell Science 127, 3699.
Verbrugghe, K.J., White, J.G., 2007. Cortical centralspindlin and G alpha have parallel roles in furrow initiation in early C. elegans embryos. J Cell Sci 120, 1772-1778.
Verma, V., Mogilner, A., Maresca, T.J., 2019. Classical and Emerging Regulatory Mechanisms of Cytokinesis in Animal Cells. Biology (Basel) 8.
von Dassow, G., 2009. Concurrent cues for cytokinetic furrow induction in animal cells. Trends in Cell Biology 19, 165-173.
Werner, M., Glotzer, M., 2008. Control of cortical contractility during cytokinesis. Biochemical Society Transactions 36, 371-377.
Werner, M., Munro, E., Glotzer, M., 2007. Astral Signals Spatially Bias Cortical Myosin Recruitment to Break Symmetry and Promote Cytokinesis. Current Biology 17, 1286-1297.
Wu, D., Zhu, X., Jimenez-Cowell, K., Mold, A.J., Sollecito, C.C., Lombana, N., Jiao, M., Wei, Q., 2015. Identification of the GTPase-activating protein DEP domain containing 1B (DEPDC1B) as a transcriptional target of Pitx2. Exp Cell Res 333, 80-92.
Wu, J.-C., Rose, L.S., 2007. PAR-3 and PAR-1 Inhibit LET-99 Localization to Generate a Cortical Band Important for Spindle Positioning in Caenorhabditis elegans Embryos. Molecular Biology of the Cell 18, 4470-4482.
Xiong, H., Mohler, W.A., Soto, M.C., 2011. The branched actin nucleator Arp2/3 promotes nuclear migrations and cell polarity in the C. elegans zygote. Developmental Biology 357, 356-369.
Yang, Y., Liu, L., Cai, J., Wu, J., Guan, H., Zhu, X., Yuan, J., Li, M., 2014. DEPDC1B enhances migration and invasion of non-small cell lung cancer cells via activating Wnt/beta-catenin signaling. Biochem Biophys Res Commun 450, 899-905.
Zanin, E., Desai, A., Poser, I., Toyoda, Y., Andree, C., Moebius, C., Bickle, M., Conradt, B., Piekny, A., Oegema, K., 2013. A conserved RhoGAP limits M phase contractility and coordinates with microtubule asters to confine RhoA during cytokinesis. Dev Cell 26, 496-510.
Zhuravlev, Y., Hirsch, S.M., Jordan, S.N., Dumont, J., Shirasu-Hiza, M., Canman, J.C., 2017. CYK-4 regulates Rac, but not Rho, during cytokinesis. Molecular Biology of the Cell.

Figures and Figure Legends

Figure 1

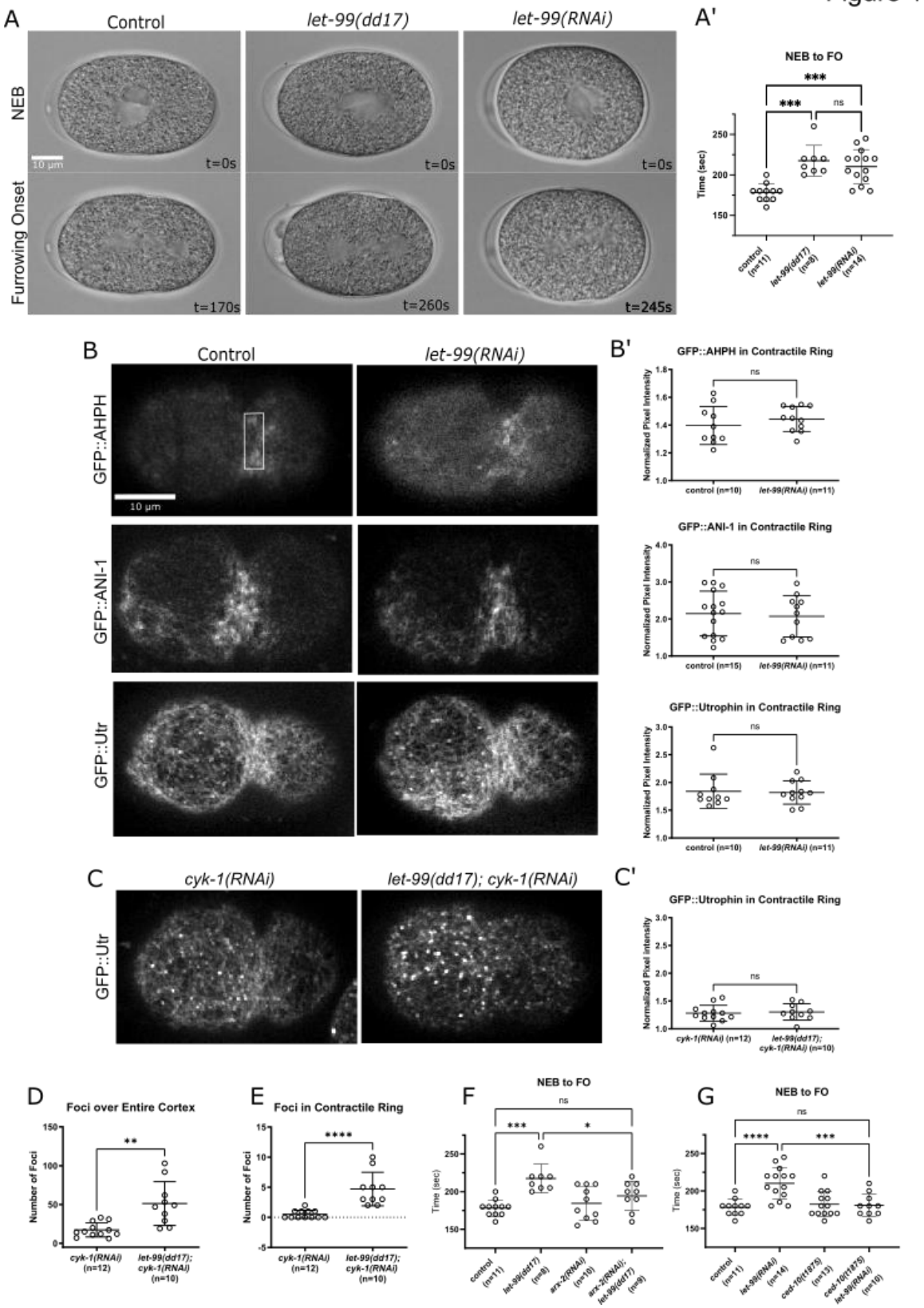

Figure 2. LET-99 antagonizes branched actin.

(A) Images from DIC time-lapse microscopy illustrating nuclear envelope breakdown (NEB) and furrowing onset (FO) for the listed genotypes during the first cell division. Scale bar is 10 microns. Time is shown relative to NEB. Anterior is to the left in this and all figures. (A') Quantification of time from NEB to FO. (B, C) Cortical images of representative embryos expressing components of the contractile ring as labeled. All images are scaled to the same pixel intensity values. Box in top left panel show the ROI of 20 x 60 pixels used to determine the average pixel intensity at the contractile ring for all quantifications shown in B' and C', where the normalized pixel intensity = value box on contractile ring/value of box on posterior cortex. (D, E) The number of foci were quantified either for the entire cortex or in an ROI of 20 x 60 pixels placed over the contractile ring. (F, G) Quantification of time from NEB to FO in the listed genotypes. Control was the wild-type N2 strain; control and dd17 data in A' and F are the same. In all, error bars represent ± SD. Statistical significance was determined using Anova with multiple comparisons via the Sidak method for graphs in panels A' and D-G. Unpaired student ttests were used for B' and C'. ns = not significant ($p > 0.05$). See Supplementary Table S1 for specific P values.

Figure 2

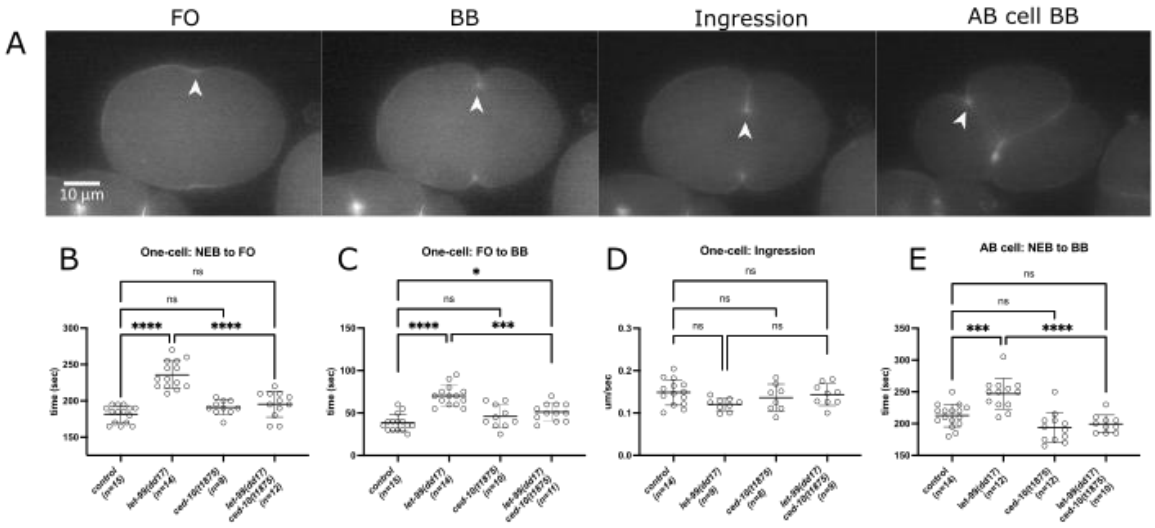

Figure 3. ***let-99*** **embryos exhibit a delay in the transition from furrowing onset to back-to-back membrane formation that is rescued by loss of CED-10.**

(A) Images from fluorescent time-lapse microscopy of a representative NMY-2::GFP control embryo during the first two divisions. Scale bar is 10 microns. Time is shown relative to NEB and stages measured are shown: furrowing onset (FO), back-to-back membrane formation (BB) and furrow ingression (at BB plus 50 sec); white arrowhead identifies the leading furrow used for measurements (see Methods). (B-E) Quantification of times for stages as labeled in the one-cell embryo and in the AB cell of two-cell embryos. Error bars represent ± SD. Statistical significance was determined using Anova with multiple comparisons via the Sidak method. ns = not significant ($p > 0.05$). See Supplementary Table S2 for specific P values.

Figure 3

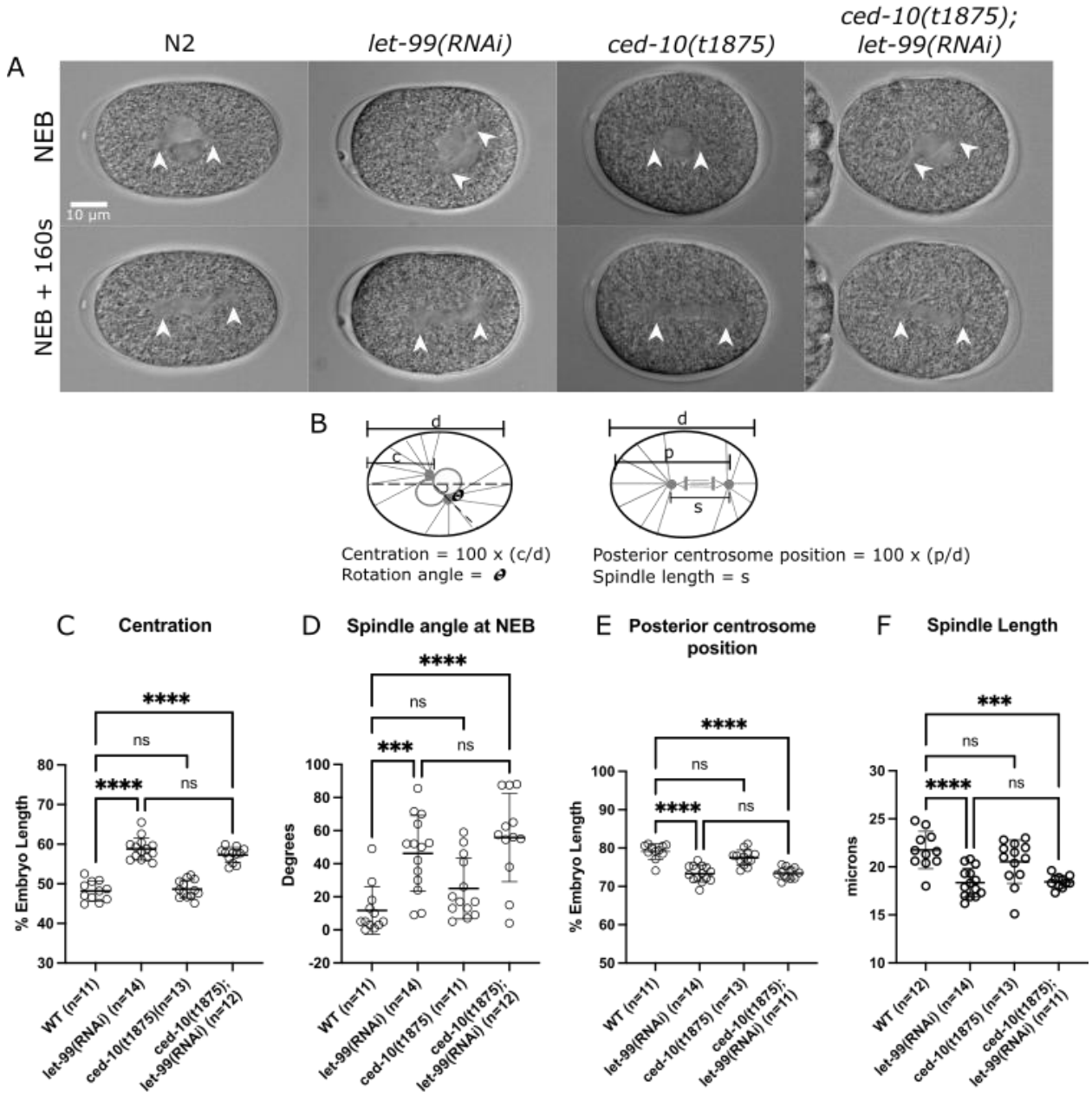
A
N2
let-99(RNAi)
ced-10(t1875)
ced-10(t1875); let-99(RNAi)
NEB
NEB + 160s
10 µm
B
d
c
θ
Centration = 100 x (c/d)
Rotation angle = θ
d
p
s
Posterior centrosome position = 100 x (p/d)
Spindle length = s
C Centration
% Embryo Length
D Spindle angle at NEB
Degrees
E Posterior centrosome position
% Embryo Length
F Spindle Length
microns
WT (n=11)
let-99(RNAi) (n=14)
ced-10(t1875)(n=13)
ced-10(t1875); let-99(RNAi) (n=12)
WT (n=12)
let-99(RNAi) (n=11)

Figure 4. Loss of CED-10 does not affect one-cell spindle positioning.

(A) Images from DIC microscopy of representative embryos with the listed genotypes at stages labeled. White arrowheads indicate the centrosomes. Anterior is to the left. Scale bar is 10 microns. (B) Schematic diagrams of measurements. Centration was determined by expressing the midpoint of the nuclear/centrosomal complex at NEB as a percentage of embryo length where anterior = 0% and posterior 100%. Rotation was measured as the angle between a line drawn along the anterior/posterior axis and a line connecting the centrosomes at NEB. As a readout for overall spindle placement, the position of the posterior centrosome as a percentage of % embryo length was measured at 160 sec after NEB. The length of the spindle was determined at 160 sec after NEB. Error bars represent ± SD. (C-F) Quantification of spindle positioning and elongation. Statistical significance was determined using Anova with multiple comparisons via the Sidak method. ns = not significant ($p > 0.05$). See Supplementary Table S3 for specific P values.

Figure 4

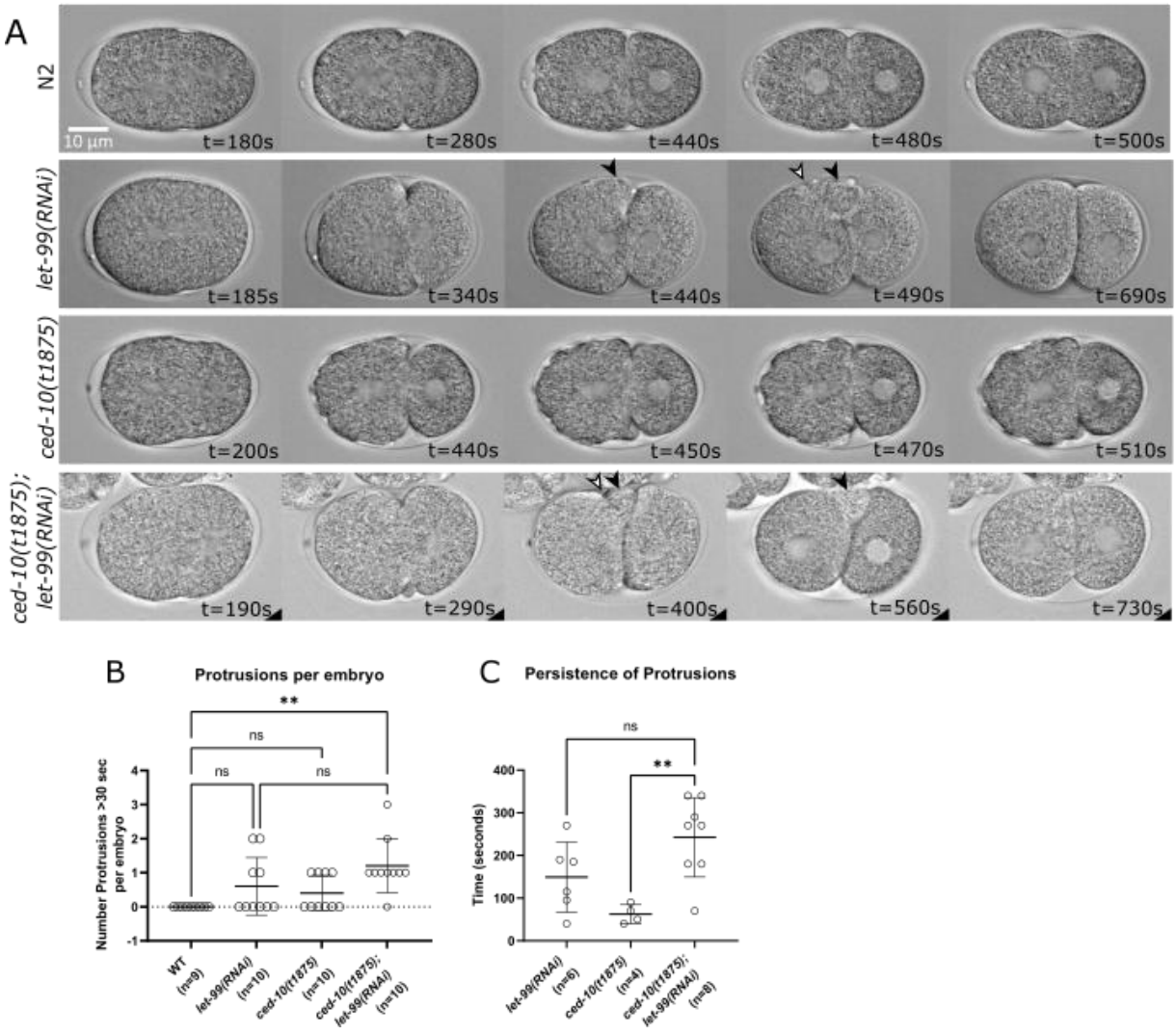

Figure 5. LET-99 and CED-10 enhance each other's cortical instability phenotypes late in cytokinesis.

(A) Stills from time-lapse DIC movies of the listed genotypes. Scale bar is 10 microns, anterior is the left. Black arrowheads mark persistent protrusions near the cytokinesis furrow; white arrowheads mark ectopic furrows that form in the protrusion. Time is shown relative to NEB = 0 seconds. Frames were chosen to illustrate the relative timing of different types of cortical activity described in the text, starting at furrowing onset or one frame after. (B) Quantification of the number of protrusions per embryo that lasted 40 sec or more. (C) Quantification of the persistence time of protrusions. Error bars represent ± SD. Statistical significance was determined using Anova with multiple comparisons via the Sidak method. ns = not significant ($p > 0.05$). See Supplementary Table S4 for specific P values.

Figure 5

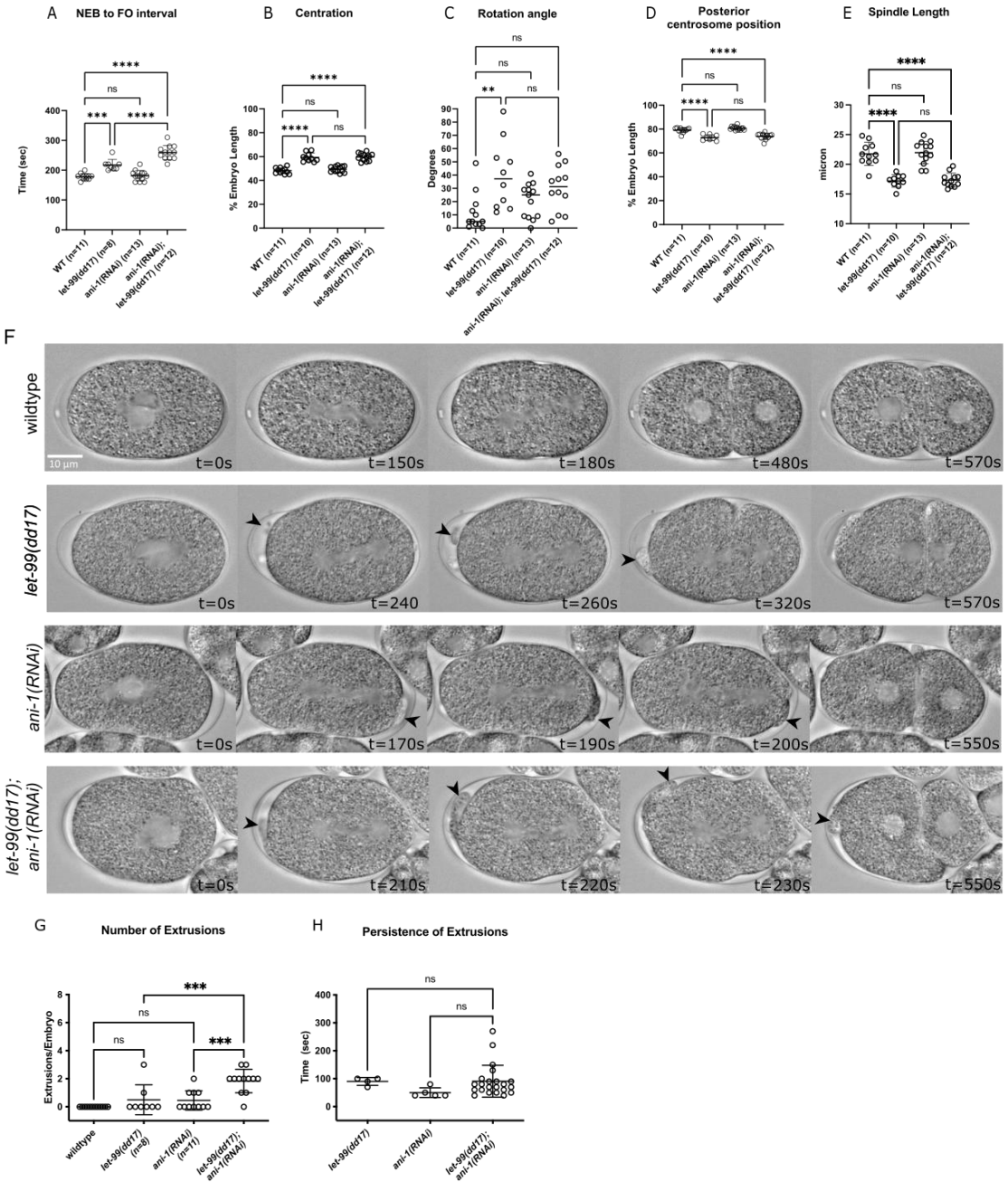
A
NEB to FO interval
Time (sec)
B
Centration
% Embryo Length
C
Rotation angle
Degrees
D
Posterior centrosome position
% Embryo Length
E
Spindle Length
micron
WT (n=11)
let-99(dd17) (n=10)
ani-1(RNAi) (n=13)
ani-1(RNAi); let-99(dd17) (n=12)
F
wildtype
let-99(dd17)
ani-1(RNAi)
let-99(dd17); ani-1(RNAi)
10 µm
t=0s
t=150s
t=180s
t=480s
t=570s
t=240
t=260s
t=320s
t=170s
t=190s
t=200s
t=550s
t=210s
t=220s
t=230s
G
Number of Extrusions
Extrusions/Embryo
wildtype
let-99(dd17) (n=8)
ani-1(RNAi) (n=11)
let-99(dd17); ani-1(RNAi)
H
Persistence of Extrusions
Time (sec)
let-99(dd17)
ani-1(RNAi)
let-99(dd17); ani-1(RNAi)

Figure 6. LET-99 and ANI-1 act in parallel to promote timely onset of furrow ingression and cortical stability.

(A) Quantification of the time to furrowing onset. (B-E) Quantification of centration, rotation, posterior spindle pole position and spindle length measured as in Fig. 4. (F) Images from time-lapse DIC movies of the listed genotypes. Anterior is to the left and times (t) are relative to NEB = 0. Arrowheads mark extrusions. Scale bar, 10 µm. (G) Quantification of the number of extrusions lasting 40 sec or more, per embryo. (H) Quantification of the persistence time of extrusions. Control and dd17 embryos are the same as in Fig. 1. Error bars represent ± SD. Statistical significance was determined using Anova with multiple comparisons via the Sidak method. ns = not significant ($p > 0.05$). See Supplementary Table S5 for specific P values.

Supplemental Files

Fig. 1A' NEB – Furrowing Onset interval (seconds)					
Condition	**Mean**	**SD**	**n**	**ANOVA, Šídák ***	
				comparison	**p-value**
control	178.2	10.8	11	N/A	N/A
let-99(dd17)	217.5	18.9	8	vs WT	0.0001
let-99(RNAi)	210.4	21.0	14	vs WT	0.0003
				vs let-99(dd17)	0.6376

Fig. 1B' Contractile ring (normalized pixel intensity)					
Condition	**Mean**	**SD**	**n**	**Unpaired t test with Welch's**	
				comparison	**p-value**
GFP::AHPH control	1.40	0.14	10	N/A	N/A
GFP::AHPH let-	1.44	0.09	11	vs control	0.3708
GFP::ANI-1 control	2.15	0.61	15	N/A	N/A
GFP::ANI-1 let-	2.07	0.56	11	vs control	0.7407
GFP::Utr control	1.84	0.31	10	N/A	N/A
GFP::Utr let-	1.82	0.21	11	vs control	0.8551

Fig. 1C' GFP::Utrophin in contractile ring (normalized pixel intensity)					
Condition	**Mean**	**SD**	**n**	**Unpaired t test with Welch's**	
				comparison	**p-value**
cyk-1(RNAi)	1.28	0.14	12	N/A	N/A
let-99(dd17);cyk-	1.30	0.15	10	vs cyk-1(RNAi)	0.7403

Fig. 1D Foci over entire cortex (number)					
Condition	**Mean**	**SD**	**n**	**Unpaired t test with Welch's**	
				comparison	**p-value**
cyk-1(RNAi)	17.3	9.2	12	N/A	N/A
let-99(dd17);cyk-1(RNAi)	51.2	28.2	10	vs cyk-1(RNAi)	0.0041

Fig. 1E Foci in contractile ring (number)					
Condition	**Mean**	**SD**	**n**	**Unpaired t test with Welch's**	
				comparison	**p-value**
cyk-1(RNAi)	0.5	0.6	12	N/A	N/A
let-99(dd17);cyk-1(RNAi)	4.7	2.8	10	vs cyk-1(RNAi)	<0.0001

Fig. 1F, G NEB – Furrowing Onset interval (seconds)					
Condition	**Mean**	**SD**	**n**	**ANOVA, Šídák ***	
				comparison	**p-value**
control	178.2	10.8	11	N/A	N/A
let-99(dd17)	217.5	18.9	8	vs WT	0.0002
arx-2(RNAi)	184.5	22.0	10	vs WT	0.8931
let-99(dd17);arx-2(RNAi)	194.4	19.4	9	vs WT	0.1952
				vs let-99(dd17)	0.0499
let-99(RNAi)	210.4	21.0	14	vs WT	<0.0001

ced-10(t1875)	182.3	16.9	13	vs WT	0.9596
ced-10(t1875);let-99(RNAi)	181.0	15.2	10	vs ced-10(t1875)	0.9922
					0.0005

***** Ordinary one-way ANOVA followed by Šídák's multiple comparisons test

Table S2. Statistics corresponding to data presented in Fig. 2

Fig. 2B NEB – Furrowing Onset interval (seconds)					
Condition	**Mean**	**SD**	**n**	**Ordinary one-way ANOVA followed by Šídák's multiple comparisons test**	
				comparison	**p-value**
control	181.7	11.6	15	N/A	N/A
let-99(dd17)	235.7	19.0	14	vs WT	<0.0001
ced-10(t1875)	191.0	9.9	10	vs WT	0.4547
ced-10(t1875);let-99(dd17)	195.4	17.7	12	vs WT	0.0938
				vs let-99(dd17)	<0.0001
Fig. 2C Furrowing – Back-to-Back interval (seconds)					
Condition	**Mean**	**SD**	**n**	**Ordinary one-way ANOVA followed by Šídák's multiple comparisons test**	
				comparison	**p-value**
control	38.3	9.9	15	N/A	N/A
let-99(dd17)	70.4	12.0	14	vs WT	<0.0001
ced-10(t1875)	46.0	13.7	10	vs WT	0.3613
ced-10(t1875);let-99(dd17)	51.3	10.3	12	vs WT	0.0209
				vs let-99(dd17)	0.0004
Fig. 2D Ingression rate (microns/second)					
Condition	**Mean**	**SD**	**n**	**Ordinary one-way ANOVA followed by Šídák's multiple comparisons test**	
				comparison	**p-value**
control	0.149	0.030	14	N/A	N/A
let-99(dd17)	0.121	0.015	9	vs WT	0.0753
ced-10(t1875)	0.136	0.032	8	vs WT	0.7608
ced-10(t1875);let-99(dd17)	0.144	0.026	9	vs WT	0.9863
				vs let-99(dd17)	0.2777
Fig. 2E AB cell NEB – Back-to-Back interval (seconds) in mKate2::NMY-2 background					
Condition	**Mean**	**SD**	**n**	**Ordinary one-way ANOVA followed by Šídák's multiple comparisons test**	
				comparison	**p-value**
control	212.8	17.9	14	N/A	N/A
let-99(dd17)	246.9	24.3	12	vs WT	0.0002
ced-10(t1875)	193.8	23.8	12	vs WT	0.0740
ced-10(t1875);let-99(dd17)	199.5	14.0	10	vs WT	0.3860
				vs let-99(dd17)	<0.0001

Table S3. Statistics corresponding to data presented in Fig. 3

Fig. 3C Centration at NEB (% Embryo Length)					
Condition	**Mean**	**SD**	**n**	**Ordinary one-way ANOVA followed by Šídák's multiple comparisons test**	
				comparison	**p-value**
WT	48.2	2.5	11	N/A	N/A
let-99(RNAi)	58.8	2.8	14	vs WT	<0.0001
ced-10(t1875)	48.7	2.2	13	vs WT	0.9805
ced-10(t1875);let-99(RNAi)	57.3	1.8	12	vs WT	<0.0001
				vs let-99(RNAi)	0.3869
Fig. 3D Spindle angle at NEB (degrees)					
Condition	**Mean**	**SD**	**n**	**Ordinary one-way ANOVA followed by Šídák's multiple comparisons test**	
				comparison	**p-value**
WT	11.8	14.4	11	N/A	N/A
let-99(RNAi)	46.3	22.8	14	vs WT	0.0005
ced-10(t1875)	25.1	18.4	11	vs WT	0.4045
ced-10(t1875);let-99(RNAi)	55.9	26.7	12	vs WT	<0.0001
				vs let-99(RNAi)	0.6904
Fig. 3E Posterior centrosome position at NEB + 160s (% Embryo Length)					
Condition	**Mean**	**SD**	**n**	**Ordinary one-way ANOVA followed by Šídák's multiple comparisons test**	
				comparison	**p-value**
WT	79.1	2.0	11	N/A	N/A
let-99(RNAi)	73.3	2.1	14	vs WT	<0.0001
ced-10(t1875)	77.5	2.0	13	vs WT	0.1828
ced-10(t1875);let-99(RNAi)	73.5	1.5	11	vs WT	<0.0001
				vs let-99(RNAi)	0.9994
Fig. 3F Spindle length at NEB + 160s (microns)					
Condition	**Mean**	**SD**	**n**	**Ordinary one-way ANOVA followed by Šídák's multiple comparisons test**	
				comparison	**p-value**
WT	21.8	1.9	11	N/A	N/A
let-99(RNAi)	18.4	1.5	14	vs WT	<0.0001
ced-10(t1875)	20.6	2.3	13	vs WT	0.3200
ced-10(t1875);let-99(RNAi)	18.5	0.6	11	vs WT	0.0002
				vs let-99(RNAi)	>0.9999

Table S4. Statistics corresponding to data presented in Fig. 4

Fig. 4B Protrusions per embryo (number)					
Condition	**Mean**	**SD**	**n**	**Ordinary one-way ANOVA followed by Šídák's multiple comparisons test**	
				comparison	**p-value**
WT	0	0	9	N/A	N/A
let-99(RNAi)	0.6	0.8	10	vs WT	0.1834
ced-10(t1875)	0.4	0.5	10	vs WT	0.5553
ced-10(t1875);let-99(RNAi)	1.2	0.8	10	vs WT	0.0010
				vs let-99(RNAi)	0.1640
Fig. 4C Persistence of protrusions (seconds)					
Condition	**Mean**	**SD**	**n**	**Ordinary one-way ANOVA followed by Šídák's multiple comparisons test**	
				comparison	**p-value**
let-99(RNAi)	149.2	81.9	6	N/A	N/A
ced-10(t1875)	62.5	22.2	4	N/A	N/A
ced-10(t1875);let-99(RNAi)	242.5	92.9	8	vs ced-10(t1875)	0.0044
				vs let-99(RNAi)	0.0913

Table S5. Statistics corresponding to data presented in Fig. 5

Fig. 5A Furrowing onset (seconds after NEB)					
Condition	**Mean**	**SD**	**n**	**ANOVA, Šídák ***	
				comparison	**p-value**
WT	178.2	10.8	11	N/A	N/A
let-99(dd17)	217.5	18.9	8	vs WT	0.0002
ani-1(RNAi)	181.5	17.2	13	vs WT	0.9864
let-99(dd17);ani-1(RNAi)	259.2	23.9	12	vs WT	<0.0001
				vs let-99(dd17)	<0.0001
Fig. 5B Centration at NEB (% Embryo Length)					
Condition	**Mean**	**SD**	**n**	**ANOVA, Šídák ***	
				comparison	**p-value**
WT	48.2	2.5	11	N/A	N/A
let-99(dd17)	59.3	3.6	10	vs WT	<0.0001
ani-1(RNAi)	49.4	2.5	13	vs WT	0.8138
let-99(dd17);ani-1(RNAi)	59.6	3.3	12	vs WT	<0.0001
				vs let-99(dd17)	0.9988
Fig. 5C Spindle angle at NEB (degrees)					
Condition	**Mean**	**SD**	**n**	**ANOVA, Šídák ***	
				comparison	**p-value**
WT	11.8	14.4	11	N/A	N/A
let-99(dd17)	40.0	25.7	10	vs WT	0.0021
ani-1(RNAi)	20.8	13.0	13	vs WT	0.6022
let-99(dd17);ani-1(RNAi)	30.5	16.8	12	vs WT	0.0500
				vs let-99(dd17)	0.6164
Fig. 5D Posterior centrosome position at NEB + 160s (% Embryo Length)					
Condition	**Mean**	**SD**	**n**	**ANOVA, Šídák ***	
				comparison	**p-value**

WT	79.1	2.0	11	N/A	N/A
let-99(dd17)	72.9	2.4	10	vs WT	<0.0001
ani-1(RNAi)	80.7	1.6	13	vs WT	0.2588
let-99(dd17);ani-1(RNAi)	73.9	2.6	12	vs WT	<0.0001
				vs let-99(dd17)	0.7624

Fig. 5E. Spindle length at NEB + 160s (microns)

Condition	Mean	SD	n	ANOVA, Šídák * comparison	p-value
WT	21.8	1.9	11	N/A	N/A
let-99(dd17)	17.2	1.1	10	vs WT	<0.0001
ani-1(RNAi)	22.0	1.9	13	vs WT	0.9962
let-99(dd17);ani-1(RNAi)	17.3	1.2	12	vs WT	<0.0001
				vs let-99(dd17)	0.9994

Fig. 5G. Extrusions per embryo (number)

Condition	Mean	SD	n	ANOVA, Šídák * comparison	p-value
WT	0	0	12	N/A	N/A
let-99(dd17)	0.5	1.1	8	vs WT	0.4476
ani-1(RNAi)	0.5	0.7	11	vs WT	0.4534
let-99(dd17);ani-1(RNAi)	1.8	0.9	12	vs ani-1(RNAi)	0.0002
				vs let-99(dd17)	0.0010

Fig. 5H. Persistence of extrusions (seconds)

Condition	Mean	SD	n	ANOVA, Šídák * comparison	p-value
let-99(dd17)	90.0	14.1	4	N/A	N/A
ani-1(RNAi)	50.0	17.3	5	N/A	N/A
let-99(dd17);ani-1(RNAi)	90.9	57.1	24	vs ani-1(RNAi)	0.2092
				vs let-99(dd17)	0.9993

***** Ordinary one-way ANOVA followed by Šídák's multiple comparisons test

Supplemental Movies

All movies are oriented with anterior to the left. Original movies were taken at either 1 frame per 5 secs or 1 frame per 10 sec as indicated, but playback speed has been adjusted so that all play at same speed; timestamp is relative to NEB=0.

Movie 1_N2_control (10-second frame interval).

Movie corresponds to embryo used for the control in Figs 1,3-5.

Movie 2_let-99(RNAi) (5-second frame interval).

Movie corresponds to embryo used for Fig. 4; embryo has time to furrowing onset in the control range, but exhibits persistent protrusions near the furrow.

Movie 3_ced-10(t1875) (10-second frame interval).

Movie corresponds to embryo used for Fig. 4; embryo exhibits excess cortical activity of the AB cell; small bleb structures are also visible early in the one-cell stage and again later at the two-cell.

Movie 4_ ced-10(t1875) let-99(RNAi) (10-second frame interval).
Movie corresponds to embryo used for Fig. 4; embryo has time to furrowing onset in the control range, but exhibits persistent protrusions near the furrow after the first division. Small bleb structures are also visible before NEB of the one-cell stage.

Movie 5_let-99(dd17) (10-second frame interval).
Movie corresponds to embryo used for Fig. 5; embryo has delayed furrow onset and exhibits polar protrusions at the anterior membrane and one persistent protrusion near the furrow.

Movie 6 _ani-1(RNAi) (10-second frame interval). Movie corresponds to embryo used for Fig. 5; embryo exhibits a posterior polar extrusion during anaphase and protrusions near the furrow after division.

Movie 7_ ani-1(RNAi); let-99(dd17) (10-second frame interval).
Movie corresponds to embryo used for Fig. 5; embryo exhibits an anterior polar extrusion during anaphase that travels from the bottom around the pole before resolving, and a second anterior extrusion that travels from the top around the pole. Embryo also exhibits a persistent furrow protrusion.

Chapter III

The Rac1 homolog CED-10 is a component of the MES-1/SRC-1 pathway for mitotic spindle positioning in the *C. elegans* EMS blastomere

Helen Lamb, Małgorzata Liro, Krista Myles, Holly Anderson, and Lesilee S. Rose

Department of Molecular and Cellular Biology, University of California, Davis

Contributions: Dr. Liro collected and scored some of the EMS spindle rotation data presented in Figure 3. Dr. Rose performed the experiment testing for presence of gut granules (Figure 5) and analyzed the resulting data. Ms. Myles acquired and analyzed the GFP::LIN-5 and GFP::CED-10 data presented in Figures 8 and S2, respectively. Under my supervision, Ms. Anderson generated the *ced-10(t1875)*;GFP::CED-10 strain used in Figures 6 and S4 and acquired and analyzed the EMS spindle rotations presented in Figure S4. I performed all other experiments and analyses and wrote the manuscript with editorial feedback from Dr. Rose.

Abstract

Asymmetric cell division is essential for the creation of cell types with different identities and functions. This study centers on the asymmetric division of the endoderm/mesoderm progenitor EMS at the four-cell stage of the *Caenorhabditis elegans* embryo. In response to two partially redundant signals from its neighbor P2, the spindle of EMS rotates onto the anterior-posterior axis of the embryo. These two signals are a Wnt/Frizzled pathway and a pathway defined by the receptor MES-1 and the kinase SRC-1. Dynein and several adaptor proteins, which together exert microtubule pulling forces in other contexts, contribute to EMS spindle orientation downstream of both pathways. Endoderm fate is specified in one resulting daughter cell by continued Wnt/Frizzled and MES-1/SRC-1 signaling from P2. A previous study identified a role for the Rac1 homolog CED-10 in EMS spindle rotation. Our genetic analyses place CED-10 in the MES-1/SRC-1, downstream of MES-1 and upstream or at the level of SRC-1. We provide evidence that CED-10 may promote EMS spindle rotation through regulation of branched actin. Finally, we show that CED-10 contributes to cortical localization of a key dynein adaptor, NuMA (LIN-5).

Introduction

Asymmetric cell division is the process by which dividing cells give rise to daughter cells with different identities and fates. This type of division occurs in all multicellular organisms and is necessary for cell type diversification during both embryonic development and adult tissue homeostasis (Inaba and Yamashita 2012), (Venkei and Yamashita 2018). A key aspect of asymmetric division is alignment of the mitotic spindle along a specific axis (D'avino, Glover et al. 2005), (Morin and Bellaiche 2011), (McNally 2013). In many metazoan cell divisions

requiring an oriented spindle, the microtubule pulling forces necessary to move the spindle are generated by the asymmetric localization of a conserved cortical complex. This complex contains the minus-end directed motor dynein, its partner dynactin, and the adaptor protein NuMA/Mud (LIN-5 in worms). The complex can be recruited to the cortex by various adaptor and anchor proteins (Morin and Bellaiche 2011), (McNally 2013), (di Pietro, Echard et al. 2016). Multiple possible sources exist for the cue that instructs spindle orientation (di Pietro, Echard et al. 2016). One mechanism that is central to many types of metazoan asymmetric divisions is the establishment of molecular asymmetry at the cortex by PAR proteins, which are highly evolutionarily conserved (Lang and Munro 2017), (Gillies and Cabernard 2011).

The early *Caenorhabditis elegans* embryo serves as an excellent model for studying the molecular mechanisms of asymmetric division: it follows an invariant division pattern that includes multiple asymmetric divisions. After fertilization, the zygote (or P0 cell) establishes molecular asymmetries that define anterior and posterior embryonic poles. Following pronuclear meeting, the newly formed mitotic spindle rotates to align with the anterior/posterior axis and thus division creates an anterior somatic cell, AB, and a posterior germ cell precursor, P1. The AB daughter divides symmetrically to give rise to ABa and ABp at the anterior and dorsal aspects of the embryo, respectively. The P1 cell divides asymmetrically to give rise to the EMS and P2 cells at the ventral and posterior aspects of the embryo, respectively (Rose and Gonczy 2014), (Griffin 2015), which both divide asymmetrically again.

The asymmetric division of the P0 cell is instructed by PAR polarity. In these cells, PAR proteins antagonize one another's cortical localization to form mutually exclusive "anterior" and "posterior" domains (Rose and Gonczy 2014), (Lang and Munro 2017). In response to the formation of the PAR domains, a cytoplasmic gradient of cell fate determinants forms, also along

the axis of PAR asymmetry (Rose and Gonczy 2014), (Griffin 2015). Also in response to PAR asymmetry, the force-generating complex described previously localizes asymmetrically on the cortex and exerts microtubule pulling forces that orient and position the spindle along the axis of PAR asymmetry (Rose and Gonczy 2014), (di Pietro, Echard et al. 2016), (Srinivasan, Fisk et al. 2003), (Park and Rose 2008). The resulting mitotic division gives rise to daughters that have inherited different quantities of PARs and cytoplasmic fate determinants and therefore proceed to adopt different fates. In the asymmetric divisions of P1 and P2, mutually exclusive cortical PAR domains form again and are thought to instruct asymmetric division through similar mechanisms (Rose and Gonczy 2014).

In contrast, the asymmetry of the EMS division is generated by two partially redundant signaling events from the neighboring cell P2: a well-described Wnt/Frizzled/β-catenin pathway and a poorly understood MES-1/SRC-1 kinase signaling pathway. In response to these pathways, the mitotic spindle orients to the anterior-posterior axis, which requires a rotation of the spindle from its initial left-right orientation (Fig. 7A). The anterior daughter of this division, MS, becomes a mesoderm progenitor, while the posterior daughter E, born adjacent to P2, is induced to become an endoderm progenitor (Fig. 7B) (Rocheleau, Downs et al. 1997), (Thorpe, Schlesinger et al. 1997), (Walston, Tuskey et al. 2004), (Bei, Hogan et al. 2002).

Double mutant analysis has been the standard mechanism for assigning genes to one of the partially redundant EMS asymmetric division pathways. Homozygous maternal loss of function in the transmembrane tyrosine kinase-like receptor MES-1, the cytoplasmic tyrosine kinase SRC-1, or any of the known Wnt pathway members causes a low rate of late or failed EMS spindle rotations and/or failure to specify endoderm, but in the same brood a significant proportion of embryos proceed normally through EMS division and endoderm induction despite

the mutation (Rocheleau, Downs et al. 1997), (Thorpe, Schlesinger et al. 1997), (Schlesinger, Shelton et al. 1999), (Berkowitz and Strome 2000). However, when either *mes-1* or *src-1* is combined with mutation of a Wnt pathway component, the rate of spindle rotation failure increases to ~95%, indicating that these two genes function redundantly with the Wnt pathway. Furthermore, *mes-1* and *src-1* mutants have the same low frequency of spindle rotation defects as *mes-1;src-1* double mutants, which means that the two genes operate in the same pathway and loss of both causes no additional consequences for EMS asymmetric division (Bei, Hogan et al. 2002).

The induction of the E cell to form endoderm is well characterized, especially for the Wnt pathway. Endoderm fate specification requires the Wnt ligand (MOM-2 in *C. elegans*, expressed in the P2 cell), the transmembrane Frizzled receptor (MOM-5), and the effector protein Disheveled (DSH-2 and MIG-2), as well as other conserved Wnt pathway components (Rocheleau, Downs et al. 1997), (Thorpe, Schlesinger et al. 1997). Activation of this pathway ultimately results in nuclear export of the LEF-1/TCF-7 ortholog POP-1 in the E cell, which allows endoderm-specific gene expression in this cell (Bei, Hogan et al. 2002), (Lin, Thompson et al. 1995), (Sugioka, Mizumoto et al. 2011). The MES-1/SRC-1 pathway also regulates POP-1 nuclear export, although the precise mechanism is unknown. The MES-1 protein is localized to the EMS/P2 cell contact, apparently in both cells (Berkowitz and Strome 2000), (Bei, Hogan et al. 2002). MES-1 is required for activation of SRC-1 at the EMS/P2 contact, based on the staining pattern of an antibody that detects SRC-1-dependent tyrosine phosphorylation (Bei, Hogan et al. 2002). Loss of SRC-1 enhances the POP-1 nuclear export defect of Wnt pathway mutants (Bei, Hogan et al. 2002), (Sumiyoshi, Takahashi et al. 2011). Thus, both pathways

converge to regulate transcription in the E cell through re-localization of the POP-1 transcription factor.

The mechanism by which the Wnt and MES-1/SRC-1 pathways regulate spindle orientation in EMS may also converge, in this case on components of the conserved force generating complex. Loss of the dynein heavy chain (DHC-1), dynactin (DNC-1), or LIN-5 results in strong spindle orientation defects, suggesting these proteins act in both pathways (Zhang, Skop et al. 2007, Liro 2017). Genetic analyses have shown that although depletion of the divergent β-catenin WRM-1 has no effect on EMS spindle orientation, loss of WRM-1 rescues the spindle orientation defects of *Wnt* (*mom-2*) and *Frizzled* (*mom-5*) mutants. Furthermore, Wnt pathway components are required to remove WRM-1 from the posterior cortex of EMS near P2. These data led to the model that removal of WRM-1 "un-masks" a cortical cue for spindle positioning that may recruit LIN-5 and/or dynein (Walston, Tuskey et al. 2004), (Kim, Ishidate et al. 2013), (Schlesinger, Shelton et al. 1999). Similar genetic analyses are consistent with the model that the MES-1/SRC-1 pathway also leads to removal of an inhibitor from the EMS/P2 contact (Liro 2017). However, for both the Wnt and MES-1/SRC-1 pathways, whether other components are involved and how they ultimately regulate the force-generating complex remain as open questions.

A previous study using a maternal-effect lethal, putative null allele of the Rac1 homolog CED-10, *ced-10(t1875),* found that CED-10 is part of a Wnt pathway for spindle orientation of the ABar blastomere in the eight-cell embryo (Cabello, Neukomm et al. 2010). Rac1 is a member of the Rho GTPase family, conserved to varying degrees throughout eukaryotes, and is primarily involved in cytoskeletal regulation across diverse developmental contexts (Boreaux, Vignal et al. 2007), (Bustelo, Sazeau et al. 2007), (Hall 2012), (Duquette and Lamache-Vane 2014). The same

study reported that *ced-10* mutant embryos exhibited abnormal EMS spindle positioning in the four-cell embryo (Cabello, Neukomm et al. 2010). However, this phenotype was not characterized, nor was the relationship between CED-10 and the signaling pathways known to promote EMS spindle positioning. Therefore, we set out to define the genetic and molecular role(s) CED-10 plays in this asymmetric division. Here we demonstrate that CED-10 works in parallel with the Wnt/Frizzled pathway in the EMS cell specifically, where it acts downstream of MES-1 and upstream or at the level of SRC-1 for both spindle orientation and endoderm specification.

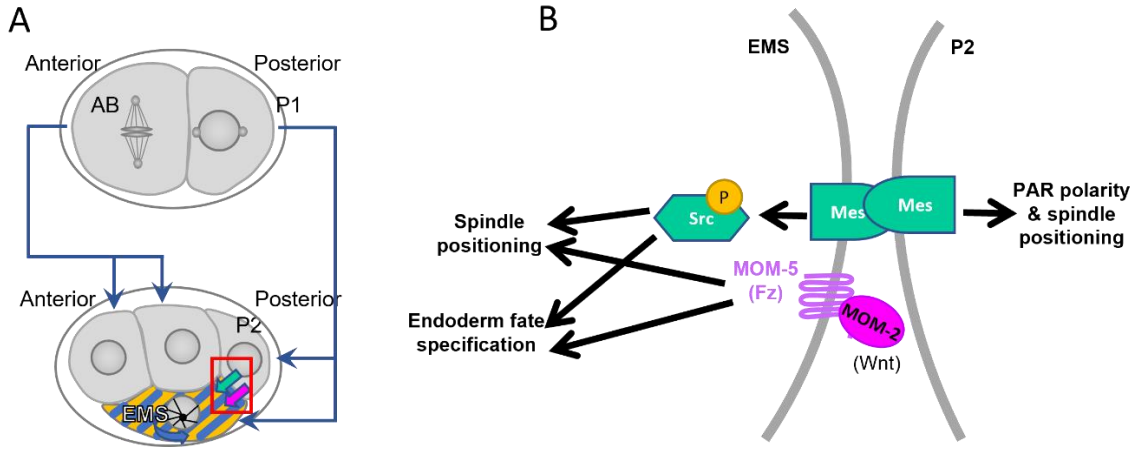

Figure 7. EMS, a daughter cell of P1, divides asymmetrically as instructed by two partially redundant signals.
(A) Diagram illustrating the progression from two cells to four cells in the early *C. elegans* embryo. In all figures throughout this paper, the anterior of the embryo is presented at the left and the posterior at the right; ventral, defined by the position of the EMS cell, is on the bottom. (B) Diagram illustrating key features of the two signaling pathways instructing EMS asymmetric division. EMS is represented on the left, P2 on the right.

Results

The Rac1 homolog CED-10 contributes to P1 spindle positioning

Prior work by Cabello and colleagues found that CED-10 plays a role in Wnt-instructed spindle positioning in the ABar cell of the eight-cell embryo. The same study proposed that

CED-10 performs the same function in EMS, but the early divisions were not analyzed in detail (Cabello, Neukomm et al. 2010). We previously found that embryos from *ced-10(t1875)* homozygous mothers, hereafter referred to as *ced-10* mutant embryos, exhibit normal nuclear and spindle positioning movements during the division of the first cell, P0 (Price, Lamb et al. 2022). Because normal EMS division requires successful completion of the first two rounds of asymmetric division (Fig. 7A), we first characterized P1 spindle orientation in *C. elegans* embryos.

To facilitate scoring of subsequent divisions, we generated a strain with *ced-10(t1875)* in a GFP::tubulin background and compared embryos from this strain to control GFP::tubulin embryos. In all control embryos, the P1 nucleo-centrosomal complex rotated onto the anterior-posterior axis prior to nuclear envelope breakdown (NEB), thus setting up the spindle to form in the correct orientation. In comparison, 21% of *ced-10*; GFP::tubulin embryos had a late or failed P1 spindle rotation (Fig. 8B, C). Consistent with prior published images, *ced-10* embryos were significantly rounder on average than control embryos ($p < 0.0001$), so we asked whether decreased aspect ratio corresponded to P1 spindle positioning defects in the GFP::tubulin background (Cabello, Neukomm et al. 2010), (Fig. 8F, G). Embryos with abnormal P1 spindles were not rounder than embryos with normal P1 spindles, so the effects of *ced-10* on P1 spindle orientation cannot be explained by abnormal embryo shape. Since P1 spindle rotation is instructed by PAR polarity, we next observed the localization of mCherry-tagged PAR-2 at the endogenous locus in a *ced-10*;GFP::tubulin strain. All embryos scored had normally oriented PAR-2 domains at the two-cell stage, indicating that CED-10 is not required for PAR polarity at the two-cell stage. Interestingly, the rate of late or failed P1 nuclear rotations in these embryos was close to 50%, suggesting that PAR-2::mCherry enhances the *ced-10* phenotype (Fig. 8D, E).

As a consequence of normal P1 asymmetric division in wild-type embryos, the EMS blastomere is larger than P2 and divides before P2. For *ced-10* embryos in which the P1 spindle oriented with normal timing or late (n=27/29), these asymmetries were present. These results suggest that CED-10 may have a subtle role in P1 nuclear rotation, but polarity is normal and in the majority of embryos the P1 cell divides asymmetrically. Because the identities of "EMS" and "P2" are unclear (i.e., cell sizes are nearly equal and cell cycles are close to synchronous) in embryos with a completely failed P1 spindle rotation (Fig. S1A, B), those embryos were excluded from further analysis (see Methods).

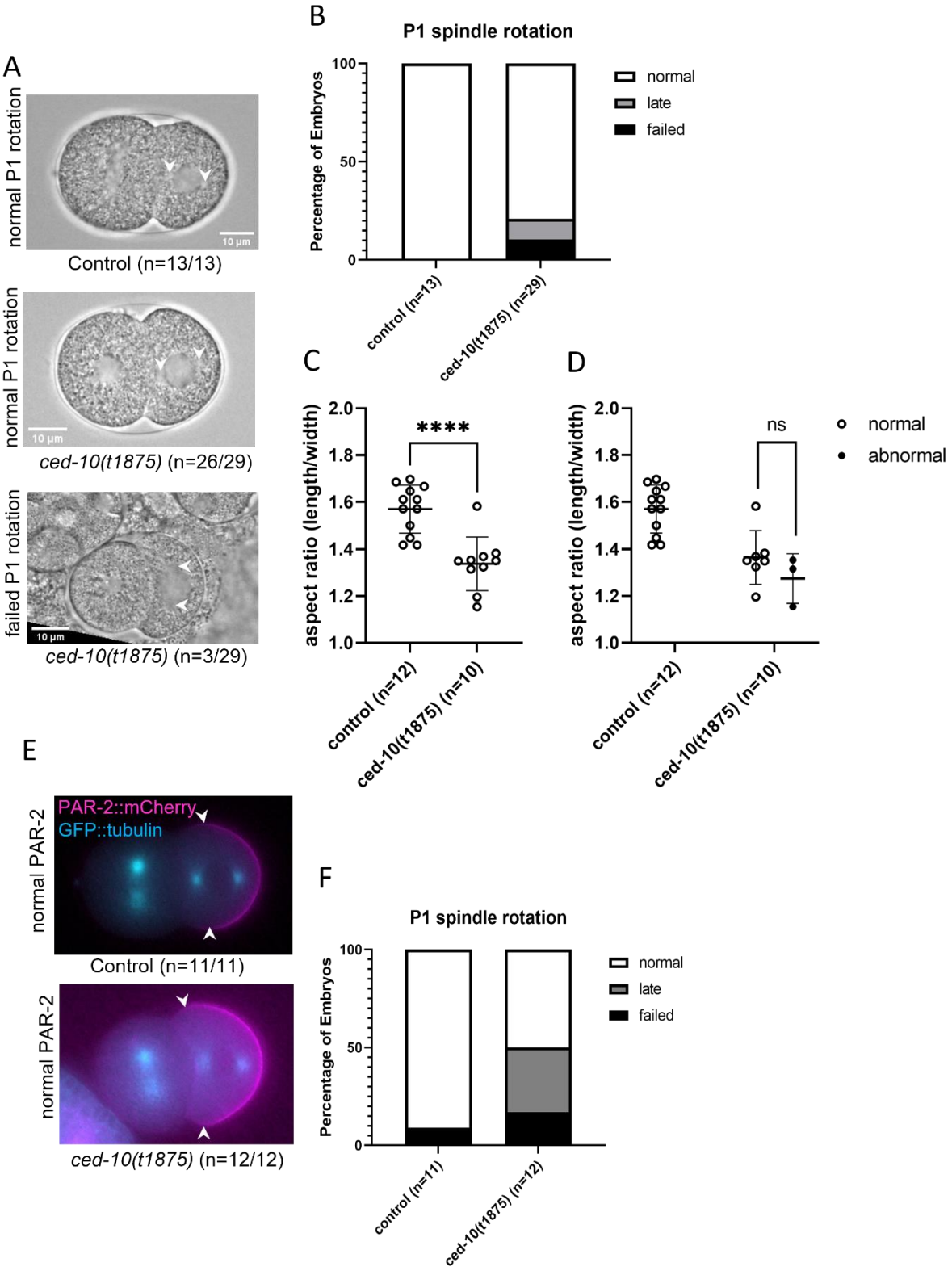
A
normal P1 rotation
10 µm
Control (n=13/13)
normal P1 rotation
10 µm
ced-10(t1875) (n=26/29)
failed P1 rotation
10 µm
ced-10(t1875) (n=3/29)
B
P1 spindle rotation
Percentage of Embryos
100
50
0
normal
late
failed
control (n=13)
ced-10(t1875) (n=29)
C
aspect ratio (length/width)
2.0
1.8
1.6
1.4
1.2
1.0
****
control (n=12)
ced-10(t1875) (n=10)
D
aspect ratio (length/width)
ns
normal
abnormal
control (n=12)
ced-10(t1875) (n=10)
E
normal PAR-2
PAR-2::mCherry
GFP::tubulin
Control (n=11/11)
normal PAR-2
ced-10(t1875) (n=12/12)
F
P1 spindle rotation
Percentage of Embryos
100
50
0
normal
late
failed
control (n=11)
ced-10(t1875) (n=12)

Figure 8. The low rate of P1 spindle defects observed in *ced-10* embryos is not caused by PAR polarity defects or embryo roundness.
(A) Representative DIC images of normal and failed P1 spindle rotation in a control and a *ced-10(t1875)* embryo, respectively.
(B) Percentage of scored embryos with normal, late, or failed P1 spindle rotation for the indicated genotypes in a GFP::tubulin background.
(C) Aspect ratio (length/width) of all scored embryos with the indicated genotypes in a GFP::tubulin background.
(D) Comparison of aspect ratios between embryos with normal vs abnormal P1 spindle rotations for each indicated genotype in a GFP::tubulin background.
(E) Representative widefield fluorescent images of normal and abnormal P1 PAR-2 domains in a *ced-10(t1875)* and a control embryo, respectively.
(F) Percentage of scored embryos with normal, late, or failed P1 spindle rotation for the indicated genotypes in a GFP::tubulin; PAR-2::mCherry background.

CED-10 is a member of the MES-1/SRC-1 pathway for EMS spindle positioning

We next examined the EMS division in *ced-10* embryos with normal or late P1 spindle rotations. We observed that 43% of *ced-10* embryos had a late or failed EMS spindle rotation, indicating that CED-10's contribution to EMS spindle orientation is separable from its role in P1 spindle orientation (Fig. 9A, B). Because CED-10 acts in a Wnt-dependent asymmetric division to orient the spindle of the ABar cell at the eight-cell stage, we considered it a candidate member of the Wnt pathway for EMS spindle positioning (Cabello, Neukomm et al. 2010). We therefore set out to score spindle positioning defects in *ced-10* mutants depleted of MES-1, expecting that if CED-10 contributes to Wnt signaling, loss of CED-10 would enhance the rate of defects in a *mes-1* background. Surprisingly, there was no difference in defect rate between *mes-1(RNAi)*, *ced-10*, and *mes-1(RNAi);ced-10* embryos. Instead, combination of *ced-10* with RNAi depletion of MOM-2 (Wnt) increased the proportion of defective EMS spindle rotation events to 50-60%, suggesting that CED-10 works through a Wnt-independent mechanism (Fig. 9B). These results are consistent with a model in which CED-10 plays a positive role in the MES-1/SRC-1 pathway.

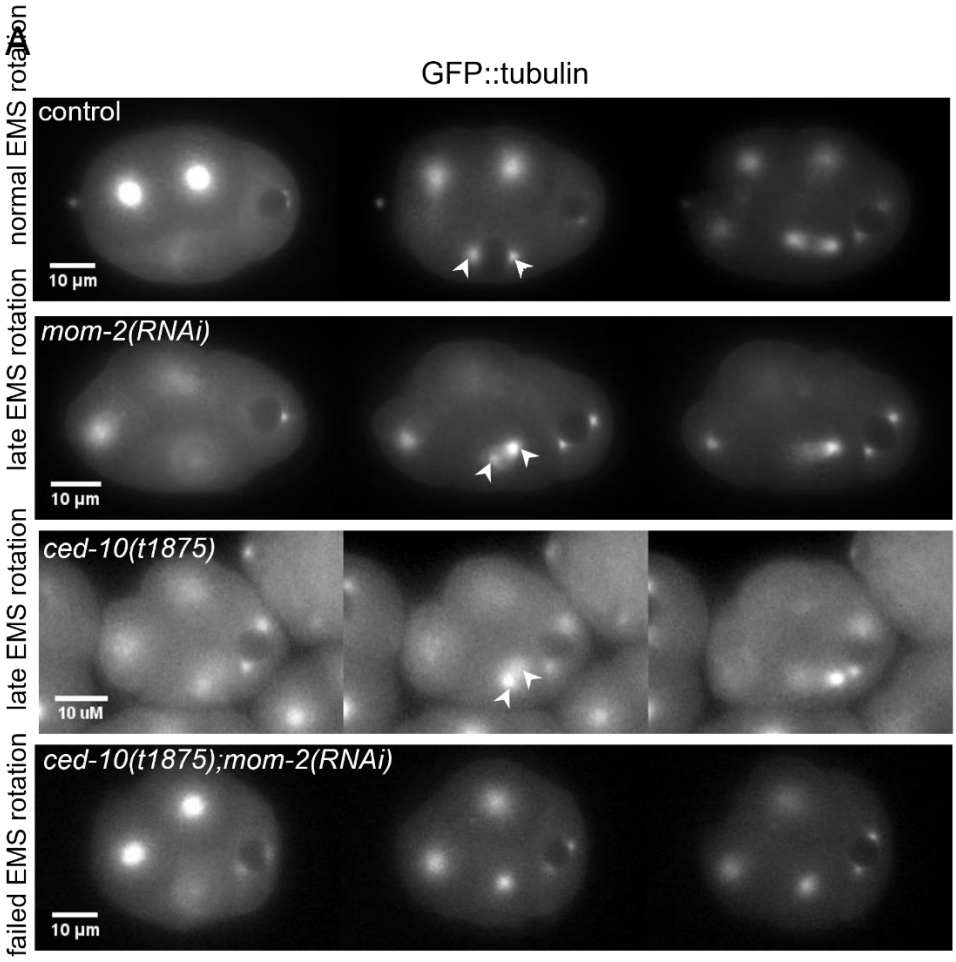
A
GFP::tubulin
normal EMS rotation
control
10 µm
late EMS rotation
mom-2(RNAi)
10 µm
late EMS rotation
ced-10(t1875)
10 uM
failed EMS rotation
ced-10(t1875);mom-2(RNAi)
10 µm

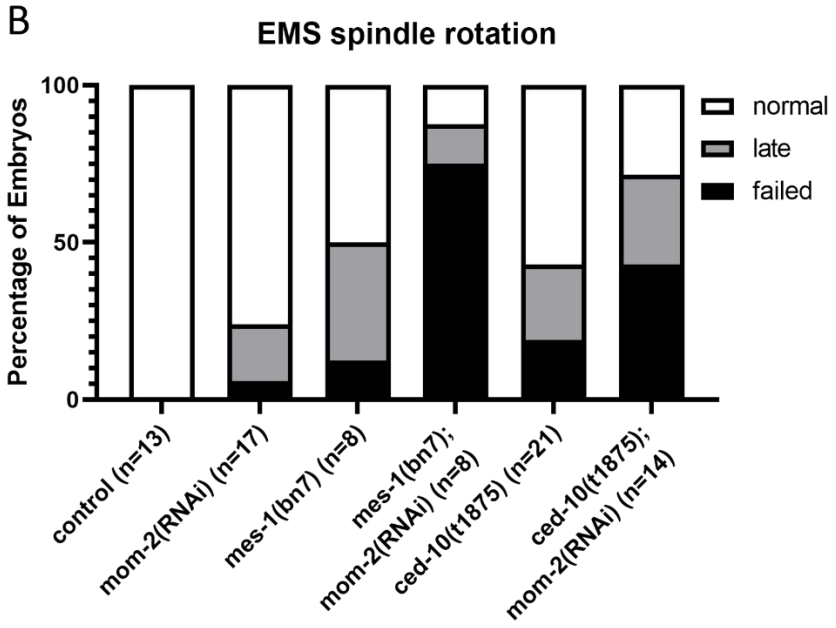
B
EMS spindle rotation
Percentage of Embryos
100
50
0
normal
late
failed
control (n=13)
mom-2(RNAi) (n=17)
mes-1(bn7) (n=8)
mes-1(bn7); mom-2(RNAi) (n=8)
ced-10(t1875) (n=21)
ced-10(t1875); mom-2(RNAi) (n=14)

Figure 9. CED-10 acts in the MES-1/SRC-1 signaling pathway for EMS spindle positioning.
(A) Representative stills from timelapse images of GFP::tubulin embryos with the indicated genotypes, illustrating the three categories of EMS spindle orientation phenotypes observed. Arrowheads indicate visible EMS centrosomes.
(B) Percentage of scored embryos for each indicated genotype with normal, late, or failed EMS rotation in a GFP::tubulin background. For *ced-10(t1875), mom-2(RNAi),* and *ced-10(t1875);mom-2(RNAi),* only embryos with normal P1 spindle rotation were included in the analysis for (E).

CED-10 acts downstream of MES-1 and upstream or at the level of SRC-1

The MES-1/SRC-1 signaling pathway, in addition to its importance in EMS spindle positioning and endoderm fate specification, is required for P2 asymmetric division (Berkowitz and Strome 2000, Bei, Hogan et al. 2002). At birth, P2 inherits the posterior PARs uniformly around the cortex. During the cell cycle, new PAR domains form, but in an orientation different from the previous P lineage divisions: "anterior" PARs such as PAR-3 localize to the anterior-dorsal aspect of the cell, while "posterior" PARs including PAR-2 occupy the posterior-ventral aspect including the EMS/P2 cell contact (Kemphues and Strome 1997, Arata, Lee et al. 2010, Rose and Gonczy 2014). The spindle orients along the axis of PAR asymmetry. This reorientation of the PAR domains requires MES-1/SRC-1 signaling (Arata, Lee et al. 2010).

Because MES-1/SRC-1 signaling is reciprocal between the EMS and P2 cells, we predicted that if *ced-10* disrupts MES-1 function, asymmetric division in both cells would be affected, similar to the *mes-1* mutant phenotype. In *mes-1* mutants, reciprocal PAR polarity domains form in the P2 cell but are misoriented in ~90% of embryos; similarly, P2 spindle orientation is perturbed in ~ 50% (Arata, Lee et al. 2010). Notably, P2 spindle positioning was normal in 100% of *ced-10(t1875)* embryos observed in the GFP::tubulin background (Fig. 10A, B). To assay for PAR polarity, we examined PAR-2::mCherry. In normal embryos, at first the "posterior" PARs are uniform on the P2 cortex. As the P2 cell cycle progresses, they are cleared from the posterior dorsal aspect of the cell and replaced by the "anterior" PARs (Arata, Lee et al.

2010) (Fig. 10C). Control embryos in this strain showed a low frequency of P2 cells that failed to clear PAR-2::mCherry from the dorsal aspect and a similar frequency of *ced-10(t1875)* mutant embryos showed failure to clear, but no misoriented PAR domains were observed. P2 spindle positioning was also unaffected in this background (Fig. 10C-E).

To further test CED-10's placement in the MES-1/SRC-1 pathway, we asked whether MES-1 localization is affected by loss of CED-10. The MES-1 protein is localized exclusively to the EMS/P2 cell contact in wild-type embryos (Berkowitz and Strome 2000). Antibody staining of mNeonGreen::3xFLAG::MES-1 expressed at the endogenous locus revealed that MES-1 enrichment at the EMS/P2 cell contact was not decreased by RNAi of CED-10, although other *ced-10* phenotypes were observed (Fig. 10F, Methods). We also confirmed the efficacy of *ced-10(RNAi)* treatment by decreased GFP::CED-10 fluorescence in parallel (Fig. S2). Together, these results indicate that CED-10 acts downstream of MES-1 for EMS spindle positioning.

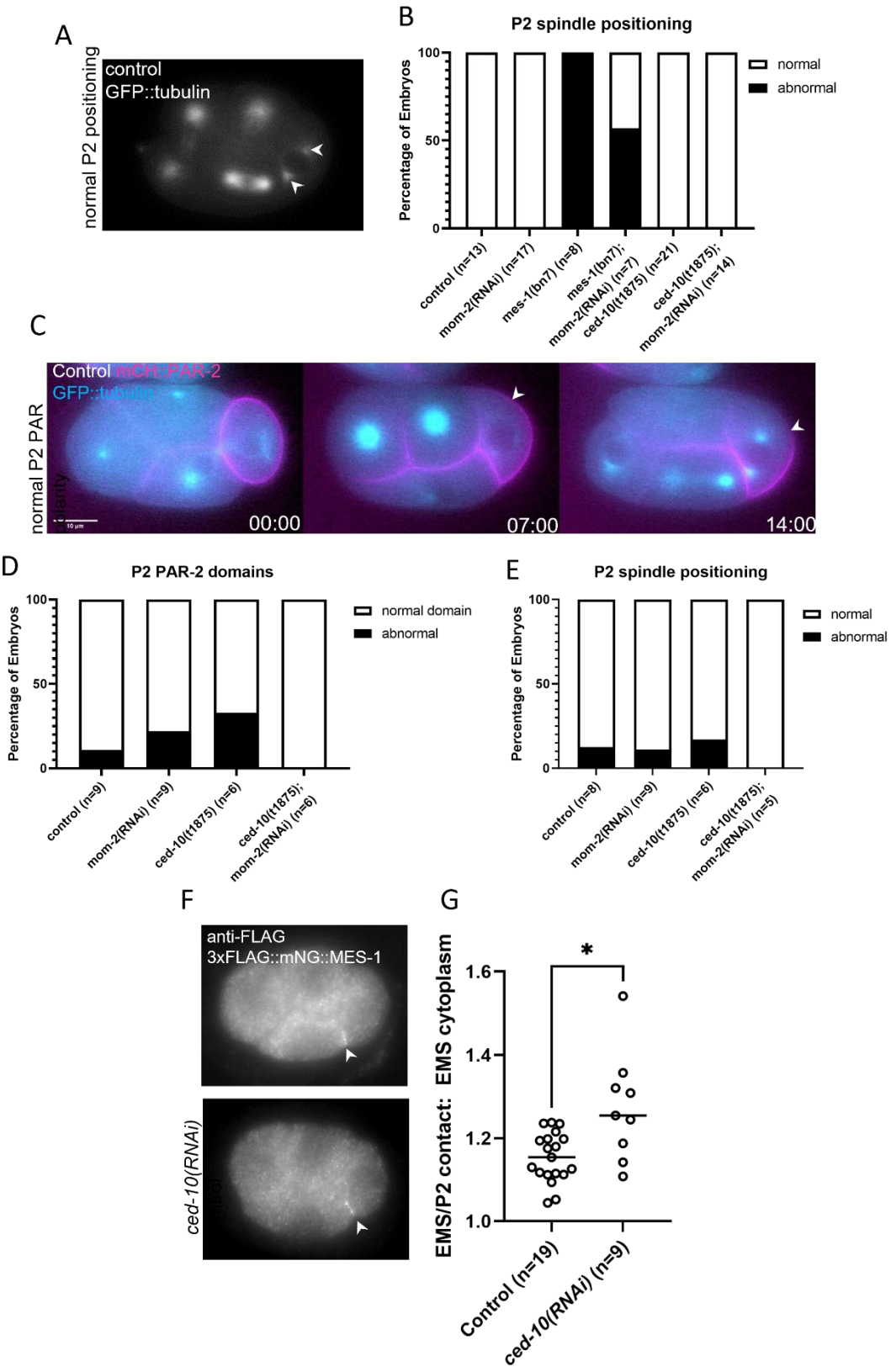
A
normal P2 positioning
control
GFP::tubulin
B
P2 spindle positioning
Percentage of Embryos
100
50
0
normal
abnormal
control (n=13)
mom-2(RNAi) (n=17)
mes-1(bn7) (n=8)
mes-1(bn7); mom-2(RNAi) (n=7)
ced-10(t1875) (n=21)
ced-10(t1875); mom-2(RNAi) (n=14)
C
normal P2 PAR polarity
Control
mCH::PAR-2
GFP::tubulin
00:00
07:00
14:00
D
P2 PAR-2 domains
Percentage of Embryos
normal domain
abnormal
control (n=9)
mom-2(RNAi) (n=9)
ced-10(t1875) (n=6)
ced-10(t1875); mom-2(RNAi) (n=6)
E
P2 spindle positioning
Percentage of Embryos
normal
abnormal
control (n=8)
mom-2(RNAi) (n=9)
ced-10(t1875) (n=6)
ced-10(t1875); mom-2(RNAi) (n=5)
F
anti-FLAG
3xFLAG::mNG::MES-1
ced-10(RNAi)
G
EMS/P2 contact: EMS cytoplasm
1.6
1.4
1.2
1.0
*
Control (n=19)
ced-10(RNAi) (n=9)

Figure 10. CED-10's role in MES-1/SRC-1 signaling is downstream of MES-1.
(A) Representative widefield fluorescence image of a control embryo expressing transgenic GFP::tubulin. Arrowheads mark positions of centrosomes in a normally oriented P2 nuclear-centrosomal complex.
(B) Percentage of scored embryos for each indicated genotype with normal or abnormal P2 spindle positioning in a GFP::tubulin background. For *ced-10(t1875), mom-2(RNAi),* and *ced-10(t1875);mom-2(RNAi),* only embryos with normal P1 spindle rotation were included in the analysis.
(C) Representative widefield fluorescence images of a control embryo expressing transgenic GFP::tubulin (cyan) and PAR-2::mCherry (magenta). As the EMS cell cycle progresses, PAR-2::mCherry clears from the dorsal aspect of P2. Arrowheads mark the approximate position of the dorsal PAR-2::mCherry domain boundary.
(D) Percentage of scored embryos for each indicated genotype with normal or abnormal P2 PAR-2::mCherry domains in a GFP::tubulin; PAR-2::mCherry background. For *ced-10(t1875), mom-2(RNAi),* and *ced-10(t1875);mom-2(RNAi),* only embryos with normal P1 spindle rotation were included in the analysis.
(E) Percentage of scored embryos for each indicated genotype with normal or abnormal P2 spindle positioning in a GFP::tubulin; PAR-2::mCherry background. For *ced-10(t1875), mom-2(RNAi),* and *ced-10(t1875);mom-2(RNAi),* only embryos with normal P1 spindle rotation were included in the analysis.
(F) Representative maximum Z projections from widefield fluorescence microscopy of control and *ced-10(RNAi)* embryos immunostained for the FLAG epitope in a mNeonGreen::3xFLAG::MES-1 background.
(G) Quantification of anti-FLAG signal intensity at the EMS/P2 contact normalized to cytoplasmic background.

We next set out to determine whether CED-10 affects SRC-1. SRC-1 has been shown to be activated by auto-phosphorylation, and immunofluorescence with an antibody that recognizes SRC-1-dependent phosphotyrosine results in an enriched signal at the EMS/P2 contact compared to other contacts (Bei et al., 2002). These two observations support a model in which elevated SRC-1 activity at the EMS/P2 contact contributes to signaling there. However, whether SRC-1 protein *per se* is enriched at that contact is unknown because the localization of SRC-1 has not been examined in the four-cell embryo. We thus hypothesized that asymmetric localization of SRC-1 in the four-cell embryo contributes to EMS spindle positioning. We observed the localization of SRC-1 tagged with GFP at the endogenous locus and found that SRC-1::GFP is cortically localized, but not enriched at the EMS/P2 contact at the four-cell stage (Zhu, Chai et

al. 2020). These results together with prior findings suggest that the asymmetric localization of SRC-1 activity is caused by asymmetric activation of SRC-1 at the EMS/P2 contact. SRC-1::GFP localization was not altered by *ced-10(RNAi)* (Fig. 11A, B).

We next stained four-cell embryos with the anti-phosphotyrosine antibody as a reporter of SRC-1 activity. While phosphotyrosine was still enriched at the EMS/P2 contact in *ced-10(t1875)* embryos compared to other contacts, many embryos showed less enrichment than in wild-type (Fig. 11C, D). However, the average enrichment of the *ced-10* embryos was higher than for *mes-1* embryos, which had no enrichment of Y99 signal at the EMS/P2 contact, as previously reported (Bei, Hogan et al. 2002). We also noted that the cytoplasm-normalized intensity of phosphotyrosine signal decreased slightly but significantly at the P2/ABp contact in *ced-10(t1875)* but not *mes-1(bn7)* embryos (Fig. S3). We interpret this as evidence that some of the observed decrease in enrichment at the EMS/P2 contact is due to a change in the P2 cell, but since there is no apparent consequence to P2 asymmetric division, we did not investigate further. Together these results indicate that CED-10 contributes to the activity of SRC-1, to the localization of the active subset of SRC-1 protein, and/or to the localization of SRC-1 phosphorylation substrates.

SRC-1 activity is required for both EMS spindle positioning and endoderm fate specification in the E daughter cell. Since CED-10 was shown to promote SRC-1 activity at the EMS/P2 contact, we asked whether loss of CED-10 perturbs both SRC-1 dependent processes by quantifying GFP::POP-1 nuclear asymmetry. As previously published, POP-1 levels in the nucleus of the E daughter cell were lower than in its sister cell MS, and RNAi depletion of the Wnt ligand MOM-2 resulted in a slight reduction in the asymmetry index between the nuclei (Fig. 11E, F) (Lin, Thompson et al. 1995), (Thorpe, Schlesinger et al. 1997), (Sugioka and Sawa

2010). A similar degree of equalization was observed in *ced-10(RNAi)*. While on average the asymmetry index was not significantly different among the three groups, 15% of both *mom-2(RNAi)* and *ced-10(RNAi)* embryos had values below the control range. In addition, we tested whether loss of CED-10 affects the differentiation of endoderm tissue by assaying the presence of gut granules in late-stage embryos. Prior work showed that although loss of MES-1 or SRC-1 alone did not affect endoderm formation, loss of either MES-1 or SRC-1 enhanced the gut granule minus phenotypes of Wnt pathway mutants (Bei et al. 2002). Virtually all *ced-10(t1875)* embryos exhibited gut granules. Although *mom-2* mutants lack gut granules with variable penetrance, most *mom-2(RNAi)* embryos form gut (Rocheleau et al. 1997, Thorpe et al. 1997). Combining *ced-10(t1875)* with *mom-2(RNAi)* enhanced the proportion of embryos without gut granules compared to loss of *mom-2* alone (Fig. 11G). These data indicate that CED-10 is required for proper specification of endoderm tissue in parallel with Wnt signaling. Together with the results of anti-phosphotyrosine staining, this observation suggests that CED-10 acts upstream of both EMS spindle positioning and endoderm fate specification by promoting enhanced SRC-1 activity at the EMS/P2 contact.

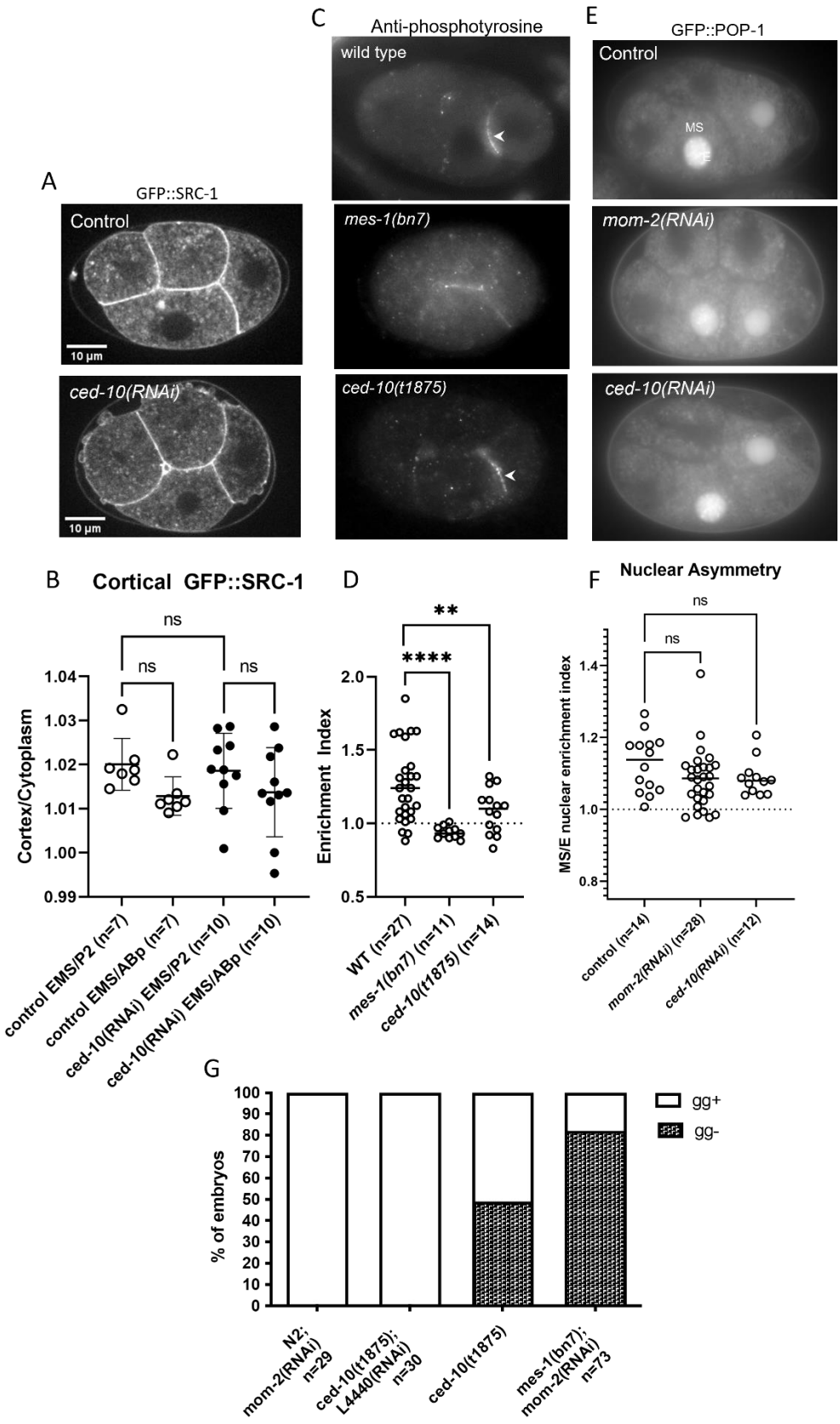
A
GFP::SRC-1
Control
10 µm
ced-10(RNAi)
10 µm
C
Anti-phosphotyrosine
wild type
mes-1(bn7)
ced-10(t1875)
E
GFP::POP-1
Control
MS
E
mom-2(RNAi)
ced-10(RNAi)
B
Cortical GFP::SRC-1
Cortex/Cytoplasm
ns
ns
ns
control EMS/P2 (n=7)
control EMS/ABp (n=7)
ced-10(RNAi) EMS/P2 (n=10)
ced-10(RNAi) EMS/ABp (n=10)
D
Enrichment Index
**
****
WT (n=27)
mes-1(bn7) (n=11)
ced-10(t1875) (n=14)
F
Nuclear Asymmetry
MS/E nuclear enrichment index
ns
ns
control (n=14)
mom-2(RNAi) (n=28)
ced-10(RNAi) (n=12)
G
% of embryos
gg+
gg-
N2; mom-2(RNAi) n=29
ced-10(t1875); L4440(RNAi) n=30
ced-10(t1875)
mes-1(bn7); mom-2(RNAi) n=73

Figure 11. CED-10's role in MES-1/SRC-1 signaling is upstream or at the level of SRC-1.
(A) Representative confocal fluorescence images of GFP::SRC-1 in control and *ced-10(RNAi)* embryos.
(B) Cortical GFP::SRC-1 fluorescence intensity, normalized to cytoplasm, at both the EMS/P2 and EMS/ABp contacts in the indicated genotypes.
(C) Representative widefield fluorescence images of embryos stained for SRC-1-dependent phosphotyrosine in the indicated genotypes.
(D) Staining Enrichment Index of EMS/P2 contact over EMS/ABp contact in the indicated genotypes ("Enrichment Index;" see Methods for details).
(E) Representative widefield fluorescence images of GFP::POP-1 in the indicated genotypes.
(F) Relative enrichment of MS nuclear fluorescence, expressed as a ratio with E nuclear fluorescence ("Nuclear Enrichment Index;" see Methods for details).
(G) Proportion of embryos with and without gut granules in the indicated genotypes.

CED-10 and ARX-2 are localized at cell contacts at the four-cell stage

To gain insight into the function of CED-10 in MES-1/SRC-1 signaling, we characterized the localization of GFP::CED-10 in four-cell embryos. We used a randomly integrated fusion transgene under transcriptional control by the *ced-10* promoter and crossed it into a *ced-10(t1875)* background (Lundquist, Reddien et al. 2001),(Ziel, Hagedorn et al. 2009). Expression of GFP::CED-10 rescued embryonic lethality sufficiently to maintain the strain as homozygous *ced-10(t1875)* and the embryos appeared less round. However, we noted qualitatively that GFP::CED-10;*ced-10(t1875)* embryos exhibited many small cortical protrusions throughout the first few mitotic divisions, similar to *ced-10(t1875)* embryos (Price, Lamb, et al. 2022). We next tested whether the fusion protein rescued CED-10 function in the early embryo by scoring EMS divisions following *mom-2(RNAi).* We found that *ced-10(t1875);*GFP::CED-10 embryos depleted of MOM-2 did not have an enhanced rate of defective spindle orientations compared to control embryos depleted of MOM-2 (Fig. S4A). This result confirmed that GFP::CED-10 expression is sufficient to rescue the EMS spindle phenotype of *ced-10(t1875).* We found that GFP::CED-10 is present on all cell-cell contacts at the four-cell stage (Fig. 12A) but did not

detect any asymmetry at the EMS/P2 contact. This localization pattern is consistent with a cortex-localized mechanism of action for CED-10.

Rac proteins can signal through the WAVE complex or WASp proteins, which both activate the Arp2/3 complex to nucleate branched actin (Shakir, Jiang et al. 2008, Saenz-Narciso, Gomez-Orte et al. 2016). Therefore we hypothesized that CED-10 contributes to EMS asymmetric division by promoting branched actin at the EMS-P2 contact. Although prior studies have shown that branched actin reporters localize to the cell surface at the one-cell stage and to cell-cell contacts during ventral enclosure, none have examined the localization of branched actin at the four-cell stage(Sawa, Suetsugu et al. 2003, Chan, Silva et al. 2018). We visualized ARX-2, a key member of the Arp2/3 branched actin nucleating complex, with a randomly integrated ARX-2::GFP fusion transgene under transcriptional control by the *arx*-2 promoter (Sarov, Murray et al. 2012). Consistent with our hypothesis, GFP::ARX-2 was present at all cortical surfaces of the embryo and enriched at the EMS/P2 contact (Fig. 12C). Furthermore, both overall cortical localization of GFP::ARX-2 and enrichment at the EMS/P2 contact were decreased with *ced-10(RNAi)*, suggesting that CED-10 increases branched actin levels globally, but especially at that cell-cell contact (Fig. 12D, E).

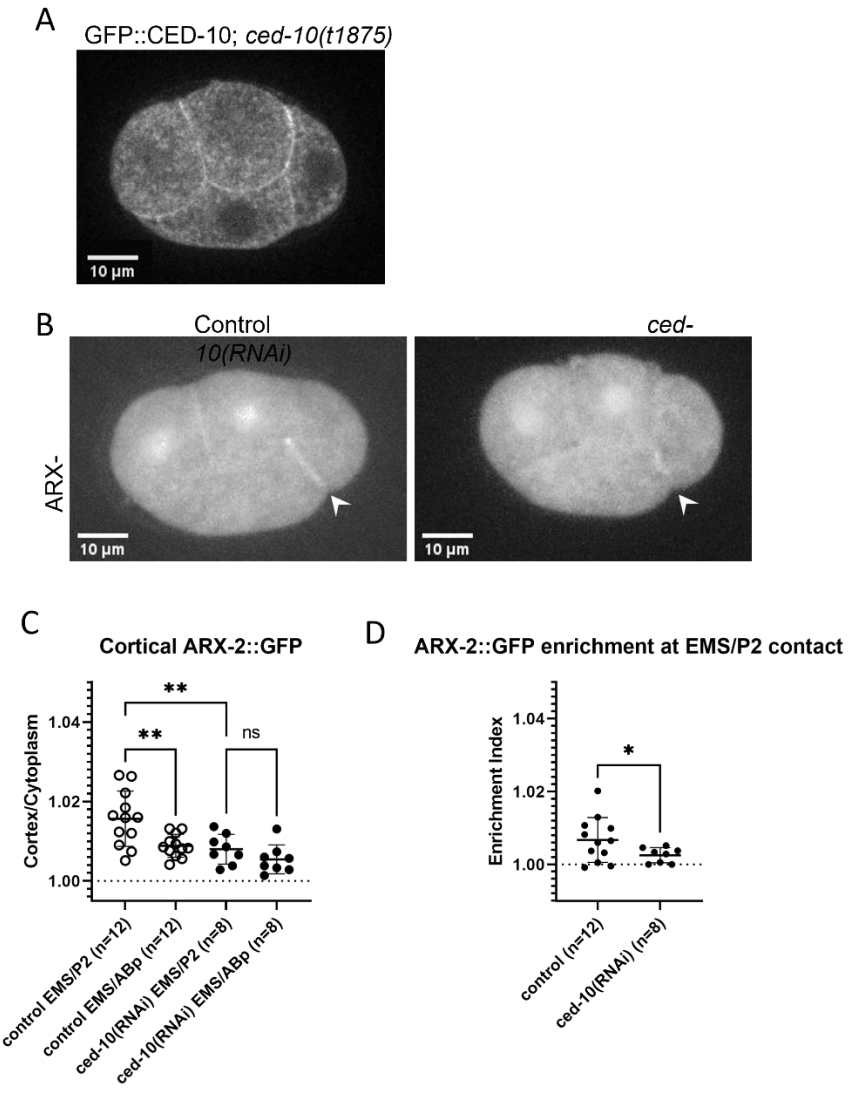

Figure 12. GFP::CED-10 and ARX-2::GFP are cortically localized and ARX-2::GFP enrichment at the EMS/P2 contact is CED-10-dependent.

(A) Representative confocal fluorescence image of GFP::CED-10 in a *ced-10(t1875)* background (n=3).

(B) Representative maximum Z projections from confocal fluorescence microscopy of ARX-2::GFP in control and *ced-10(RNAi)* embryos.

(C) Cortical ARX-2::GFP fluorescence intensity, normalized to cytoplasm, at both the EMS/P2 and EMS/ABp contacts in the indicated genotypes.

(D) Relative enrichment of cortical fluorescence at EMS/P2 contact in control and *ced-10(RNAi)* embryos, expressed as a ratio with EMS/ABp contact ("Enrichment Index;" see Methods for details).

Branched actin interacts with Frizzled for proper P1 and EMS spindle rotation

To test whether branched actin contributes to EMS spindle positioning, we examined spindle rotation events in embryos depleted of ARX-2 by RNAi and in *mom*-5*(zu193)* (*Frizzled* null) embryos depleted of ARX-2, both in a GFP::tubulin background. Unexpectedly, we found that 75% of *mom-5(zu193);arx-2(RNAi)* embryos displayed defective P1 spindle rotation at the 2-cell stage (Fig. 13A); only 15% of *mom-5(zu193)* and 13% of *arx-2(RNAi)* embryos had P1 spindle defects. EMS spindle positioning was then scored in only the embryos with a normal or late rotation, which would allow for normal fating of the EMS and P2 blastomeres. In this small subset, 100% of *arx-2(RNAi)* embryos had normal EMS spindles, but depletion of ARX-2 in a *mom-5(zu193)* background enhanced the rate of defective spindle rotations observed in *mom-5* alone from 9% to 43% (Fig. 13B).

While *ced-10(RNAi)* on *mom-5(zu193)* resulted in a similarly enhanced rate of P1 spindle defects (45% failed compared to 9% late or failed in *mom-5(zu193)* and 0% in *ced-10(RNAi)*), *mom-2(RNAi)* on *ced-10(t1875)* did not cause the same strong enhancement (32% defect rate in the double, most of which were late, vs ~10-20% in the singles), nor did *mom-2(RNAi)* on *mes-1(bn7)*, which resulted in 100% normal P1 rotations (n=4) (Fig. S5A, B). These results suggest the phenotype is due to a specific interaction between the Frizzled ortholog MOM-5 and the branched actin cytoskeleton.

The unexpected P1 phenotype raised the possibility that PAR polarity is perturbed in these embryos, since P1 spindle rotation is instructed by asymmetric PAR localization and branched actin has been implicated previously both in robust PAR polarity maintenance and in nuclear positioning in PAR-instructed systems (Rose and Gonczy 2014), (Kemphues, Priess et al. 1988), (Xiong, Mohler et al. 2011), (Shivas and Skop 2012). We therefore observed

mCherry::PAR-2 localization at the 2-cell stage in *arx-2(RNAi)*, *mom-5(zu193)*, and *mom-5(zu193);arx-2(RNAi)* embryos. Contrary to our hypothesis, 100% of PAR-2 domains appeared normal in *mom-5(zu193)*, *arx-2(RNAi)*, and *mom-5(zu193);arx-2(RNAi)* embryos (Fig. 13D); in this data set 1/11 control embryos had a misoriented PAR-2 domain with PAR-2 signal appearing on the lateral cortices of both P1 and AB. Furthermore, the presence of mCherry::PAR-2 appeared to suppress the genetic interaction of MOM-5 and branched actin observed in the background of GFP::tubulin alone: only 1/9 *mom-5(zu193);arx-2(RNAi)* embryos had defective P1 spindle rotations (Fig. 13C). However, in this background *arx-2(RNAi)* on *mom-5(zu193)* still enhanced the rate of late and failed EMS spindle rotations compared to *mom-5(zu193)* alone (69% defective vs 43% in *mom-5* and 0% in *arx-2*), which corroborates our findings in embryos without mCherry::PAR-2 (Fig. 13E).

In the late *C. elegans* embryo, CED-10 has been shown to act preferentially through the WAVE complex, which in worms includes the subunits WVE-1(WAVE), GEX-2 (CYFIP), and GEX-3 (NCKAP1) (Shakir, Jiang et al. 2008), (Saenz-Narciso, Gomez-Orte et al. 2016) (Soto, Qadota et al. 2002). Thus to try to target more specifically the population of branched actin that is regulated by CED-10 and avoid the high rate of defective P1 nuclear rotations, we depleted MOM-2 in a *gex-3(zu196)* background. All EMS/P2 pairs appeared to be fated correctly as determined by unequal size and asynchronous cell cycles; the few P1 rotations we observed in this data set were normal (n=1 for *gex-3(zu196)* and n=2 for *gex-3(zu196);mom-2(RNAi)*). We observed no defective EMS rotations in *gex-3(zu196)* embryos and only one late EMS rotation out of 9 *gex-3(zu196);mom-2(RNAi)* embryos, despite strong RNAi of MOM-2 as determined by the enhancement of the *mes-1(bn7)* phenotype (Fig. 13F).

Together, these results point to a previously unidentified mechanism involving branched actin and Frizzled that regulates P1 spindle rotation. In addition to and possibly separate from this mechanism, our observations support a role for branched actin in MES-1/SRC-1 signaling for EMS spindle positioning. However, this possible role does not appear to be mediated by GEX-3, which represents the WAVE/SCAR complex.

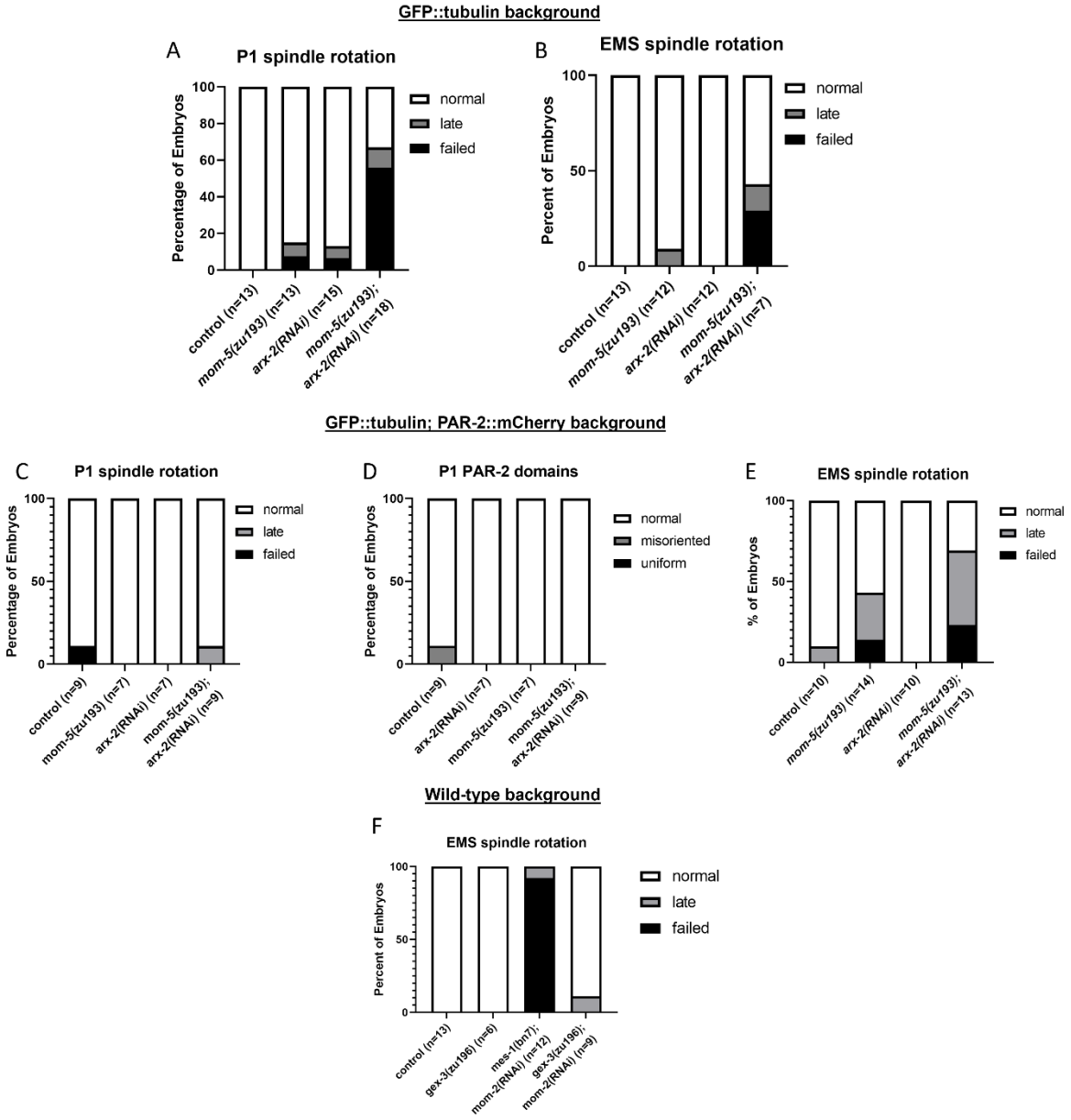

Figure 13. Branched actin works with Frizzled to promote P1 spindle rotation and also contributes to EMS spindle positioning.
(A) Percentage of scored embryos for each indicated genotype with normal, late, or failed P1 rotation in a GFP::tubulin background.
(B) Percentage of scored embryos for each indicated genotype with normal, late, or failed EMS rotation in a GFP::tubulin background. Only embryos with normal P1 spindle rotation were included in the analysis.
(C) Percentage of scored embryos for each indicated genotype with normal, late, or failed P1 rotation in a GFP::tubulin; mCherry::PAR-2 background.
(D) Percentage of scored embryos for each indicated genotype with normal, uniform, or misoriented P1 PAR-2 domains in a GFP::tubulin; mCherry::PAR-2 background.
(E) Percentage of scored embryos for each indicated genotype with normal, late, or failed EMS rotation in a GFP::tubulin; mCherry::PAR-2 background.
(F) Percentage of scored embryos for each indicated genotype with normal, late, or failed EMS rotation in a wild-type background.

CED-10 contributes globally to cortical localization of the dynein adaptor LIN-5/NuMA

Several components of the force-generating complex responsible for asymmetric spindle positioning at the one- and two-cell stages have been implicated in EMS spindle positioning. For example, the dynein adaptor LIN-5/NuMA, the dynein heavy chain (DHC-1), and the dynein partner dynactin (DNC-1) have been shown to be genetically required for the process (Liro and Rose 2016), (Zhang, Skop et al. 2007). Additionally, LIN-5 localizes to the cortex at the four-cell stage and is enriched at the EMS/P2 contact (Srinivasan, Fisk et al. 2003), although this enrichment may be P2 specific (Heppert, Pani et al. 2018). We therefore tested whether loss of CED-10 affects the localization of LIN-5 (Fig. 14A). Consistent with previously reported LIN-5 localization patterns, LIN-5 tagged with GFP at the endogenous locus was localized to the cortex at the four-cell stage and enriched at the EMS/P2 contact in control embryos (Srinivasan, Fisk et al. 2003), (Portegijs, Fielmich et al. 2016), (Heppert, Pani et al. 2018); (Fig. 14B). We found that the ratio of signal intensities at the EMS/P2 contact vs the EMS/ABp contact was not affected (Fig. 14C). However, *ced-10(RNAi)* embryos did have lower overall levels of cortical GFP::LIN-5, indicating that CED-10 promotes LIN-5 cortical localization on a global scale (Fig. 14B).

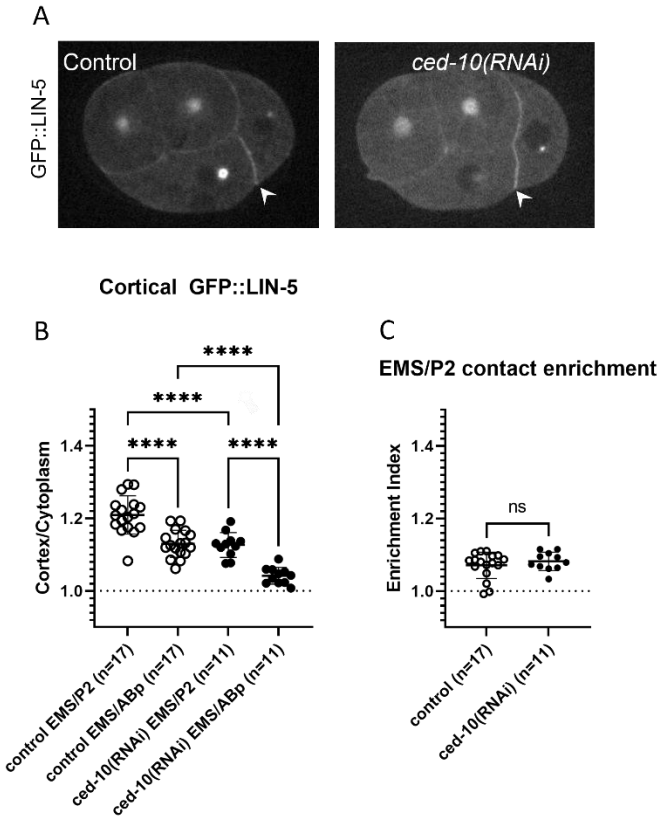

Figure 14. CED-10 contributes globally to localization of the dynein adaptor LIN-5 at the four-cell stage.
(A) Representative confocal fluorescence images of GFP::LIN-5 in control and *ced-10(RNAi)* embryos.
(B) Cortical GFP::LIN-5 fluorescence intensity, normalized to cytoplasm, at both the EMS/P2 and EMS/ABp contacts in the indicated genotypes.
(C) Relative enrichment of cortical fluorescence at EMS/P2 contact in control and *ced-10(RNAi)* embryos, expressed as a ratio with EMS/ABp contact ("Enrichment Index;" see Methods for details).

Discussion

The same studies that originally identified a role for Wnt signaling components in EMS asymmetric division also found that one of the four granddaughters of AB, ABar, requires Wnt (MOM-2), Frizzled (MOM-5), and Disheveled (DSH-2, MIG-5) to orient its mitotic spindle with the left-right axis of the embryo, in contrast with the anterior-posterior orientations of the other three AB4 spindles (Rocheleau, Downs et al. 1997), (Thorpe, Schlesinger et al. 1997). This

spindle orientation, like the analogous process in EMS, was shown to be transcription-independent (Schlesinger, Shelton et al. 1999), (Walston, Tuskey et al. 2004). In many contexts throughout the animal kingdom, including in left/right symmetry breaking in *C. elegans*, non-canonical Wnt signaling can regulate the actin cytoskeleton to alter cell behavior in a transcription-independent manner (Schlessinger, Hall et al. 2009), (Pohl and Bao 2010). Thus when the Rac1 homolog CED-10, an actin regulator, was found to act in the Wnt pathway for cell corpse engulfment and to contribute to EMS and ABar spindle positioning, the rational prediction was that its role in EMS spindle positioning was also as a member of the Wnt pathway (Cabello, Neukomm et al. 2010).

Here we demonstrate that in the four-cell embryo, CED-10 does play a role in EMS asymmetric division, but it works as a member of the MES-1/SRC-1 pathway in parallel to Wnt signaling. SRC-1 has also been shown to contribute to ABar spindle positioning, where its precise role is unknown, but it is thought to be part of the Wnt pathway (Walston, Tuskey et al. 2004, Sumiyoshi, Takahashi et al. 2011). Thus, the two systems, although similar, may not be directly comparable.

Our analyses demonstrate that CED-10 acts downstream of MES-1 and upstream or at the level of SRC-1, to influence both spindle positioning and endoderm fate specification. Notably, this function of CED-10 is specific to the EMS cell, as we observed no defects in the asymmetric division of the P2 cell in *ced-10* embryos.

Given that MES-1 and anti-phosphotyrosine immunostaining are both enriched at the EMS/P2 contact, we hypothesized that asymmetric localization of other components of the MES-1/SRC-1 pathway might contribute to the molecular mechanisms involved in signaling. GFP-tagged versions of SRC-1 and CED-10 were present at cell-cell contacts, but they were not

enriched at the EMS/P2 contact, nor was SRC-1 localization altered by *ced-10(RNAi)*. We did find that CED-10 contributes to the enrichment of SRC-1-dependent phosphotyrosine at that contact. However, the nature of the antibody used for this immunostaining experiment, the ability of SRC-1 to autophosphorylate, and the lack of known SRC-1 phosphorylation targets in this context make it impossible to distinguish whether CED-10 affects phosphorylated (active) SRC-1, other phosphorylated SRC-1 targets, or both. Together, these observations do not support a model dependent on asymmetrically localized CED-10 or SRC-1. Instead, we propose that asymmetrically activated CED-10 promotes the cortical recruitment, organization, and/or retention of active SRC-1 and/or SRC-1 phosphorylation targets at the EMS/P2 contact.

Two additional pieces of evidence support our conclusion that CED-10 acts upstream or at the level of SRC-1 as a regulator not only of EMS spindle positioning but also of endoderm fate specification. First, the levels of GFP::POP-1 transcription factor were partially equalized between the E and MS blastomeres in *ced-10(RNAi)* embryos. Second, the proportion of embryos without gut granules was enhanced in *ced-10(t1875);mom-2(RNAi)* embryos compared to embryos lacking either CED-10 or MOM-2. The fact that loss of CED-10 affects both aspects of EMS asymmetric division suggests that CED-10 regulates either SRC-1 itself, or SRC-1 phosphorylation targets common to both processes.

The mechanistic link, if any, between SRC-1 regulation by CED-10 and the regulation of spindle positioning and endoderm fate specification remains unclear. Understanding this mechanism requires identification of the effector(s) directly regulated by CED-10 and SRC-1. One possible connection between CED-10 and SRC is myosin: SRC-1 localization has been previously shown to require activated myosin, and a known effector of CED-10 in other contexts is the PAK family member PAK-1, which can phosphorylate and activate the myosin light chain

(Liu, Maduzia et al. 2010), (Chircop 2014), (Nguyen, Kholodenko et al. 2018). Another possible link is the actin cytoskeleton: one of the major roles of CED-10 and other Rac1 homologs is to promote the formation of branched actin in various contexts, and cortical actin dynamics are critical in maintaining signaling molecules such as SRC-1 at the cortex (Mattila, Batista et al. 2016). Indeed, in this study we showed not only that the branched actin nucleator ARX-2/Arp2 is enriched in a CED-10 dependent manner at the EMS/P2 contact during EMS spindle rotation, but also that depletion of ARX-2 enhanced the rate of EMS spindle defects in a *mom-5*/*Frizzled* background. Intriguingly, the EMS spindle defect enhancement was not observed when we combined *mom-2* depletion with mutation of the WAVE/SCAR complex member GEX-3 (NCKAP1). This result suggests that while CED-10 dependent branched actin may have a role in EMS asymmetric division, this role is not mediated by the WAVE/SCAR complex as in other contexts where CED-10 promotes branched actin formation.

Our results support the hypothesis that a key consequence of CED-10 activity in the MES-1/SRC-1 pathway is cortical recruitment of the dynein adaptor LIN-5 (NuMA). We found that CED-10 contributes globally to absolute cortical GFP::LIN-5 levels, but the relative enrichment of GFP::LIN-5 at the EMS/P2 contact was unaffected by *ced-10(RNAi)*. This finding presents a plausible mechanism for CED-10's connection to the dynein-containing force-generating complex previously implicated in EMS spindle positioning. Furthermore, it is consistent with previous observations implicating asymmetric LIN-5 localization in the asymmetric division of P2 but not that of EMS (Heppert, Pani et al. 2018).

During our studies focused on EMS asymmetric division, we unexpectedly identified a previously unreported role for CED-10 in P1 spindle positioning. We also uncovered an apparent genetic interaction between branched actin and the Frizzled ortholog MOM-5 at the two-cell

stage. In the absence of MOM-5, branched actin depletion with RNAi against *arx-2* or *ced-10* caused a high rate of failed P1 spindle rotations. This interaction may also be enhanced by the presence of GFP-labeled tubulin in the strain background, since there was a low rate of P1 spindle defects in the *mom-5* mutant strain alone, and this phenotype has never been reported for this allele previously. Interestingly, the presence of mCherry-labeled PAR-2 appeared to suppress the enhancement.

One possible interpretation of these observations is that CED-10-mediated branched actin promotes P1 spindle rotation in parallel to a mechanism requiring MOM-5 and properly tuned microtubule dynamics. This model would be consistent with previous findings implicating both Frizzled/MOM-5 and the adenomatous polyposis coli (APC) homolog APR-1 in regulation of microtubule dynamics during mitotic spindle positioning. Key observations reported in these prior studies include 1) the ligand-independent enrichment of MOM-5 on the posterior cortices of various asymmetrically dividing somatic cells; 2) the MOM-5 and PAR-3 dependent enrichment of APR-1 on the anterior cortex of the zygote P0; 3) the MOM-5 dependent enrichment of APR-1 on the anterior cortex of EMS itself; and 4) the ability of cortical APR-1 to stabilize astral microtubules and thus attenuate spindle pulling forces (Park, Tenlen et al. 2005), (Sugioka, Mizumoto et al. 2011), (Sugioka, Fielmich et al. 2017). We propose that like P0 spindle positioning, P1 spindle rotation is driven in part by APR-1 modulation of microtubule pulling forces. Considering the enhanced rate of P1 rotation defects observed with loss of both branched actin regulators and MOM-5, we further propose that branched actin is required in the absence of this mechanism.

The results of this study add detail and complexity to our knowledge of the diverse functions of Rac1 and shed light on a relatively poorly understood type of asymmetric division.

Not only do these insights contribute to a deeper understanding of the cellular and molecular principles of asymmetric division and Rac1 signaling under normal conditions; we may also leverage them to address diseases associated with dysregulation of the process.

Acknowledgements

We thank members of the Rose and McNally labs for helpful discussions. Thanks to Daniel A. Starr and Bruce W. Draper for critical reading of the manuscript. We are grateful to Guangshuo Ou, Martha Soto, Karen Oegema, and Francis McNally for strains. We also thank the *Caenorhabditis* Genetics Center, which is funded by the National Institutes of Health Office of Research Infrastructure Programs (P40 OD010440) for strains. Erik Lundquist provided strains and plasmids. Jennifer Heppert advised on anti-FLAG staining protocol. The 3i Marianas spinning disk confocal and the Nikon laser scanning confocal used in this study were purchased using a National Institutes of Health Shared Instrumentation Grant [1S10RR024543-01]. We thank the MCB Light Microscopy Imaging Facility, which is a UC-Davis Campus Core Research Facility, for the use of this microscope. This work was funded by the National Institutes of Health Grant to LSR [R01GM68744]. Support for HL and ML was also provided by the UC Davis BMCDB Graduate Group and a National Institutes of Health training grant to HL [T32 GM 007377].

Methods

Nematodes were maintained on Modified Youngren's, Only Bacto-Peptone (MYOB) seeded with *E. coli* OP50; worms were maintained at ambient temperature (22-24°C), except during RNAi treatment (see below) or in the case of temperature sensitive strains (RL292 [*mes-1(bn7)*; GFP::tubulin] was maintained at 16°C)(Church, Guan et al. 1995),(Stiernagle 2006).

Table of strains used with attributions

Strain number	Genotype	Source
FM126	unc-119 (ed3); ruIs57 [pAZ147: pie-1/B-tubulin::GFP; unc-119 (+)]; itIs37 [unc-119(+) pie-1::mCherry::H2B]; him-8 (e1489) IV	Cortez et al. 2015. eLife 4:e06056.
GOU3475	src-1(cas605[src-1::gfp CRISPR knock-in]) I	Zhu et al. 2020. *PNAS* 117(25): 14270-14279
JR1904	wIs117 [med-1p::GFP::pop-1::med-1 3'UTR + rol-6(su1006)]	Maduro MF, Lin R & Rothman JH. 2002. *Dev Biol* 248: 128-142.
LP527	mes-1(cp240[mes-1::mNG-C1^3xFlag]	Heppert et al. 2018. *Genetics* 208, 1147–1164.
NK336	qyIs28 [ced-10p::GFP::ced-10; unc-119(+); unc-119(ed4)	Lundquist et al. 2001. *Development* 128: 4475-4488.
RL262	mom-5(zu193)unc-13(e1091)/hT2 I; hT2/+ III; ruIs57[pie-1::GFP::tubulin unc-119(+)]	Liro & Rose 2016. Genetics 204: 1177–1189.
RL292	mes-1(bn7) IV; ruIs57[pie-1::GFP::tubulin unc-119(+)]	Liro & Rose 2016. Genetics 204: 1177–1189.
RL359	ced-10(t1875)dpy-20(e1282)/nT1[qIs51]	This study
RL393	ced-10(t1875) dpy-20(e1282)/ nT1 [qIs51(pha::GFP)] IV; ruIs57[pie-1::GFP::tubulin unc-119(+)]	This study
RL412	PAR-2::mCherry unc-119+ II; unc-119(ed3) III; ced-10(t1875)dpy-20(e1282)/nT1[qIs51] IV; ruIs57[pie-1::GFP::tubulin unc-119(+)]; +/nT1[qIs51] V	This study
RL440	qyIs28 [ced-10p::GFP::ced-10; unc-119(+); unc-119(ed4); ced-10(t1875)dpy-20(?)/nT1[qIs51] IV; +/nT1[qIs51] V	This study
RL443	par-2(it315[mCherry::PAR-2 unc-119(+)]) III; unc-119(ed3) III; GFP::tubulin V	This study
SV1589	lin-5 (he244[egfp::lin-5]) II	Portegijs et al. 2016. PLOS Genetics 12(10): e1006291.

TH246	unc-119(ed3) III; ddIs159[arx-2::TY1::EGFP::3xFLAG(92C12) + Cbr-unc-119(+)].	Sarov et al. 2012. Cell 150(4):855-66.

RNA interference

For all target genes, RNAi was performed by feeding as described, with the modification of adding IPTG to the bacterial culture, to a final concentration of 1mM, just prior to seeding the culture on the feeding plates(Ahringer 2006). Plates were kept in the dark at 4°C for no more than 5 days prior to use. Except for *ced-10*, all constructs were obtained from the Ahringer library (Kamath et al. 2003). Construct information, feeding conditions, and criteria for inclusion are listed in Table 3.

Table 3. Constructs and conditions used for RNAi

Construct (Cosmid no.)	Hours feeding	Temperature	Criteria for inclusion
arx-2 (V-7M13)	48-52h	20°C	Many small cortical extrusions at early embryonic stages (Pohl & Bao 2010); older siblings from same brood with failed ventral enclosure (Patel et al. 2008).
mom-2 (V-6A13)	36-48h	20°C	*mom-2(or42)* performed in parallel on *mes-1(bn7)* resulted in enhanced rate of late or failed EMS spindle rotations.
wve-1 (I-6A05)	48-52h	20°C	Many small cortical extrusions; older siblings from same brood with failed ventral enclosure (Shakir et al. 2008).

The *ced-10* RNAi clone we obtained from our institution's Ahringer library (IV-1J04) was sequenced and found to contain empty L4440 vector with no insert. We therefore generated an RNAi feeding construct by subcloning the *ced-10* cDNA region of pPR37 (constructed by Peter Reddien, courtesy of Erik Lundquist) into the L4440 vector using NcoI and SacI restriction enzymes. After confirming the sequence of the transformant clone in *E. coli* strain HT115, we scored EMS spindle rotation in *mom-5(zu193); ced-10(RNAi)* embryos to determine that CED-10 knockdown was sufficient to induce an enhanced EMS spindle phenotype after 48-52h feeding at

20°C. We also noted the presence of many small cortical extrusions at early embryonic stages, similar to the cortical instability we previously reported for *ced-10(t1875)* (Price, Lamb et al. 2022). We further demonstrated knockdown efficacy by quantifying the depletion of fluorescent protein in GFP::CED-10; *ced-10(RNAi)* embryos after 48-52h at 20°C. Exact protocols for each experiment using *ced-10(RNAi)* are listed in Table 4:

Table 4. Detailed protocols for RNAi depletion of CED-10

Reporter	Hours feeding	Temperature	Criteria for inclusion
anti-FLAG staining on mNG::3xFLAG::MES-1	28-29	Ambient (21-23°C)	Round embryos with many small cortical extrusions
GFP::SRC-1	48-52	16°C	*ced-10(RNAi)* on *mom-2(or42)* performed in parallel resulted in enhanced rate of late or failed EMS spindle rotations
GFP::POP-1	27-38	Ambient (21-23°C)	Round embryos with many small cortical extrusions, ~20% late or failed EMS spindle rotations
Gut granules	40-48	16°C	*ced-10(RNAi)* on *mom-2(or42)* performed in parallel resulted in enhanced rate of late or failed EMS spindle rotations
ARX-2::GFP	48-52	16°C	*ced-10(RNAi)* on *mom-2(or42)* performed in parallel resulted in enhanced rate of late or failed EMS spindle rotations
GFP::LIN-5	20-40	20°C	*ced-10(RNAi)* on GFP::CED-10 performed in parallel resulted in total absence of GFP::CED-10 cortical fluorescence

Live widefield microscopy

Embryos were removed from gravid hermaphrodites in 1x Egg Buffer, mounted on 2% agarose pads under coverslips, and observed on an Olympus BX60 microscope equipped with PlanApo N 60X, 1.42 NA oil immersion objective lens, a CoolLED light source, a Hamamatsu Orca 12-bit digital camera, and MicroManager software(Strange, Christensen et al. 2007),(Hardin 2011).

To score P1, EMS, and P2 spindle positioning, images were acquired every 10 s with an exposure of 10 ms in bright field illumination. Focus was manually adjusted to follow centrosomes during each division. In strains expressing GFP::tubulin, acquisition was switched to 488 nm light at approximately NEB of ABa and ABp to follow centrosomes and spindles more easily. Two strains without GFP::tubulin were used: WM43 [*gex-3(zu196)*] and [*mom-2(or42)*]. For these, centrosomes were followed by imaging with DIC microscopy and manually adjusting the focus.

To visualize P1 and P2 PAR-2::mCherry localization, single-plane images were acquired every 10 s from approximately NEB of ABa and ABp until the completion of P2 cytokinesis. Each acquisition exposed the sample to 200 ms of 560 nm light.

To visualize GFP::POP-1, 4-cell embryos were identified and observed under brightfield illumination until the completion of P2 cytokinesis. 5-6 minutes after P2 cytokinesis, two single-plane images were taken of each embryo, one in the central focal plane of the MS blastomere and one in the central focal plane of the E blastomere, with an exposure of 250 ms of 488 nm light for each image.

To visualize GFP::CED-10, single-plane images were acquired with an exposure of 100 ms every 30 s.

Confocal microscopy

Embryos were removed from gravid hermaphrodites and mounted on 2% agarose pads under coverslips. All the following fluorescent GFP reporters, except for GFP::LIN-5, were observed using the spinning disc module of an Intelligent Imaging Innovations (3i) Marianas SDC Real-Time 3D Confocal-TIRF microscope fit with a Yokogawa spinning disc head, a 60x 1.4 numerical aperture oil-immersion objective, and EMCCD camera. A 488 nm laser at 100%

power was used to illuminate samples. Acquisition was controlled by Slidebook 6 software (3i Incorporated). To visualize GFP::SRC-1, single-plane images were acquired with an exposure of 500 ms every 30 s. To visualize GFP::CED-10, single-plane images were acquired with an exposure of 250 ms every 30 s. To visualize ARX-2::GFP, Z-stack images were acquired with a total depth of 14 um and a step size of 2 um at an exposure of 500 ms every 30 s. Maximum Z projections were generated for a timepoint 30-90 s prior to EMS NEB, as scored by the loss of exclusion of fluorescent signal from the nucleus.

GFP::LIN-5 was observed on a Nikon Ti2 with a Yokogawa CSU-X1 spinning disc head, a 100x 1.45 numerical aperture oil-immersion objective, and a Hamamatsu ORCA Flash 4.0 camera. To visualize GFP::LIN-5, single-plane images were acquired with an exposure of 250 ms of 488 nm light at 25% laser power every 30 s.

Scoring of asymmetric division

P1 centrosomes were clearly visible under brightfield illumination. A “normal” P1 rotation was defined as a nucleo-centrosomal complex that achieved a near-perpendicular angle relative to the AB mitotic spindle prior to P1 NEB. A “late” P1 rotation was defined as a spindle that rotated onto a near-perpendicular angle after P1 NEB, but prior to P1 cytokinesis onset, and where the centrosome maintained close contact with the AB/P1 cell contact. A “failed” P1 rotation was defined as a spindle that did not rotate but maintained a near-parallel orientation relative to the AB mitotic spindle throughout the P1 division. Only embryos with “normal” P1 rotations, or “late” P1 rotations followed by asynchronous cell cycle timing of EMS and P2, were included in analysis of EMS and P2 spindle positioning.

A “normal” P1 PAR-2 domain was defined as a cap of mCherry::PAR-2 that formed on the posterior surface of the P1 cell before P1 NEB. A “misoriented” P1 PAR-2 domain was defined

as a restricted domain of mCherry::PAR-2 that formed on a part of the P1 surface other than the posterior.

EMS and P2 spindles were scored using GFP::tubulin labeled spindles. A “normal” EMS spindle rotation was defined as a nucleo-centrosomal complex that achieved a near-parallel orientation relative to the anterior/posterior body axis prior to EMS NEB. A “late” EMS rotation was defined as a spindle that rotated onto a parallel angle after EMS NEB, but prior to EMS cytokinesis onset. A “failed” EMS rotation was defined as a spindle that divided more than 45° off the anterior-posterior axis in any direction.

A “normal” P2 spindle orientation was defined as a nucleo-centrosomal complex that achieved an approximately 45 angle relative to the EMS spindle and oriented toward the EMS/P2 contact so that one centrosome appeared to be touching the contact. We noted that in all GFP::tubulin backgrounds, some P2 centrosomes appeared to migrate into the correct positions rather than migrating to opposite sides of the nucleus and then rotating as a unit into the correct orientation. An “abnormal” P2 spindle orientation was defined as a spindle that did not orient and translocate as just described.

A “normal” P2 PAR-2 domain was defined as a restricted domain of mCherry::PAR-2 that formed on the posterior-ventral corner of P2 before P2 NEB. “Abnormal” P2 PAR-2 domains included uniform presence of mCherry::PAR-2 on the entire surface of P2 and the presence of two distinct domains on the dorsal and ventral corners of P2 with clearing of mCherry::PAR-2 from the posterior cell surface in between.

To determine if embryos produced intestinal cells (an E derivative), embryos were mounted on agar pads as outlined for imaging of early divisions above. After filming some embryos to confirm spindle positioning phenotypes (e.g., in RNAi conditions), these and sibling embryos on

agar pads were incubated in a moist chamber at 16°C for 18-24 hr (a time by which wild type embryos hatched). Polarization optics were used to identify the presence of birefringent gut granules, which are a marker of intestinal differentiation (Laufer, Bazzicalupo et al. 1980).

Immunostaining

For immunostaining, embryos were dissected in PBS from gravid hermaphrodites onto slides coated with poly-L-lysine, then they were freeze-cracked according to (Duerr 2006). To stain SRC-1 dependent phosphotyrosine, slides were immediately fixed in prechilled methanol at -20°C for 5 min, followed by 5 min in ice-cold acetone. Slides were then air-dried at room temperature for 5-10 min or until fixatives had completely evaporated. Slides were rehydrated in PBS for 5 min. Nonspecific binding was prevented by gently pipetting 50 uL of blocking solution (5% w/v bovine serum albumin in PBS + 0.1% v/v Tween) onto the samples and incubating slides in a moist chamber for 2 hr at room temperature. After wicking excess blocking solution away with a Kimwipe on the edge of the slide, samples were incubated overnight in a 4°C moist chamber in 50 uL of primary antibody solution (Santa Cruz Biotech mouse monoclonal PY99 diluted 1:200 in PBS + 1% w/v bovine serum albumin + 0.1% v/v Tween). The following morning, slides were washed 3x in PBS + 0.1% v/v Tween. Excess PBS + Tween was wicked away with a Kimwipe; samples were covered with 50 uL secondary antibody solution (Alexa594-congugated goat monoclonal anti-mouse diluted 1:200 in PBS + 1% w/v bovine serum albumin + 0.1% v/v Tween) and incubated in a moist chamber for 2 hr at room temperature. Slides were washed 3x in PBS + 0.1% v/v Tween, once in PBS, and excess PBS was wicked away with a Kimwipe before mounting in 20 uL of Vectashield mounting medium with a 20 x 40 mm coverslip. The edges of the coverslip were carefully sealed with nail polish.

To stain mNG::3xFLAG::MES-1, the same protocol was used, omitting the acetone fixation and subsequent air-drying step. The primary antibody was Invitrogen mouse monoclonal anti-FLAG, diluted 1:500.

To visualize SRC-1-dependent phosphotyrosine staining and anti-FLAG staining on mNeonGreen::3xFLAG::MES-1, images were acquired in the focal plane of the EMS/P2 contact with an exposure of 200 ms of 560 nm light on the Olympus BX60 microscope described above. 4-cell embryos between EMS prophase and EMS anaphase onset, as scored by the appearance of DAPI-stained chromosomes in the UV channel, were analyzed.

Analysis of cortical fluorescence intensity

To quantify the relative enrichment of various fluorescent reporters at the EMS/P2 contact over other cell-cell contacts, the "Segmented Line" tool in ImageJ was used to trace a 3-pixel-wide line along the EMS/P2 contact as well as the EMS/ABp contact. The "Measure" function was used to determine the mean fluorescence intensity within the area covered by the line traces. The same line traces were placed approximately 5 pixels from the cell-cell contacts and well outside the dark nuclear regions to sample mean cytoplasmic fluorescence intensity within EMS, P2, and ABp. The fluorescence intensity of each cell-cell contact was then normalized to the mean cytoplasmic intensity of the two cells on either side of it. "Enrichment Index" was calculated as the ratio of cytoplasm-normalized EMS/P2 contact fluorescence to the ratio of cytoplasm-normalized EMS/ABp contact fluorescence. A value of 1 indicates no difference in relative cortical fluorescence intensity between the two cell-cell contacts, i.e., no enrichment.

Analysis of nuclear fluorescence intensity

To quantify the relative enrichment of GFP::POP-1 in the MS blastomere nucleus over the E blastomere nucleus, a circular region of interest (ROI) with a diameter of 55 pixels (~8μm) was

created in ImageJ and placed over each nucleus measured as well as the adjacent cytoplasm of the respective cell. The “Measure” function was used to determine the mean fluorescence intensity within the area covered by the ROI. The fluorescence intensity of each nucleus was then normalized to the mean cytoplasmic intensity of the cell containing it. “Nuclear Enrichment Index” was calculated as the ratio of cytoplasm-normalized MS nuclear fluorescence to the ratio of cytoplasm-normalized E nuclear fluorescence. A value of 1 indicates equally bright nuclei.

References

Arata, Y., Lee, J.-Y., Goldstein, B., & Sawa, H. (2010). Extracellular control of PAR protein localization during asymmetric cell division in the C. elegans embryo. *Development*(137), 3337-3345.

Bailly, C., Beignet, J., Loirand, G., & Sazeau, V. (2022). Rac1 as a therapeutic anticancer target: Promises and limitations. *Biochemical Pharmachology, 203*. doi:10.1016/j.bcp.2022.115180

Bei, Y., Hogan, J., Berkowitz, L. A., Soto, M., Rocheleau, C. E., Pang, K. M., . . . Mello, C. C. (2002). SRC-1 and Wnt signaling act together to specify endoderm and to control cleavage orientation in early C. elegans embryos. *Developmental Cell*, 113-125.

Berkowitz, L. A., & Strome, S. (2000). MES-1, a protein required for unequal divisions of the germline in early C. elegans embryos, resembles receptor tyrosine kinases and is localized to the boundary between the germline and gut cells. *Development, 127*, 4419-4431.

Bernadskaya, Y. Y., Patel, F. B., Hsu, H.-T., & Soto, S. C. (2011). Arp2/3 promotes junction formation and maintenance in the Caenorhabditis elegans intestine by regulating membrane association of apical proteins. *Molecular Biology of the Cell*, 2886-2899.

Boreaux, A., Vignal, E., Faure, S., & Fort, P. (2007). Evolution of the Rho Family of Ras-like GTPases in Eukaryotes. *Molecular Biology and Evolution, 24*(1), 203-216. doi:10.1093/molbev/msl145

Boyd, L., Guo, S., Levitan, D., Stinchcomb, D. T., & Kemphues, K. J. (1996). PAR-2 is asymmetrically distributed and promotes association of P granules and PAR-1 with the cortex in C. elegans embryos. *Development, 122*, 3075-3084.

Bustelo, X. R., Sazeau, V., & Berenjeno, I. M. (2007). GTP-binding proteins of the Rho/Rac family: regulation, effectors and functions in vivo. *BioEssays, 29*(4), 356-370. doi:10.1002/bies.2055

Cabello, J., Neukomm, L. J., Gunesdogan, U., Burkart, K., Charette, S. J., Lochnit, G., . . . Schnabel, R. (2010). The Wnt pathway controls cell death engulfment, spindle orientation, and migration through CED-10/Rac. *PLOS Biology*, e1000297.

Carminati, M., Gallini, S., Pirovano, L., Alfieri, A., Bisi, S., & Mapelli, M. (2016). Concomitant binding of Afadin to LGN and F-actin directs planar spindle orientation. *Nature Structural & Molecular Biology*, 155-163.

Chan, F.-Y., Silva, A. M., Saramago, J., Pereira-Sousa, J., Brighton, H. E., Pereira, M., . . . Carvalho, A. X. (2018). The ARP2/3 complex prevents excessive formin activity during cytokinesis. *Molecular Biology of the Cell, 30*, 96-107.

Chen, C., Fingerhut, J. M., & Yamashita, Y. M. (2016). The ins(ide) and outs(ide) of asymmetric stem cell division. *Current Opinion in Cell Biology*, 1-6.

Chircop, M. (2014). Rho GTPases as regulators of mitosis and cytokinesis in mammalian cells. *Small GTPases*. doi:10.4161/sgtp.29770

D'avino, P. P., Glover, D., & Glover, D. M. (2005). Cleavage furrow formation and ingression during animal cytokinesis: a microtubule legacy. *Journal of Cell Science*, 1549-1558.

Dewey, E. B., & Johnston, C. A. (2017). Diverse mitotic functions of the cytoskeletal cross-linking protein Shortstop suggest a role in Dynein/Dynactin activity. *Molecular Biology of the Cell*, 2555-2568.

di Pietro, F., Echard, A., & Morin, X. (2016). Regulation of mitotic spindle orientation: an integrated view. *EMBO reports*, 1106-1130.
Dickinson, D. J., Schwager, F., Pintard, L., Gotta, M., & Goldstein, B. (2017). A single-cell biochemistry approach reveals PAR complex dynamics during cell polarization. *Developmental Cell, 42*, 416-434.
Duquette, P. M., & Lamache-Vane, N. (2014). Rho GTPases in embryonic development. *Small GTPases, 5*(2), 1-9. doi:10.4161/sgtp29716
Gillies, T. E., & Cabernard, C. (2011). Cell Division Orientation in Animals. *Current Biology, 21*, R599-R609. doi:10.1016/j.cub.2011.06.055
Griffin, E. (2015). Cytoplasmic localization and asymmetric division in the early embryo of Caenorhabditis elegans. *WIREs Dev Biol*(4), 267-282. doi:10.1002/wdev.177
Griffin, E. E., Odde, D. J., & Seydoux, G. (2011). Regulation of the MEX-5 gradient by a spatially segregated kinase/phosphate cycle. *Cell, 146*, 955-958.
Guo, S., & Kemphues, K. J. (1995). par-1, a gene required for establishing polarity in C. elegans embryos, encodes a putative Ser/Thr kinase that is asymmetrically distributed. *Cell, 81*, 611-620.
Hall, A. (2012). Rho family GTPases. *Biochemical Society Transactions, 40*(6), 1378-1383. doi:10.1042/BST20120103
Heppert, J. K., Pani, A. M., Roberts, A. M., Dickinson, D. J., & Goldstein, B. (2018). A CRISPR tagging-based screen reveals localized players in Wnt-directed asymmetric cell division. *Genetics*, 1147-1164.
Hsu, T.-Y., & Wu, Y.-C. (2010). Engulfment of apoptotic cells in C. elegans is mediated by integrin alpha/SRC signaling. *Current Biology*, 477-486.
Inaba, M., & Yamashita, Y. M. (2012). Asymmetric Stem Cell Division: Precision for Robustness. *Cell Stem Cell*(11), 461-469.
Ishidate, T., Elewa, A., Kim, S., Mello, C. C., & Shirayama, M. (2014). Divide and differentiate: CDK/cyclins and the art of development. *Cell Cycle, 13*(9), 1384-1391.
Kemphues, K. J., Priess, J. R., Morton, D. G., & Cheng, N. S. (1988). Identification of genes required for cytoplasmic localization in early C. elegans embryos. *Cell, 52*, 311-320.
Kim, S., Ishidate, T., Sharma, R., Soto, M. C., Conte, D., Mello, C. C., & Shirayama, M. (2013). Wnt and CDK-1 regulate cortical release of WRM-1/beta-catenin to control cell division orientation in early Caenorhabditis elegans embryos. *PNAS*, E918-E927.
Kiyomitsu, T., & Cheeseman, I. M. (2013). Cortical dynein and asymmetric membrane elongation coordinately position the spindle in anaphase. *Cell*, 391-402.
Krueger, L. E., Wu, J. C., Tsou, M. F., & Rose, L. S. (2010). LET-99 inhibits lateral posterior pulling forces during asymmetric spindle elongation in C. elegans embryos. *Journal of Cell Biology, 189*, 481-495.
Kwon, M., Bagonis, M., Danuser, G., & Pellman, D. (2015). Direct microtubule-binding by Myosin-10 orients centrosomes toward retraction fibers and subcortical actin clouds. *Developmental Cell*, 323-337.
Lancaster, O. M., & Baum, B. (2014). Shaping up to divide: Coordinating actin and microtubule cytoskeletal remodelling during mitosis. *Seminars in Cell & Developmental Biology, 34*, 109-115.
Lang, C. F., & Munro, E. (2017). The PAR proteins: from molecular circuits to dynamic self-stabilizing cell polarity. *Development, 144*, 3405-3416. doi:10.1242/dev.139063

Lin, R., Thompson, S., & Priess, J. R. (1995). pop-1 encodes an HMG box protein required for the specification of a mesoderm precursor in early C. elegans embryos. *Cell, 83*, 599-609.
Liro, M. L., & Rose, L. S. (2016). Mitotic spindle positioning in the EMS cell of C. elegans requires LET-99 and LIN-5/NuMA. *Genetics*, 1177-1189.
Liro, M. L., Morton, D., & Rose, L. S. (2018). The kinases PIG-1 and PAR-1 act in redundant pathways to regulate asymmetric division in the EMS blastomere of C. elegans. *Developmental Biology*, 9-19.
Liu, J., Maduzia, L. L., Shirayama, M., & Mello, C. C. (2010). NMY-2 maintains cellular asymmetry and cell boundaries, and promotes a SRC-dependent asymmetric cell division. *Developmental Biology*(339), 366-373. doi:10.1016/j.ydbio.2009.12.04
Lundquist, E. A., Reddien, P. W., Hartwieg, E., Horvitz, H., & Bargmann, C. I. (2001). Three C. elegans Rac proteins and several alternative Rac regulators control axon guidance, cell migration and apoptotic cell phagocytosis. *Development, 128*, 4475-4488.
Machicoane, M., de Frutos, C. A., Fink, J., Rocancourt, M., Lombardi, Y., Garel, S., . . . Echard, A. (2014). SLK-dependent activation of ERMs controls LGN-NuMA localization and spindle orientation. *Journal of Cell Biology*, 791-799.
Mattila, P. K., Batista, F. D., & Treanor, B. (2016). Dynamics of the actin cytoskeleton mediates receptor cross talk: An emerging concept in tuning receptor signaling. *J Cell Biol, 212*(3), 267-280.
McNally, F. J. (2013). Mechanisms of spindle positioning. *Journal of Cell Biology*, 131-140.
Morin, X., & Bellaiche, Y. (2011). Mitotic spindle orientation in asymmetric and symmetric cell divisions during animal development. *Developmental Cell*, 102-119.
Morton, D. G., Hoose, W. A., & Kemphues, K. J. (2012). A genome-wide RNAi screen for enhancers of par mutants reveals new contributors to early embryonic polarity in Caenorhabditis elegans. *Genetics, 192*, 929-942.
Nakamura, K., Kim, S., Ishidate, T., Bei, Y., Pang, K., Shirayama, M., . . . Mello, C. C. (2005). Wnt signaling drives WRM-1/beta-catenin asymmetries in early C. elegans embryos. *Genes & Development, 19*, 1749-1754.
Nguyen, L. K., Kholodenko, B. N., & von Kriegsheim, A. (2018). Rac1 and RhoA: Networks, loops and bistability. *Small GTPases, 9*(4), 316-321. doi:10.1080/21541248.2018.1224399
Park, D. H., & Rose, L. S. (2008). Dynamic localization of LIN-5 and GPR-1/2 to cortical force generation domains during spindle positioning. *Developmental Biology*, 42-52.
Park, F. D., Tenlen, J. R., & Priess, J. R. (2005). C. elegans MOM-5/Frizzled functions in MOM-2/Wnt-independent cell polarity and is localized asymmetrically prior to division. *Curr. Biol., 14*, 22582-2258. doi:10.1016/j.cub.2004.12.019
Patel, F. B., Bernadskaya, Y. Y., Chen, E., Jobanputra, A., Pooladi, Z., Freeman, K. L., . . . Soto, M. C. (2008). The WAVE/SCAR complex promotes polarized cell movements and actin enrichment in epithelia during C. elegans embryogensis. *Developmental Biology, 324*, 297-309.
Portegijs, V., Fielmich, L.-E., Galli, M., Schmidt, R., Munoz, J., van Mourik, T., . . . van den Heuvel, S. (2016). Multisite phosphorylation of NuMA-related LIN-5 controls mitotic spindle positioning in C. elegans. *PLoS Genetics*. doi:10.1371/journal.pgen.1006291
Rakotomamonjy, J., Brunner, M., Juschke, C., Zang, K., Huang, E. J., Reichardt, L. F., & A., C. (2017). Afadin controls cell polarization and mitotic spindle orientation in developing cortical radial glia. *Neuronal Development*, 7.

Rocheleau, C. E., Downs, W. D., Lin, R., Wittmann, C., Bei, Y., Cha, Y. H., . . . Mello, C. C. (1997). Wnt signaling and an APC-related gene specify endoderm in early C. elegans embryos. *Cell*(90), 707-716.

Rodriguez, J., Peglion, F., Martin, J., Hubatsch, L., Reich, J., Hirani, N., . . . Goehring, N. W. (2017). aPKC cycles between functionally distinct PAR protein assemblies to drive cell polarity. *Developmental Cell, 42*, 400-415.

Rose, L. S., & Gonczy, P. (2014). Polarity establishment, asymmetric division and segregation of fate determinants in early C. elegans embryos. *WormBook: The Online Review of C. Elegans Biology*.

Rose, L. S., & Kemphues, K. (1998). The let-99 gene is required for proper spindle orientation during cleavage of the C. elegans embryo. *Development, 125*, 1337-1346.

Saenz-Narciso, B., Gomez-Orte, E., Zheleya, A., Gastaca, I., & Cabello, J. (2016). Control of developmental networks by Rac/Rho small GTPases: How cytoskeletal changes during embryogenesis are orchestrated. *Bioessays*, 1246-1254.

Sandquist, J. C., Kita, A. M., & Bement, W. M. (2011). And the dead shall rise: Actin and myosin return to the spindle. *Developmental Cell*, 410-419.

Sandquist, J. C., Larson, M. E., & Hine, K. J. (2016). Myosin-10 independently influences mitotic spindle structure and mitotic progression. *Cytoskeleton*, 351-364.

Sarov, M., Murray, J. I., Schanze, K., Pozniakovski, A., Niu, W., Angermann, K., . . . Hyman, A. A. (2012). A genome-scale resource for in vivo tag-based protein function exploration in C. elegans. *Cell, 150*(4), 855-866.

Sawa, M., Suetsugu, S., Sugimoto, A., Miki, H., Yamamoto, M., & Takenawa, T. (2003). Essential role of the C. elegans Arp2/3 complex in cell migration during ventral enclosure. *Journal of Cell Science*, 1505-1518.

Schierenberg, E. (1987). Reversal of cellular polarity and early cell-cell interaction in the embryo of Caenorhabditis elegans. *Developmental Biology, 122*, 452-463.

Schlesinger, A., Shelton, C. A., Maloof, J. N., Meneghini, M., & Bowerman, B. (1999). Wnt pathway components orient a mitotic spindle in the early Caenorhabditis elegans embryo without requiring gene transcription in the responding cell. *Genes & Development, 13*, 2028-2038.

Seldin, L., Poulson, N. D., Foote, H. P., & Lechler, T. (2013). NuMA localization, stability, and function in spindle orientation involve 4.1 and Cdk1 interactions. *Molecular Biology of the Cell*, 3651-3662.

Shakir, A. M., Jiang, K., Struckhoff, E. C., Demarco, R. S., Patel, F. B., Soto, M. C., & Lundquist, E. A. (2008). The Arp2/3 activators WAVE and WASP have distinct genetic interactions with Rac GTPases in Caenorhabditis elegans axon guidance. *Genetics, 179*, 1957-1971. doi:10.1534/genetics.108.088963

Shivas, J. M., & Skop, A. R. (2012). Arp2/3 mediates early endosome dynamics necessary for the maintenance of PAR asymmetry in C. elegans . *Mol. Biol. of the Cell, 23*, 1917-1927.

Soto, M. C., Qadota, H., Kasuya, K., Inoue, M., Tsuboi, D., Mello, C. C., & Kaibuchi, K. (2002). The GEX-2 and GEX-3 proteins are required for tissue morphogenesis and cell migrations in C. elegans. *Genes & Development*, 620-632.

Srinivasan, D. G., Fisk, R. M., Xu, H., & van den Heuvel, S. (2003). A complex of LIN-5 and GPR proteins regulates G protein signaling and spindle function in C. elegans. *Genes & Development*, 1225-1239.

Sugioka, K., & Sawa, H. (2010). Regulation of asymmetric positioning of nuclei by Wnt and Src signaling and its roles in POP-1/TCF nuclear asymmetry in Caenorhabditis elegans. *Genes to Cells*(15), 397-407. doi:10.1111/j.1365-2443.2010.01388.x

Sugioka, K., Fielmich, L.-E., Mizumoto, K., Bowerman, B., van den Heuvel, S., Kimura, A., & Sawa, H. (2017). Tumor suppressor APC is an attenuator of spindle-pulling forces during C. elegans asymmetric cell division. *Proc. Natl. Acad. Sci.*, 954-963. doi:www.pnas.org/cgi/doi/10.1073/pnas.1712052115

Sugioka, K., Mizumoto, K., & Sawa, H. (2011). Wnt regulates spindle asymmetry to generate asymmetric nuclear B-catenin in C. elegans. *Cell, 146*(6), 942-954. doi:https://doi.org/10.1016/j.cell.2011.07.043

Sugioka, K., Mizumoto, K., & Sawa, H. (2011). Wnt regulates spindle asymmetry to generate asymmetric nuclear beta-catenin in C. elegans. *Cell, 146*, 942-954.

Sumiyoshi, E., Takahashi, S., Obata, H., Sugimoto, A., & Kohara, Y. (2011). The b-catenin HMP-2 functions downstream of Src in parallel with the Wnt pathway in early embryogenesis of C. elegans. *Developmental Biology, 355*, 302-312. doi:10.1016/j.ydbio.2011.04.034

Thorpe, C. J., Schlesinger, A., Carter, J. C., & Bowerman, B. (1997). Wnt signaling polarizes an early C. elegans blastomere to distinguish endoderm from mesoderm. *Cell*(90), 695-705.

Venkei, Z. G., & Yamashita, Y. M. (2018). Emerging mechanisms of asymmetric stem cell division. *Journal of Cell Biology*, 3785-3795.

Walston, T., Tuskey, C., Edgar, L., Hawkins, N., Ellis, G., Bowerman, B., . . . Hardin, J. (2004). Multiple Wnt signaling pathways converge to orient the mitotic spindle in early C. elegans embryos. *Developmental Cell*, 831-841.

Wang, S.-C., Low, T. Y., Nishimura, Y., Gole, L., Yu, W., & Motegi, F. (2017). Cortical forces and CDC-42 control clustering of PAR proteins for Caenorhabditis elegans embryonic polarization. *Nature Cell Biology, 19*(8), 988-995.

Werts, A. D., Roh-Johnson, M., & Goldstein, B. (2011). Dynamic localization of C. elegans TPR-GoLoco proteins mediates mitotic spindle orientation by extrinsic signaling. *Development*, 4411-4422.

Wodarz, A., Ramrath, A., Grimm, A., & Knust, E. (2000). Drosophila atypical protein kinase C associates with Bazooka and controls polarity of epithelia and neuroblasts. *Journal of Cell Biology, 150*, 1361-1374.

Woolner, S., O'Brien, L. L., Wiese, C., & Bement, W. M. (2008). Myosin-10 and actin filaments are essential for mitotic spindle function. *Journal of Cell Biology*, 77-88.

Xiong, H., Mohler, W. A., & Soto, M. C. (2011). The branched actin nucleator Arp2/3 promotes nuclear migrations and cell polarity in the C. elegans zygote. *Dev. Biol*, 356-369.

Zhang, H., Skop, A. R., & White, J. G. (2007). Src and Wnt signaling regulate dynactin accumulation to the P2-EMS cell border in C. elegans embryos. *Journal of Cell Science*, 155-161.

Zhu, Z., Chai, Y., Hu, H., Li, W., Li, W.-J., Dong, M.-Q., . . . Ou, G. (2020). Spatial confinement of receptor activity by tyrosine phosphatase during directional cell migration. *Proc. Natl. Acad. Sci., 117*(25), 14270-14279. doi:10.1073/pnas.200301911

Ziel, J. W., Hagedorn, E. J., Audhya, A., & Sherwood, D. R. (2009). UNC-6 (netrin) orients the invasive membrane of the anchor cell in C. elegans. *Nature Cell Biology, 11*, 183-189. doi:10.1038/ncb1825

Supplements

Table S1. Comparison of aspect ratios across selected genotypes.

Genotype	Mean	SD	n	vs control (Dunnett's Multiple Comparisons Test)
Control	1.57	0.10	12	--
mom-2(RNAi)	1.55	0.09	9	0.5644
ced-10(t1875)	1.34	0.11	10	0.0002
ced-10(t1875); mom-2(RNAi)	1.30	0.16	11	<0.0001

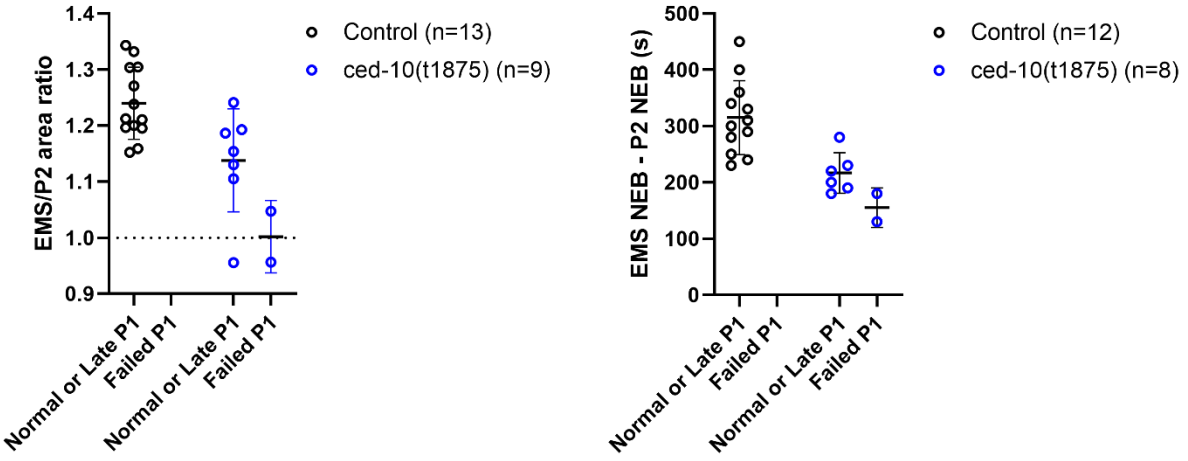

Figure S1. Failed P1 spindle rotation corresponds with equalized daughter cell sizes and synchronized cell cycles at the four-cell stage.
(A) Comparison between control embryos and *ced-10(t1875)* embryos of the ratio of EMS area to P2 area immediately following P1 cytokinesis.
(B) Comparison between control embryos and *ced-10(t1875)* embryos of the interval in seconds between EMS NEB and P2 NEB.

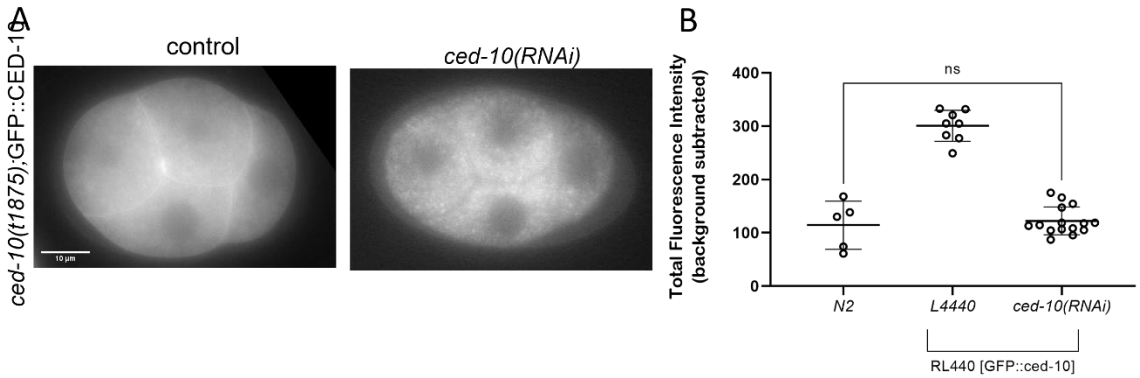

Figure S2. *ced-10* RNAi decreases fluorescence in a GFP::CED-10 transgenic line.
(A) Representative images from widefield fluorescent microscopy of GFP::CED-10 rescue embryos with and without *ced-10(RNAi)*.
(B) Quantification of total background-corrected embryonic fluorescence intensity of GFP::CED-10 rescue embryos with and without *ced-10(RNAi)*.

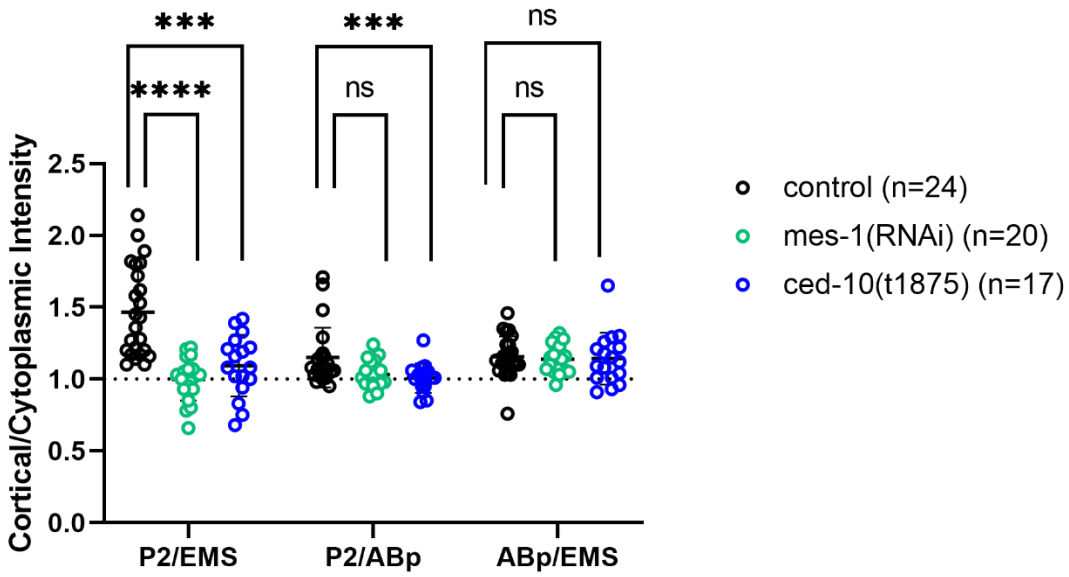

Figure S3. Cortical phosphotyrosine signal in *ced-10(t1875)* embryos is decreased substantially at the EMS/P2 contact and slightly at the P2/ABp contact. The cortical signal intensity, normalized to cytoplasm, at the EMS/P2 contact, the P2/ABp contact, and the EMS/ABp contact are compared across the indicated genotypes.

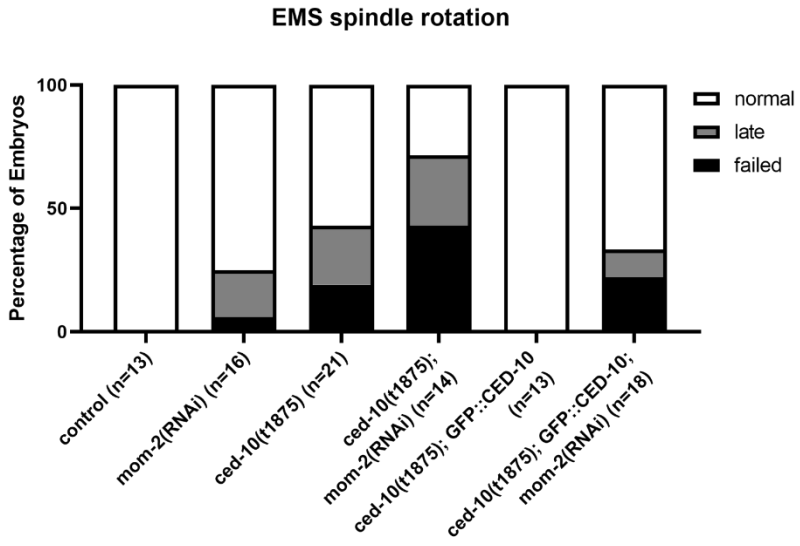

Fig. S4. GFP::CED-10 transgene rescues key *ced-10* phenotypes in a *ced-10(t1875)* background.
(A) Percentage of scored embryos with normal, late, and failed EMS spindle rotations for the indicated genotypes in a GFP::tubulin background vs a GFP::CED-10 transgenic rescue background. Note that the datasets used for "control," "*mom-2(RNAi)*," "*ced-10(t1875)*," and "*ced-10(t1875);mom-2(RNAi)*" are the same as in Figure 1.

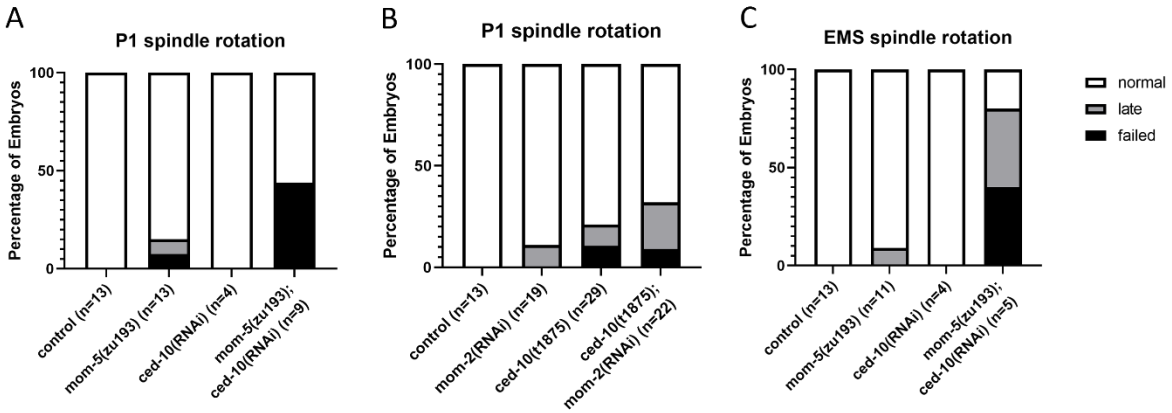

Figure S5. *ced-10(RNAi)* enhances the rate of *mom-5(zu193)* spindle rotation defects in P1 and EMS.
(A) Percentage of scored embryos with normal, late, and failed P1 spindle rotations for the indicated genotypes in a GFP::tubulin background.
(B) Percentage of scored embryos with normal, late, and failed P1 spindle rotations for the indicated genotypes in a GFP::tubulin background.
(C) Percentage of scored embryos with normal, late, and failed EMS spindle rotations for the indicated genotypes in a GFP::tubulin background. Only embryos with normal P1 spindle rotation were included in the analysis.

Chapter IV

Conclusions and Future Directions

Asymmetric cell division is essential for the creation of cell types with different identities and functions. The cytoskeleton is an essential component of the molecular machinery required to achieve asymmetric cell division: a molecular cue prompts the microtubule based mitotic spindle to align according to the axis of cellular asymmetry, following which the mitotic spindle instructs the formation of an actin- and myosin-based contractile ring that performs cytokinesis, or the physical separation of the two daughter cells. Coordination of the microtubule cytoskeleton and the actomyosin cytoskeleton is therefore critically important for successful asymmetric division.

Here I have presented my contributions to two research projects related to cytoskeletal regulation during asymmetric cell division, with an emphasis on identifying regulators of the actin cytoskeleton, defining their roles, and understanding how they work together to modulate the balance of different forms of actin. The first project aims to understand the role of the DEPDC1 homolog LET-99, previously characterized as a negative regulator of the dynein-containing force generating complex during spindle positioning. With others, I demonstrated that during the first mitotic division LET-99 and a Rac1 homolog, CED-10, play opposing roles in the regulation of cortical branched actin. The precise balance between the activities of these two proteins promotes robust and timely cytokinesis. In the second project, I investigated the role of CED-10 in spindle orientation of the asymmetrically dividing EMS cell. I determined that CED-10 works upstream or at the level of SRC-1 in the previously identified MES-1/SRC-1 signaling pathway that promotes EMS spindle orientation and furthermore that CED-10 contributes to cortical localization of the same dynein-containing force generating complex.

Although this research was performed in nematodes, the results have broad implications for all animals because most of the molecular components involved are evolutionarily conserved. By understanding in detail the mechanisms of different types of asymmetric divisions, we can understand both normal development and diseases such as cancer, which involves the dysregulation of asymmetric division.

Summary of key findings

LET-99 and CED-10 have antagonistic roles in regulating the balance of branched vs linear actin during cytokinesis. These roles appear to be global rather than spatially restricted to the contractile ring. LET-99's role as a regulator of cytokinesis is separable from its role in spindle positioning; furthermore, CED-10 has no role in P0 spindle positioning. However, CED-10 does regulate spindle positioning at the four-cell stage, where it acts downstream of MES-1, but upstream of SRC-1, to promote EMS spindle rotation and endoderm fate specification. There is some evidence that CED-10's molecular function in this context may be to promote branched actin formation at the EMS/P2 contact, but this evidence is partially contradicted by our findings that loss of the branched-actin regulator GEX-3 does not enhance the rate of EMS spindle rotation defects in Wnt/MOM-2-depleted embryos. An additional curious finding is that CED-10 has a previously unreported role in P1 spindle rotation, as do the branched actin nucleator Arp2/ARX-2 (Arp2) and the Frizzled ortholog MOM-5.

Outstanding questions regarding CED-10's role in EMS asymmetric division

Two key experiments demonstrated that CED-10 does not affect MES-1 protein localization, nor is it required for MES-1 dependent asymmetric division in the P2 cell. However, the reverse relationship was not tested. It is possible that in CED-10 works

independently of MES-1 to regulate SRC-1 and/or SRC-1 phosphorylation targets. Future experiments should test whether MES-1 affects the cortical localization and/or activity of CED-10 during EMS asymmetric division. This information could inform more detailed hypotheses regarding the mechanism of SRC-1 regulation by CED-10.

A possible mechanistic connection between CED-10 and SRC-1 exists in p21-associated kinases (PAKs). In mammalian systems as well as in worms, Rac1/CED-10 activates not only branched actin regulators, but also myosin and a host of other targets through PAKs (Chircop 2014), (Kumar, Sanawar et al. 2017), (Nguyen, Kholodenko et al. 2018). Importantly, in the four-cell *C. elegans* embryo, proper localization of SRC-1 dependent phosphotyrosine has been shown to require activated myosin (Liu, Maduzia et al. 2010). On a related note, although we have ruled out a model in which CED-10 promotes the enrichment of SRC-1 protein itself at the EMS/P2 contact, our limited knowledge of SRC-1 phosphorylation targets in this context and our lack of a reporter for active SRC-1 make it impossible to distinguish whether CED-10 is required for SRC-1 activation, for recruitment and/or retention of active SRC-1 at the EMS/P2 contact, or for recruitment and/or retention of some or all SRC-phosphorylation targets at the EMS/P2 contact. However, at least one promising avenue of investigation exists: the divergent β-catenin HMP-2 has been identified as a possible substrate for SRC-1 kinase activity in EMS asymmetric division, where it is removed from the EMS/P2 contact in an SRC-1 dependent manner. In the E daughter cell, HMP-2 localization to the nucleus is required for endoderm fate specification redundantly with Wnt-instructed nuclear import of a different β-catenin, WRM-1. HMP-2 is further required for ABar spindle positioning in parallel with the Wnt pathway (Sumiyoshi, Takahashi et al. 2011). Although HMP-2 was not tested directly for a role in EMS spindle positioning, the existing evidence provides a strong rationale for doing so. I did attempt to

characterize HMP-2 localization in the four-cell embryo using a GFP reporter generated by CRISPR/Cas9 (Marston, Higgins et al. 2016), but fluorescent signal was not detectable at this stage. Future studies could use immunofluorescence to detect HMP-2.

Because CED-10 has been identified as a member of a Wnt/Frizzled pathway in the asymmetric division of the ABar cell, we expected that our genetic analyses would place CED-10 in the Wnt/Frizzled pathway for EMS spindle positioning as well (Cabello, Neukomm et al. 2010). However, we found that CED-10 works in the MES-1/SRC-1 pathway rather than the Wnt/Frizzled pathway. Several of our other results were surprising as well. First were the seemingly contradictory observations that depletion of the branched actin nucleator ARP-2, which is enriched at the EMS/P2 contact in a CED-10 dependent manner, enhances the EMS spindle defect of *mom-5* (Frizzled), but the WAVE complex component GEX-3 (NCKAP1) has no EMS phenotype even in combination with MOM-2 (Wnt) depletion. A possible explanation for this finding is that mammalian Rac1 can promote branched actin formation through not only the WAVE complex but also the WASp complex, although others have shown that in the later *C. elegans* embryo CED-10 works preferentially through WAVE for morphogenesis and axon guidance (Soto, Qadota et al. 2002), (Bustelo, Sazeau et al. 2007), (Shakir, Jiang et al. 2008), (Saenz-Narciso, Gomez-Orte et al. 2016). Another possibility, not mutually exclusive with the first, is that we uncovered a ligand-independent role for MOM-5 parallel with both the MES-1/SRC-1 pathway and MOM-5's known function as a receptor for MOM-2. In many other model organisms, the Frizzled receptor can initiate signaling by localizing to a restricted domain on the cell membrane; this mechanism is the basis of planar cell polarity signaling (Yang and Mlodzik 2015). Evidence for a similar phenomenon in worms exists in the one-cell embryo, where MOM-5 is required to restrict localization of the Adenomatous Polyposis Coli (APC) homolog APR-1

to the anterior cortex. APR-1, in turn, attenuates microtubule pulling forces and thereby contributes to spindle positioning (Sugioka, Fielmich et al. 2017). Importantly, MOM-5 localizes to the posterior membrane of multiple asymmetrically dividing somatic cells, and APR-1 localizes to the anterior cortex of EMS itself (Park, Tenlen et al. 2005), (Sugioka, Mizumoto et al. 2011). An interesting note is that APR-1 has previously been implicated in endoderm fate specification, but not in EMS spindle positioning (Rocheleau, Downs et al. 1997). This would be consistent with not two but three partially redundant pathways ensuring a robust spindle rotation in EMS.

Additional support for this notion of a third, MOM-5 and APR-1 dependent, spindle positioning mechanism comes from the fact that in a substantial proportion of embryos lacking both MOM-5 and Arp2 or CED-10, the asymmetric division of P1 at the two-cell stage was defective. Although P1 division is thought to be instructed by a PAR and dynein-dependent mechanism very similar to the one at work in P0, the existing evidence does not rule out a second, redundant pathway to ensure normal P1 spindle rotation (Rose and Gonczy 2014). The role of branched actin here is not obvious; although branched actin has been shown to promote the maintenance of robust PAR domains in the zygote and other embryonic stages, our results indicate that PAR-2 localization in these embryos is grossly normal (Shivas and Skop 2012). Regardless, it is apparent that branched actin does play a role in P1 spindle rotation, and that it does so in parallel with a mechanism involving the Frizzled homolog MOM-5. Whether APR-1 contributes to P1 division remains to be seen.

Another open question is the nature of the relationships between CED-10 and two other recently identified members of the MES-1/SRC-1 signaling pathway, PIG-1 and LET-99. First implicated in asymmetric neuroblast division, PIG-1 is the worm ortholog of the maternal

embryonic leucine zipper kinase (MELK). Mammalian MELK requires phosphorylation for its own kinase activity, and in *C. elegans* neuroblast division PIG-1 is phospho-activated by PAR-4 (Ganguly, Mohyeldin et al. 2015). Work by Liro and colleagues has identified an additional role for PIG-1 in EMS asymmetric division, where it works in the MES-1/SRC-1 pathway for both spindle orientation and endoderm specification but only slightly influences the accumulation of enriched phosphotyrosine at the EMS/P2 contact (Liro, Morton et al. 2018). These observations place PIG-1 downstream of SRC-1 but upstream of both SRC-1-dependent processes, pointing to the possibility that SRC-1 could phospho-activate PIG-1 in this context. If this is the case, I predict CED-10 would be required for PIG-1 activation.

LET-99, a homolog of mammalian DEP Domain Containing 1 (DEPDC1) that is best known for its role in spindle positioning during the first asymmetric division of P0, was also recently found by our lab to contribute to the MES-1/SRC-1 pathway for EMS asymmetric division (Liro and Rose 2016). In the context of P0 division, it localizes primarily in a posterior-lateral band at the cortex where it functions as a negative regulator of the dynein-containing force generating complex to promote asymmetric microtubule pulling forces (Tsou 2002), (Krueger, Wu et al. 2010). At the four-cell stage, it initially localizes to cell-cell contacts and is removed from the EMS/P2 contact over the course of the EMS cell cycle. Given these observations and the fact that loss of LET-99 suppresses rather than enhances the EMS spindle rotation defects observed in Wnt pathway mutants, the authors concluded that LET-99 works as a negative regulator of unknown targets, possibly including the same force generating complex, during the asymmetric division of EMS (Liro and Rose 2016). It would be interesting to test whether CED-10 and LET-99 interact genetically and/or at a molecular level during EMS asymmetric division.

Finally, our results are consistent with previous reports that LIN-5 localization is not asymmetric in EMS (Heppert, Pani et al. 2018). How does the EMS spindle rotate (i.e., how are asymmetric microtubule pulling forces generated) if that is the case? I propose that APR-1 and LET-99 could be the downstream signaling targets of Wnt/Frizzled and MES-1/SRC-1, respectively, that are partially or completely responsible for asymmetric pulling forces. The localization pattern of LET-99 opposes almost precisely the localization patterns of MES-1 and SRC-1 dependent phosphotyrosine, and indeed its removal from the EMS/P2 contact requires MES-1 function (Berkowitz and Strome 2000), (Bei, Hogan et al. 2002), (Tsou, Hayashi et al. 2003). Similarly, APR-1 localizes to the anterior, dorsal, and ventral cortices of EMS, but not the EMS/P2 contact, in a Wnt and Disheveled dependent manner (Sugioka, Mizumoto et al. 2011), (Heppert et al. 2018). These observations lend plausibility to the hypothesis that dynein-dependent cortical microtubule pulling forces are negatively regulated globally in EMS, except at the EMS/P2 contact where Wnt/Frizzled and MES-1/SRC-1 signaling remove the negative regulators.

Outstanding questions regarding LET-99's role in cytokinesis

In addition to its function as a negative regulator of spindle positioning in both the P lineage and now EMS, LET-99 has also been shown to contribute to cytokinesis in both symmetric and asymmetric division (Bringmann, Cowan et al. 2007), (Price and Rose 2017). Chapter II reports work done in collaboration with Kari Price and others that further characterizes the role of LET-99 in cytokinesis of not only P0 but also the first somatic cell, AB. During anaphase, LET-99 localizes to the nascent cytokinetic furrow via a PAR-independent, spindle-dependent mechanism. Two redundant signaling pathways from the mitotic spindle promote the concentration of RhoA, a small G protein and key cytoskeletal regulator, to the same

region of the cortex to initiate assembly of the actin and myosin based contractile ring (Miller 2011), (Chircop 2014). Our lab recently showed that LET-99 can respond to either pathway (Price and Rose 2017). Here we demonstrate that loss of LET-99 does not affect localization of a fluorescent reporter for active RhoA, which implies that LET-99 works either downstream of or in parallel with RhoA. Furthermore, we found that LET-99 globally downregulates the formation of branched actin in favor of linear actin, and that this function is central to LET-99's ability to ensure robust furrow formation and timely cytokinesis.

These findings, and the fact that LET-99 possesses a RhoGAP like domain that might allow interaction with Rho family GTP aces, raise two interesting questions: first, does RhoA regulate LET-99, or does LET-99 function independently? Second, what effectors or intermediates are required for LET-99 regulation of branched actin? Intriguingly, we identified a genetic interaction between LET-99 and CED-10, the same RAC-1 homolog found to act in EMS spindle positioning as well as multiple branched actin dependent developmental processes. Specifically, we showed that loss of CED-10 restores the timing of cytokinesis onset in *let-99* mutants. Do these two proteins interact directly or through an intermediate, or do they work independently to regulate branched vs linear actin? Our lab has identified a candidate intermediate in Calponin Homology Domain Protein 1 (CHDP-1), which has previously been shown to work as a cortical anchor for CED-10 during formation of actin-rich cell protrusions (Guan, Ma et al. 2016). In unpublished immunoprecipitation experiments, Kari Price and Małgorzata Liro have identified CHDP-1 as a binding partner of LET-99. Future work will investigate the possibility that these three proteins work together to regulate cortical branched actin.

Any discussion of cytokinesis that does not mention the central role of myosin in generating contractile forces is incomplete. This motor protein "walks" on and crosslinks actin filaments, whether they are in a branched or linear configuration, and is required for PAR polarity establishment in the zygote, cytokinesis in all cells, and numerous other processes (Miller 2011, Lang and Munro 2017). As mentioned previously, active RhoA recruits myosin to the contractile ring. Our lab has recently shown that loss of LET-99 reduces nonmuscle myosin levels is it the contractile ring (Price and Rose 2017). It will be interesting to investigate whether LET-99 promotes myosin accumulationto the furrow as a downstream effector of RhoA or via an independent mechanism, and whether it does so through a specific mechanism or simply as a consequence of altered actin dynamics. Another key question is whether CED-10 has any effect on myosin concentration at the furrow, in which case I would predict that the normal timing of cytokinesis onset in *ced-10;let-99* double mutants could be explained by restored levels of myosin there. I have made extensive attempts to address this latter question, but have been unable to draw strong conclusions from the resulting unpublished data because of various technical limitations.

One striking aspect of the LET-99 cytokinesis phenotype is the presence in many embryos of a large cortical protrusion near the cytokinetic furrow, which we call a "wedge." Despite CED-10's ability to rescue cytokinesis timing in *let-99* embryos, these double mutant embryos exhibit this wedge more frequently and the wedge persists longer. This finding implies that overall cortical structure or organization is perturbed by loss of both proteins. Since the organization of the cortex determines its mechanical properties including rigidity, and properly tuned cortical rigidity has been implicated in both spindle positioning and cytokinetic dynamics, it would be interesting to investigate whether LET-99 and CED-10 have antagonistic effects on

cortical rigidity as they do on branched actin and whether the wedge might be the result of excessive or insufficient cortical rigidity (Redemann, Pecreaux et al. 2010), (Gilden and Krummel 2010).

Over the course of my studies, it has become evident that LET-99 is a multifunctional protein with important roles in at least three contexts: a specific PAR-dependent role in spindle positioning in P0, a general role in cytokinesis in both P lineage and somatic cells, and an apparently MES-1/SRC-1 dependent role in EMS spindle positioning. The impressive versatility of this protein raises the question of how these different functions are possible and how the molecular mechanisms may be similar or different across contexts. A LET-99 structure/function analysis would reveal how LET-99 can interact with context-specific regulators and effectors for separable roles in spindle positioning and cytokinesis.

Connections between systems and concluding thoughts

Chapters II and III of this dissertation center on different types of asymmetric cell divisions, but a common theme in both is the importance of coordinating the actin cytoskeleton with the microtubule-based mitotic spindle. The best described interaction between these two structures occurs during cytokinesis, when an actomyosin contractile ring forms in response to signals from the spindle (Miller 2011, Green, Paluch et al. 2012). However, the actin cytoskeleton and the mitotic spindle must work together throughout the process of division, not only during cytokinesis. The mechanical stiffness of the cortex, which is determined by the organization of the actin cytoskeleton, must be tuned precisely so that the dynein anchored there can generate microtubule pulling forces to position the spindle; the contractile ring can deform the membrane; and the cortex can maintain integrity throughout (Gilden and Krummel 2010, Redemann, Pecreaux et al. 2010). The studies presented in Chapter II highlight the importance of

the second and third points: we identified an oppositional relationship between LET-99 and CED-10 in organizing actin at the cell cortex during the first mitotic division of the *C. elegans* zygote. The studies presented in Chapter III hint at the first point: I showed that CED-10 is important for early events in the MES-1/SRC-1 signaling pathway at the four-cell stage and provided some evidence that its role in this pathway may be via its functions as a regulator of the actomyosin cytoskeleton. Intriguingly, a role for LET-99 in this pathway has also been identified (Liro and Rose 2016). The possible connection between LET-99 and CED-10 in the four-cell embryo should be investigated with a special emphasis on how their relationship might compare with their antagonistic roles in the first division.

References

Bei, Y., J. Hogan, L. A. Berkowitz, M. Soto, C. E. Rocheleau, K. M. Pang, J. Collins and C. C. Mello (2002). "SRC-1 and Wnt signaling act together to specify endoderm and to control cleavage orientation in early C. elegans embryos." Developmental Cell: 113-125.

Berkowitz, L. A. and S. Strome (2000). "MES-1, a protein required for unequal divisions of the germline in early C. elegans embryos, resembles receptor tyrosine kinases and is localized to the boundary between the germline and gut cells." Development **127**: 4419-4431.

Bringmann, H., C. R. Cowan, J. Kong and A. A. Hyman (2007). "LET-99, GOA-1/GPA-16, and GPR-1/2 are required for aster-positioned cytokinesis." Curr Biol **17**(2): 185-191.

Bringmann, H., C. R. Cowan, J. Kong and A. A. Hyman (2007). "LET-99, GOA-1/GPA-16, and GPR-1/2 Are Required for Aster-Positioned Cytokinesis." Current Biology **17**(2): 185-191.

Bustelo, X. R., V. Sauzeau and I. M. Berenjeno (2007). "GTP-binding proteins of the Rho/Rac family: regulation, effectors and functions in vivo." Bioessays **29**(4): 356-370.

Bustelo, X. R., V. Sazeau and I. M. Berenjeno (2007). "GTP-binding proteins of the Rho/Rac family: regulation, effectors and functions in vivo." BioEssays **29**(4): 356-370.

Cabello, J., L. J. Neukomm, U. Gunesdogan, K. Burkart, S. J. Charette, G. Lochnit, M. O. Hengartner and R. Schnabel (2010). "The Wnt pathway controls cell death engulfment, spindle orientation, and migration through CED-10/Rac." PLOS Biology: e1000297.

Cabello, J., L. J. Neukomm, U. Gunesdogan, K. Burkart, S. J. Charette, G. Lochnit, M. O. Hengartner and R. Schnabel (2010). "The Wnt pathway controls cell death engulfment, spindle orientation, and migration through CED-10/Rac." PLoS Biol **8**(2): e1000297.

Chircop, M. (2014). "Rho GTPases as regulators of mitosis and cytokinesis in mammalian cells." Small GTPases **5**.

Ganguly, R., A. Mohyeldin, J. Thiel, H. I. Kornblum, M. Beullens, I. Nakano (2015). "MELK -- a conserved kinase: functions, signaling, cancer, and controversy." Clin & Transl Med 4(1): e11.

Gilden, J. and M. F. Krummel (2010). "Control of cortical rigidity by the cytoskeleton: emerging roles for septins." Cytoskeleton (Hoboken) **67**(8): 477-486.
Green, R. A., E. Paluch and K. Oegema (2012). "Cytokinesis in Animal Cells." Annual Review of Cell and Developmental Biology **28**(1): 29-58.
Guan, L., X. Ma, J. Zhang, J. J. Liu, Y. Wang and M. Ding (2016). "The Calponin Family Member CHDP-1 Interacts with Rac/CED-10 to Promote Cell Protrusions." PLoS Genet **12**(7): e1006163.
Hall, A. (2012). "Rho family GTPases." Biochemical Society Transactions **40**(6): 1378-1383.
Heppert, J. K., A. M. Pani, A. M. Roberts, D. J. Dickinson and B. Goldstein (2018). "A CRISPR tagging-based screen reveals localized players in Wnt-directed asymmetric cell division." Genetics: 1147-1164.
Inaba, M. and Y. M. Yamashita (2012). "Asymmetric Stem Cell Division: Precision for Robustness." Cell Stem Cell(11): 461-469.
Krueger, L. E., J.-C. Wu, M.-F. B. Tsou and L. S. Rose (2010). "LET-99 inhibits lateral posterior pulling forces during asymmetric spindle elongation in C. elegans embryos." The Journal of Cell Biology **189**(3): 481-495.
Kumar, R., R. Sanawar, X. Li and F. Li (2017). "Structure, biochemistry, and biology of PAK kinases." Gene **605**: 20-31.
Lang, C. F. and E. Munro (2017). "The PAR proteins: from molecular circuits to dynamic self-stabilizing cell polarity." Development **144**: 3405-3416.
Liro, M. J., D. Morton and L. S. Rose (2018). "The kinases PIG-1 and PAR-1 act in redundant pathways to regulate asymmetric division in the EMS blastomere of C. elegans." Developmental Biology: 9-19.
Liro, M. L. and L. S. Rose (2016). "Mitotic spindle positioning in the EMS cell of C. elegans requires LET-99 and LIN-5/NuMA." Genetics: 1177-1189.
Lundquist, E. A., P. W. Reddien, E. Hartwieg, H. R. Horvitz and C. I. Bargmann (2001). "Three C. elegans Rac proteins and several alternative Rac regulators control axon guidance, cell migration and apoptotic cell phagocytosis." Development **128**: 4475-4488.
Marston, D. J., C. D. Higgins, K. A. Peters, T. D. Cupp, D. J. Dickinson, A. M. Pani, R. P.
Mattila, P. K., F. D. Batista and B. Treanor (2016). "Dynamics of the actin cytoskeleton mediates receptor cross talk: An emerging concept in tuning receptor signaling." J Cell Biol **212**(3): 267-280.
Miller, A. L. (2011). "The contractile ring." Curr Biol **21**(24): R976-978.
Nguyen, L. K., B. N. Kholodenko and A. von Kriegsheim (2018). "Rac1 and RhoA: Networks, loops and bistability." Small GTPases **9**(4): 316-321.
Park, F. D., J. R. Tenlen and J. R. Priess (2005). "C. elegans MOM-5/Frizzled functions in MOM-2/Wnt-independent cell polarity and is localized asymmetrically prior to division." Curr. Biol. **14**: 22582-22258.
Price, K. L. and L. S. Rose (2017). "LET-99 functions in the astral furrowing pathway, where it is required for myosin enrichment in the contractile ring." Mol Biol Cell **28**(18): 2360-2373.
Redemann, S., J. Pecreaux, N. W. Goehring, K. Khairy, E. H. Stelzer, A. A. Hyman and J. Howard (2010). "Membrane invaginations reveal cortical sites that pull on mitotic spindles in one-cell C. elegans embryos." PLoS One **5**(8): e12301.
Rocheleau, C. E., W. D. Downs, R. Lin, C. Wittmann, Y. Bei, Y. H. Cha, M. Ali, J. R. Priess and C. C. Mello (1997). "Wnt signaling and an APC-related gene specify endoderm in early C. elegans embryos." Cell(90): 707-716.

Rose, L. and P. Gonczy (2014). "Polarity establishment, asymmetric division and segregation of fate determinants in early C. elegans embryos." WormBook: 1-43.
Rose, L. S. and P. Gonczy (2014). "Polarity establishment, asymmetric division and segregation of fate determinants in early C. elegans embryos." WormBook: The Online Review of C. Elegans Biology.
Saenz-Narciso, B., E. Gomez-Orte, A. Zheleya, I. Gastaca and J. Cabello (2016). "Control of developmental networks by Rac/Rho small GTPases: How cytoskeletal changes during embryogenesis are orchestrated." Bioessays: 1246-1254.
Shakir, A. M., K. Jiang, E. C. Struckhoff, R. S. Demarco, F. B. Patel, M. C. Soto and E. A. Lundquist (2008). "The Arp2/3 activators WAVE and WASP have distinct genetic interactions with Rac GTPases in Caenorhabditis elegans axon guidance." Genetics **179**: 1957-1971.
Shivas, J. M. and A. R. Skop (2012). "Arp2/3 mediates early endosome dynamics necessary for the maintenance of PAR asymmetry in C. elegans " Mol. Biol. of the Cell **23**: 1917-1927.
Shivas, J. M. and A. R. Skop (2012). "Arp2/3 mediates early endosome dynamics necessary for the maintenance of PAR asymmetry in Caenorhabditis elegans." Molecular Biology of the Cell **23**(10): 1917-1927.
Soto, M. C., H. Qadota, K. Kasuya, M. Inoue, D. Tsuboi, C. C. Mello and K. Kaibuchi (2002). "The GEX-2 and GEX-3 proteins are required for tissue morphogenesis and cell migrations in C. elegans." Genes & Development: 620-632.
Sugioka, K., L.-E. Fielmich, K. Mizumoto, B. Bowerman, S. van den Heuvel, A. Kimura and H. Sawa (2017). "Tumor suppressor APC is an attenuator of spindle-pulling forces during C. elegans asymmetric cell division." Proc. Natl. Acad. Sci.: 954-963.
Sugioka, K., K. Mizumoto and H. Sawa (2011). "Wnt regulates spindle asymmetry to generate asymmetric nuclear B-catenin in C. elegans." Cell **146**(6): 942-954.
Sumiyoshi, E., S. Takahashi, H. Obata, A. Sugimoto and Y. Kohara (2011). "The β-catenin HMP-2 functions downstream of Src in parallel with the Wnt pathway in early embryogenesis of C. elegans." Dev Biol **355**(2): 302-312.
Tsou, M.-F. B., A. Hayashi, L. R. DeBella, G. McGrath and L. S. Rose (2002). "LET-99 determines spindle position and is asymmetrically enriched in response to PAR polarity cues in C. elegans embryos." Development **129**(19): 4469-4481.
Tsou, M.-F. B., A. Hayashi and L. S. Rose (2003). "LET-99 opposes G-alpha/GPR signaling to generate asymmetry for spindle positioning in response to PAR and MES-1/SRC-1 signaling." Development: 5717-5730.
Yang, Y. and M. Mlodzik (2015). "Wnt-Frizzled/planar cell polarity signaling: cellular orientation by facing the wind (Wnt)." Annu Rev Cell Dev Biol **31**: 623-646.